Development of an Analytical Tool for Thrust Load Calculations of a Turbocharger Considering Effect of Exhaust Braking

A Dissertation

Submitted in partial fulfilment of the requirements for the degree of

Master of Engineering

in

CAD/CAM

by

Mohit Sharma

Registration No: 801784010

Under the guidance of

Mr. A.S. Jawanda	**Mr. J.M. Ramamoorthy**	**Mr. Atif B. Bhagat**
Associate Professor, Mechanical Engineering Department Thapar Institute of Engineering and Technology, Patiala	Product Engineer-Senior, Rotor system and seals Cummins India Limited, Pune	Product Engineer-Senior, Platform engineering Cummins India Limited, Pune

MECHANICAL ENGINEERING DEPARTMENT

THAPAR INSTITUTE OF ENGINEERING &TECHNOLOGY, PATIALA, INDIA

(DEEMED TO BE UNIVERSITY)

JULY, 2019

DECLARATION

I hereby declare that the work done in thesis report entitled, " ***Development of an Analytical Tool for Thrust Load Calculations of a Turbocharger Considering Effect of Exhaust Braking*** *" submitted towards partial fulfilment of award of* ***Master of Engineering degree*** *in* ***CAD/CAM Engineering*** *in* ***Mechanical Engineering Department*** *of* ***Thapar Institute of Engineering and Technology, Patiala*** *is an authentic record of work carried out by me under the supervision and guidance of* ***Mr. A.S. Jawanda, Associate Professor, Mechanical Engineering Department*** *of* ***Thapar Institute*** *of* ***Engineering and Technology, Patiala, Mr. J.M. Ramamoorthy, Product Engineer-Senior, Cummins India Limited, Pune and Mr. Atif B. Bhagat, Product Engineer-Senior, Cummins India Limited, Pune.***

Mohit Sharma

Date: 15th July, 2019 **Mohit Sharma**

This is to certify that above declaration made by the student concerned is correct to the best of my knowledge and belief.

Mr. A.S. Jawanda **Associate Professor,** **Mechanical Engineering Department,** **Thapar Institute of Engineering and Technology, Patiala**	**Mr. J.M. Ramamoorthy** **Product Engineer-Senior,** **Cummins India Limited, Pune**	**Mr. Atif B. Bhagat** **Product Engineer-Senior, Cummins India Limited, Pune**

ACKNOWLEDGEMENT

I am highly thankful to **Dr. Tejinder Paul Singh,** professor and head of Mechanical Engineering Department, Thapar Institute of Engineering and Technology, Patiala for providing me with the opportunity to do an internship at Cummins India Limited, Pune. I am grateful to **Mr**. **A.S Jawanda**, Associate Professor, Thapar Institute of Engineering and Technology, for providing me with the opportunity to work with him and supporting me to complete the project. He has always been a source of inspiration for me and his persona motivates me to take up challenging tasks.

I am grateful to **Mr. J.M. Ramamoorthy,** Product Engineer-Senior, Cummins India Limited, Pune, for keeping faith in me and providing me persistent support and guidance throughout the course of the project. He gave me opportunities to learn new technologies and analysis tools. I am deeply indebted by the efforts made by **Mr**. **Siddharth Sane,** Thermal and Fluid Science Engineer-Senior, Cummins India Limited, Pune and **Mr. Prasanna Ramanan Surendiran**, Thermal and Fluid Science Engineer-Senior, Cummins India Limited, Pune to make the project successful. I am also thankful to **Mr. Arindam Mahato**, Product Chief Engineer, Cummins India Limited and **Mr. Atif Bhagat,** Product Engineer-Senior, Cummins India Limited, Pune, for making me the part of medium-duty platform team. I am grateful to the members of Cummins Turbo Technologies, a component wing of Cummins India Limited, for actively assisting me at the times of need.

I am grateful to my grandmother, **Mrs. Krishna Devi,** who always supported and motivated me in my endeavours. I would like to express my gratitude to my parents, **Mr. Navdeep Sharma** and **Mrs. Sunita Rani** for being the pillars of strength whenever I felt demotivated during this challenging project and also my sister, **Miss Rusheen Sharma** for inspiring me to work hard throughout the course of the project.

Mohit Sharma

ABSTRACT

Turbocharging is a way of enhancing the power output of the engine by suppling higher density and high-pressure air. Turbocharging not only compensated the loss of power due to engine downsizing but also reduced the particulate matter into the atmosphere. So, turbocharging is highly preferred in the present scenario. It is vital for the turbocharger to work very effectively so as give good engine performance. A turbocharger comprises of compressor stage, turbine stage and the bearing system. The impeller is assembled along with the turbine wheel and shaft assembly, supported in radial and thrust bearings for effective power transmission. It is necessary that the bearing system works effectively to transmit energy. The thrust bearing system is a major contributor to the energy losses so it is vital to predict and optimise the design of new thrust bearings. This project aims to predict the thrust loads and improve upon the current CTT methods of prediction. The project also aims to co-relate the predicted loads well with the experimentally determined loads even under high exhaust back pressure conditions because the new emission norms demand new components in the downstream of the engine after the turbocharger, which results in high back pressure.

To accomplish this task, the biggest assumption of a degree of reaction which is assumed to be constant and equal for both turbine and compressor stages have been eliminated. For this, the critical parameter tree for the compressor and turbine stage has been created and important parameters have been collected. Using the CFD data as the base, the parameters and their effect on the pressures have been studied. Non-dimensional parameters have been used in the new approach to making the analytical method applicable to all turbocharger frames and operating conditions. Non-dimensional parameters collected using CFD data are trained in MATLAB regression tool to extract a regression model that can predict the degree of reaction for both the compressor and turbine stages. The degree of reaction value is used to estimate the pressures needed to predict thrust loads in analytical tool and the results are compared with the thrust loads obtained using test data. The results obtained are co-relate better than the current CTT method and fit in agreement with the results obtained using the test data.

Keywords: Critical parameter tree, Thrust load, MATLAB regression tool, Degree of reaction

LIST OF ABBREVIATIONS

Abbreviations	Expansion
M.E.	Master of Engineering
CTT	Cummins Turbo Technologies
DOR	Degree of reaction
CFD	Computational Fluid Dynamics
1-D	One dimensional
MWE	Map Width Enhancement
RPM	Revolutions per minute
VGT	Variable geometry turbine
NDSP	Non-dimensional speed parameter
TMFP	True mass flow parameter
PR	Pressure ratio
ER	Expansion ratio
CP tree	Critical parameter tree
MFT	Mixed flow turbine
RFT	Radial flow turbine
GPR	Gaussian process regression
BS	Bharat stage emission norms
RMSE	Root mean square error
TIT	Turbine inlet temperature
MSE	Mean square error
MAE	Mean absolute error

LIST OF SYMBOLS

Symbol	Meaning, Unit
A/R	Area/Radius - Turbine volute geometric parameter
Δhc	Compressor wheel enthalpy change, J/kg
Δhst	Compressor stage enthalpy change, J/kg
Δht	Turbine wheel enthalpy change, J/kg
Δhst	Turbine stage enthalpy change, J/kg
rc	DOR of compressor
rt	DOR of turbine
p1	Compressor stage inlet stagnation pressure, Pa
p2	Compressor stage outlet stagnation pressure, Pa
p2*	Impeller outlet static pressure, Pa
p3	Turbine stage inlet stagnation pressure, Pa
p3*	Turbine wheel inlet static pressure, Pa
p4	Turbine stage outlet stagnation pressure, Pa
$\frac{p2}{p1}$	Pressure ratio of compressor stage
$\frac{p3}{p4}$	Expansion ratio of turbine stage
U_1	Inlet blade velocity, m/sec
U_2	Exit blade velocity, m/sec
V_1	Absolute velocity at inlet of compressor, m/sec
V_2	Absolute velocity at exit of compressor, m/sec
V_{r1}	Relative velocity at inlet of compressor, m/sec
V_{r2}	Relative velocity at exit of compressor, m/sec
V_{f1}	Flow velocity at compressor inlet, m/sec
V_{f2}	Flow velocity at compressor outlet, m/sec
V_{w1}	Whirl velocity at compressor inlet, m/sec
V_{w2}	Whirl velocity at compressor outlet, m/sec
β_1	Blade inlet angle, radian
β_2	Blade outlet angle, radian
γ	Isentropic exponent of gas for compressor/turbine
C_p	Specific heat at constant pressure, J/kgK

C_v	Specific heat at constant volume, J/kgK
$\dot{m}$	Compressor mass flow rate in kg/sec
P	Compressor inlet pressure in MPa
R	Gas constant in J/KgK
T	Inlet temperature of compressor or turbine, K
D	Tip diameter of compressor or turbine wheel, mm
N/ω	Rotational speed of rotor in rpm
h	Height of thrust bearing in mm
M	Fundamental unit of mass
L	Fundamental unit of length
T	Fundamental unit of time
θ	Fundamental unit of temperature
η	Oil dynamic viscosity, kg/m-sec
$\frac{\partial}{\partial x}$	Partial differentiation in x direction
$\frac{\partial}{\partial z}$	Partial differentiation in z direction
$\frac{\partial p}{\partial x}$	Partial differentiation of pressure in x direction
$\frac{\partial p}{\partial z}$	Partial differentiation of pressure in z direction
$\frac{\partial h}{\partial x}$	Partial differentiation of thrust bearing height in x direction
$\frac{\partial h}{\partial z}$	Partial differentiation of thrust bearing height in z direction
U	Circumferential velocity at mean diameter of thrust bearing, m/sec
L	Bearing segment (pad) length, mm
W	Width of bearing, mm
p(x,z)	Induced pressure in the bearing, Pa
h(x,z)	Oil film thickness in the bearing, mm
D_o	Outer diameter of thrust bearing, mm
D_m	Mean diameter of thrust bearing, mm
D_i	Inner diameter of thrust bearing, mm
l_{wed}	Wedth length, mm

c_{wed}	Wedth height, mm
θ_L	Angle subtended by thrust bearing circumferential length, radian
θ_W	Angle subtended by tapered land, radian
θ_{oil}	Angle subtended by oil groove, radian
p_o	Oil pressure at the thrust bearing, Pa
FC1	Compressor wheel inducer force, N
FC2	Compressor wheel shroud force, N
FC3	Compressor wheel back face force, N
FT1	Turbine wheel back face force, N
FT2	Turbine wheel shroud force, N
FT3	Turbine wheel exducer force, N
$D_{inducer}$	Impeller inducer diameter, m
$D_{impeller\ tip}$	Impeller tip diameter, m
$D_{scalloped}$	Turbine wheel scalloped diameter, m
D_{boss}	Turbine wheel boss diameter, m
$D_{exducer}$	Turbine wheel exducer diameter, m
$D_{slinger}$	Diamter of oil slinger in contact with impeller, m
ρ	Density of fluid, kg/m^3

LIST OF FIGURES

Contents

CHAPTER 1: INTRODUCTION

Background and Motivation

The M.E thesis is the result of the joint efforts made by the college and Cummins India Limited. It is a product of the paid internship that was offered by Cummins at CTT, which is a component wing of Cummins specialised in dealing with turbochargers. The turbocharger design, compressor and turbine stage analysis, bearing system design and analysis, rotor stability and balancing and turbo matching to the engine are some of the technical areas in which Cummins turbocharger wing is specialised. Cummins deals with turbochargers from the low to medium, heavy-duty and high horsepower operations. This project originated because of the implementation of more stringent norms related to automotive emissions. To meet these norms in the present scenario when India is migrating from BSIV to BSVI, it was the need of the hour to come up with new technology in addition to after treatment devices.

Fig. 1 Secondary brake valve (En.wikipedia.org, 2016)

The after-treatment devices and secondary brake valve which is shown in figure 1 obstructs the path of exhaust flow gas which tends to affect the turbine motion and slows it down. As the turbine is retarded, the turbocharger is not capable of pulling enough fresh air into the inlet manifold thus boost pressure gets lowered. In addition to a turbocharger, it results in high back pressure and increase in temperature in exhaust

manifold which impacts the piston motion by generating negative torque (En.wikipedia.org, 2016).

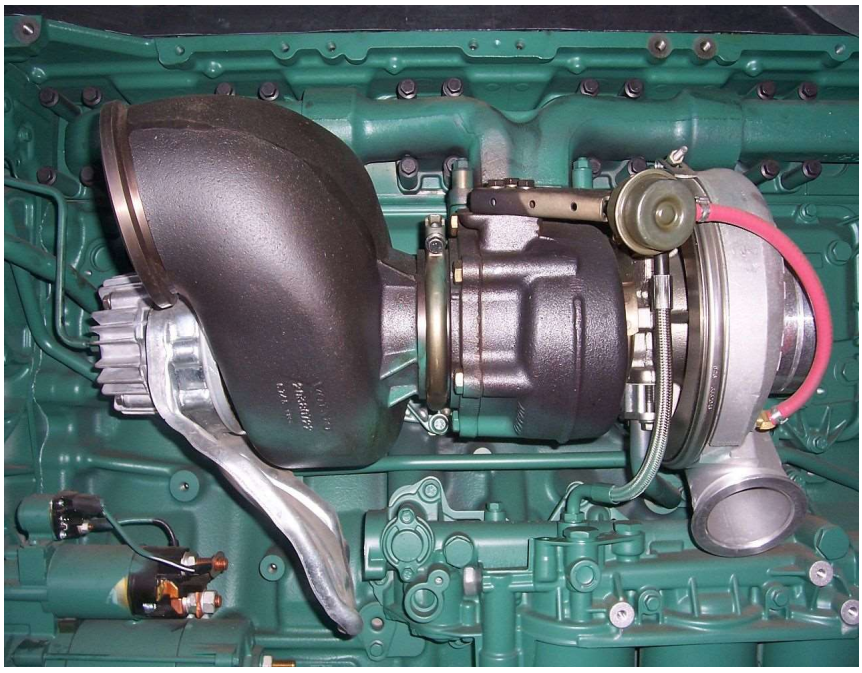

Fig. 2 Secondary brake valve with turbo charger mounted on the engine (En.wikipedia.org, 2016)

Though secondary brake valve is quite helpful in safeguarding vehicle, it has a negative impact on turbocharger operation causing oil leakage, higher blow-by and higher temperature. As it creates drastic pressure difference, it impacts turbocharger's axial stability. This raises loads on the thrust bearing system. So, it's vital to estimate the thrust loads when the secondary brake valve is operated so that turbocharger thrust system failure can be avoided. The accurate prediction of thrust loads helps to develop thrust bearing with higher capacity.

Problem Statement

Shortcomings of Current CTT Approach

The project aims to reduce the gap between the thrust load prediction between the experimental pressure tapping method and the analytical one-dimensional method. The analytical method available with CTT makes use of equal value of the degree of reaction for all operating ranges of turbocharger for both the compressor and turbine side. Because of this, there was significant variation between the results obtained from the pressure tapped method and the analytical method. The results deviated from the test

cell results at all operating points and under predicted the thrust loads. Thrust bearing design is affected due to lower prediction of thrust loads.

Deviation between the two methods is given in the figure below:

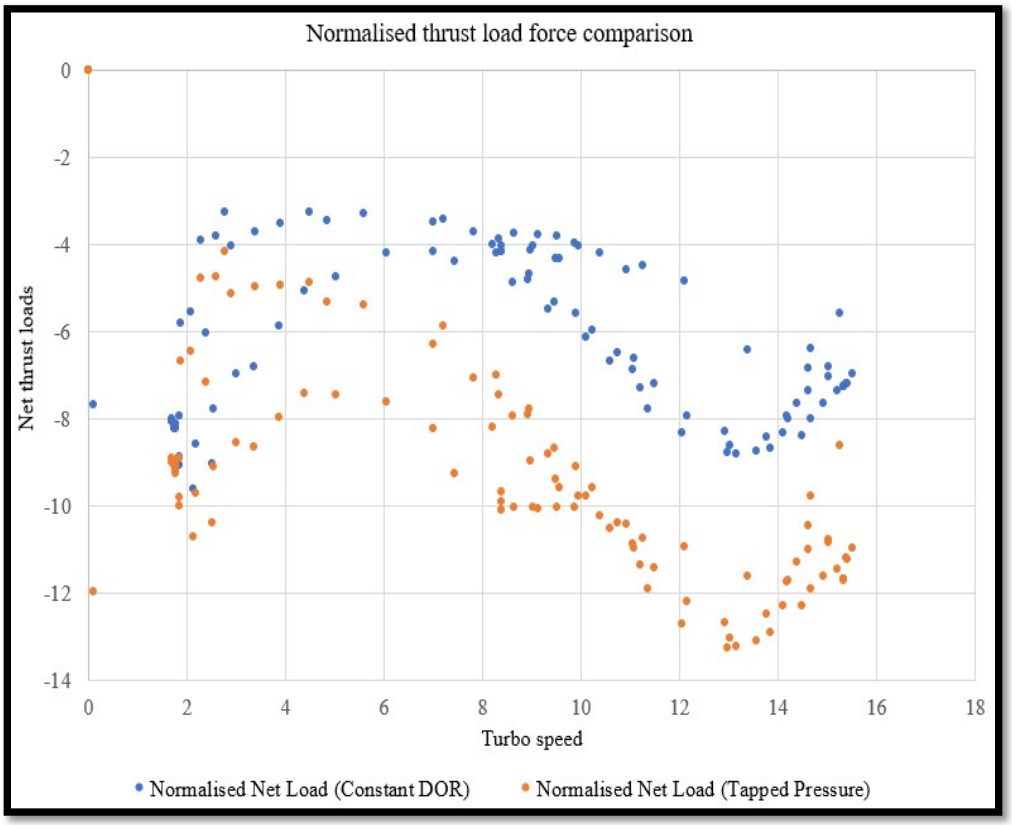

Fig. 3 Constant DOR method under predicts values with higher variation © Cummins

In the current CTT analytical approach, the pressure behind the seal on the turbine side has not been considered which is significant at the time when the secondary brake valve is operated. This resulted in the wrong prediction of forces on the turbine side. Moreover, the assumption of a constant degree of reaction did not fare well in all frames of the turbocharger. There are various geometric and operating parameters that vary when there are significant pressure changes. Moreover, CFD used for computing thrust loads involves a lot of time and resources while the experimentation involves a lot of costs.

Importance of the Proposed Work

Learning from the previous results, it was felt that there is a need to bring the co-relation between the experimental results and results predicted by the analytical tool.

Considering that the analytical tool is based on 1-D equations in the literature, there are assumptions involved in calculating the forces acting on the thrust load bearings under the turbocharger operating conditions. So, this project aims to decrease the variation of the thrust load prediction from the current CTT approach. The project aims to test the newly developed tool in the conditions when the turbocharger is operated under high exhaust back pressures. The transient and steady-state variation of the thrust loads estimated by the tool needs to be calculated and the variation with the test cell results must be studied. The comparison of deviation with the new analytical tool and the current CTT method is presented in figure 4 below taking the engine running data:

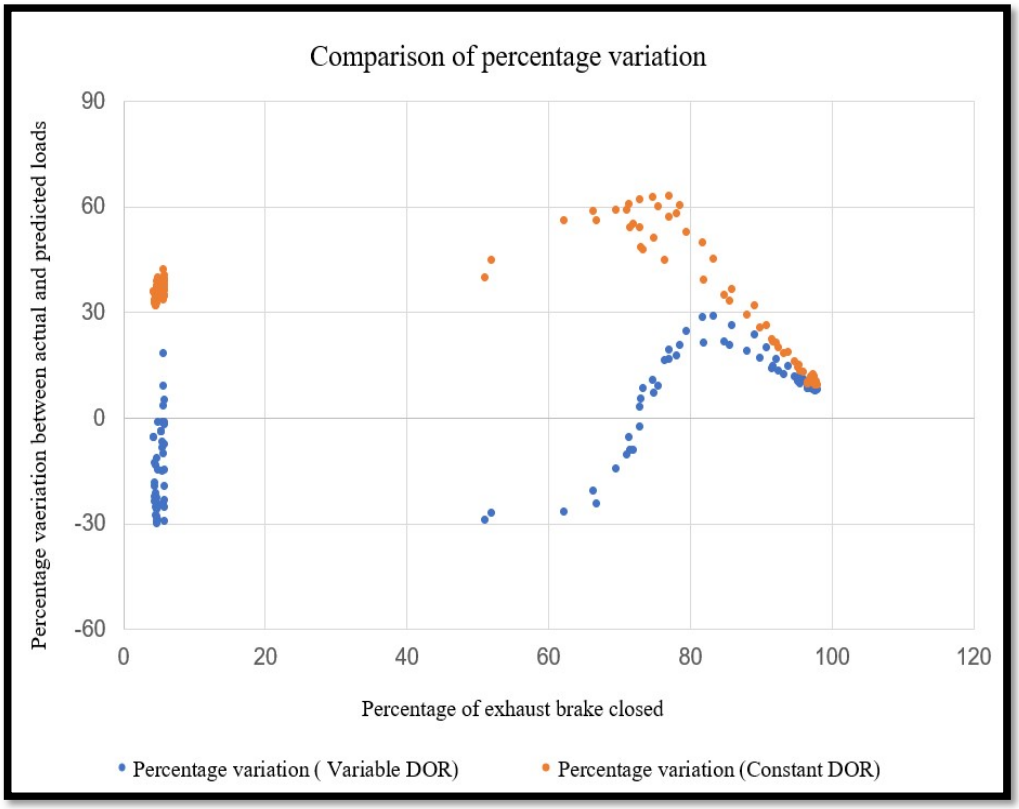

Fig. 4 Improvements made in prediction of axial thrust loads © Cummins

Hypothesis Considered to Build Analytical Thrust Load Calculation Model

- In the analytical model developed to predict thrust loads under high exhaust back pressures momentum forces have been excluded which is a function of meridional velocity. As it's difficult to capture the velocity and area on which impulse forces

act so their effect is assumed to be insignificant as compared to other contributing forces (Lüddecke *et al.*, 2015).

- Control volume (Lüddecke *et al.*, 2015) approach has been followed based on the previous research work. The geometry of impeller and turbine is complex so it's complicated to capture the exact areas on which forces act. Moreover, on the basis of various research findings, it has been assumed to agree well with test results.
- The thermal processes involved are isentropic (Nguyen-Schäfer, 2012). Isentropic processes are taken at baseline and all the theoretical equations used are based on it. Although in practice it is not able to capture the real situation in which the processes are considered adiabatic and irreversible.
- The intermediate value of pressures has been taken when there is a pressure difference at two different points within the geometry (Lüddecke *et al.*, 2015). The exact variation of pressures is unknown and it does not capture the practical situation of flow. But it has been assumed to keep the model simple.

CHAPTER 2: LITERATURE REVIEW

International Status

Chapter 2 deals with the historical developments in the field of the turbocharger, its use in passenger cars and the importance of the study. Various research studies have been under to manage the power transmission in turbocharger by improving the bearing design and operating parameters. Various research studies have been performed to predict thrust loads under operating conditions. The exhaust brake in the engine has also been used in modern automotive engines whose effect in relation to turbocharger thrust loads is a part of the research. The turbocharger fundamentals throw light on various types of turbines and compressor involved and the types of turbochargers available in the automotive industry. The operating principles of compressor and turbine have also been discussed along with different ways of turbo charging (Hannu Jääskeläinen, 2017). There are various ways of reducing the turbocharger lag to improve the acceleration in passenger car vehicles. The first of which is introducing the twin entry turbine housing to capture enough pulse energy to derive the turbocharger, second is to use mixed flow turbine, third is to use to ball bearings. These methods help to improve the passenger car experience by improving acceleration (Watanabe and Koike, 1996). The experimentation performed between aspirated and turbocharged engine shows less pollution emission particles and increased thermal efficiency (Chiatti, Chiavola and Recco, 2017). The turbocharger bearings play a vital role to keep the rotor in position and are responsible for power transmission. There are journal bearings, ball bearings and thrust bearings employed in turbocharger with various designs depending upon applications (Jääskeläinen, 2017). It has been found that the axial force is the major contributor to the friction which brings down turbocharger efficiency. So, the design of thrust bearings is crucial for the power supply in the rotor system and turbocharger operation. An experimental and numerical method has been designed to accurately determine the thrust loads in turbocharger (Lee, Hong and Choi, 2018). The thrust loads have been estimated using analytical and CFD approach. It is necessary to estimate the thrust loads to avoid turbocharger failure at extreme speeds (Sun *et al.*, 2010). The tilted pad thrust bearings are mostly used in the turbocharger and it is necessary to estimate the friction and the oil film lubrication in operating range. The experimentation has been successfully carried out in this regard and the numerical results are in tune with the experimentally determined values (Tieu, 1991).The flow

type in which the thrust bearing is operated play an important role in determining the stiffness and bearing capacity. For the specific angles between 0° and 50° of tapered land bearing the performance remains the same in both laminar and turbulent regions and it shows variations later (Frene, 1978). The thrust bearing is governed by the lubricating regions given by the Stribeck curve and also by the Reynolds equation (Huebner, 1974). The experimental findings of the parameters of temperature, oil film thickness and friction on thrust bearings in hydrodynamic region has been in good agreement with the test and theoretical predictions. Though the parameters showed considerable variations on each pad of the thrust bearing but it's the result of non-uniform temperature and pressure at all pads (Henry, Bouyer and Fillon, 2014). The axial thrust load calculation by the experimental results and the analytical approach shows good agreement in the axial thrust load prediction. To carry out the test a specialized test rig was developed and turbocharger testing has been carried out both in the steady state and transient regions (Gjika and LaRue, 2008). The power loss testing has been carried out in which the results show positive response to experimental values. The radial and thrust bearings both have been studied (Lamquin, 2009). The experimentation has been carried out to investigate the frictional losses occurring in the bearings. The radial and thrust bearings have been put to test and the results show that the thrust bearings show higher frictional losses when temperature and speeds are higher. So the design of thrust bearing is crucial to the automotive industry to minimize the power loss (Deligant, Podevin and Descombes, 2012). The theoretical model is in resonance with experimental values. Frictional losses have been found to contribute as much as 32% under full load (Hoepke *et al.*, 2015). The aerodynamic forces which are impacting the bearing frictions due to axial thrust loads have been put to study and have been compared with CFX analysis of compressor and turbine (Raetz *et al.*, 2017). Exhaust brakes have been used in engines as a secondary braking system to safeguard the loaded vehicles during operation (En.wikipedia.org, 2016). The rotor dynamics take care of the vibrations involved in the rotor during the turbocharger operation. The various modes of vibration including the thickness of oil film are vital to its operation. The radial and thrust bearing design is crucial in keeping the rotor balanced within its operating range (Nguyen-Schäfer, 2012).

National Status

The review paper shows the importance of using exhaust brakes in the vehicle (Palanisamy *et al.*, 2018). Exhaust brakes have been crucial in modern days for commercial vehicles for effective engine operation and to control the vehicle during operation. It is a part of research in the automotive industry and its use is essential as per the latest emission norms (Khan *et al.*, 2005). To reduce the impact of harmful emissions on the environment, turbo charging has been employed in engines and uses different types of turbochargers as per applications. The variable geometry turbocharger has found to increase performance at lower engine speeds and reduced turbo lag (Muqeem, Ahmad and Sherwani, 2015).

Objectives of the Proposed Project

Project aims to fulfil the following objectives which are listed below:

1. To eliminate the constant value of the degree of reaction used in previous research studies and to develop a method that can predict the degree of reaction based on the dependent parameters.
2. To predict the pressures behind the turbine effectively so that pressure variations can be taken care of when the turbocharger is operated under high back pressures.
3. To reduce the variation between the pressure tapped estimated thrust loads and the ones predicted by analytical approach making use of a variable degree of reaction.
4. To determine thrust loads accurately even under high back pressures generated as a result of after-treatment devices.

CHAPTER 3: THEORETICAL FOUNDATION

Chapter 3 describes the phenomenon of turbo charging and its principle. The various components involved in turbocharger are also discussed. It also throws light on the need to opt for turbocharged diesel engines than the naturally aspirated ones (En.wikipedia.org, 2016).

The turbocharger is a device which is used in the engine to increase the boost pressure, to supply compressed and higher density air into the engine which is accomplished by turbine wheel causing forced induction of charged air. Thus, a turbocharged engine increases thermal efficiency(En.wikipedia.org, 2016). The engine performance gets enhanced as considerable amount of fuel is burnt with the charged supply of air. The figure below shows the turbocharger working and operation:

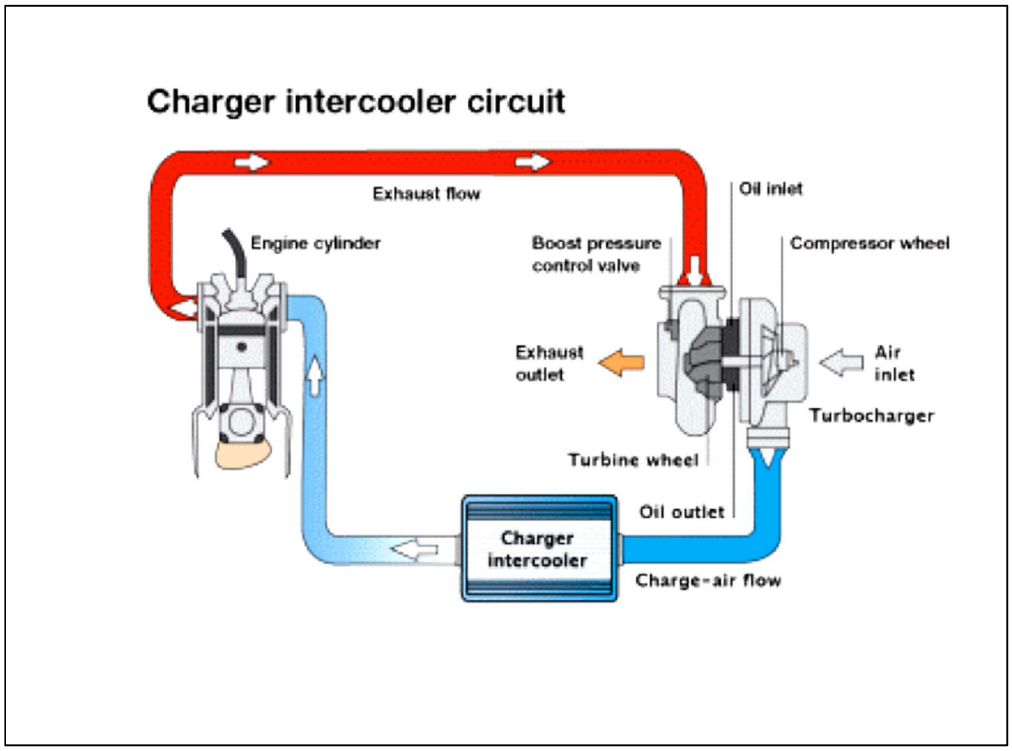

Fig. 5 Principle of turbocharger operation (Rais, 2016)

The charged air is sucked in by centrifugal compressor and it undergoes compression but the compressed air still does have a higher temperature. Air density is raised when it passes through an intercooler. It lowers down its temperature and enriches it with higher amounts of oxygen. The compressed and denser air is then supplied to the inlet manifold, which then enters the combustion chamber. After combustion, the

combustion gases are expanded over turbine to extract energy. In turbocharger, the turbine is the driver and the compressor is the driven component connected with a common shaft. The idea of turbo charging came into automotive scenario because of the implementation of higher stringent emission norms and to reduce the emissions of harmful gases into the atmosphere. Moreover, it was the need of the hour to develop smaller displacement engines having higher power and minimal emissions which were supported by the turbocharger device fitted to the engines. The turbocharged engines work better at a higher altitude than the naturally aspirated engines. So, at higher altitudes, the conditions are quite favourable for the turbocharged engine (En.wikipedia.org, 2016).

Turbocharger Components

Compressor Stage

Compressor Working

The most preferred type of compressors in turbochargers are of centrifugal nature. Centrifugal compressors can withstand higher and variable mass flow rates and can be operated under higher pressure ratios. Centrifugal compressors are designed to operate in the subsonic range. The compressor wheel is called impeller. The impeller has a compressor housing to guide the compressor flow in the stage and noise baffle is placed at the air entry passage. As the impeller is rotated at high speeds in turbocharger the fluid flow occurs in towards impeller eye with an increased velocity which results in a slight drop of static pressure. The kinetic energy is imparted to fluid due to the centrifugal action of impeller. The dynamic energy of fluid partially converts into static pressure within the impeller and the diffuser. The diffuser can be classified as having vanes or vaneless with the sole purpose of decelerating the fluid flow in designed limits to increase the static pressure and to guide the flow for the entry into the volute casing and further to the inlet manifold (En.wikipedia.org, 2016). The diffuser vanes are diverging in nature and are tangential to impeller outlet flow. The figure 6 shows the various geometric components of the compressor stage. The blades of the impeller are a combination of full and splitter blades which helps to create optimum mass flow rate. The compressor covers are generally made of cast aluminium. For higher operating temperatures above 300°C, the titanium wheels are generally preferred both in the cast and machined from solid while the compressor cover is made from cast iron. Axial

compressors were not selected due to various limitations. The smaller operational bounds of the axial compressor makes it unfit for the turbocharged engines. Moreover, the axial compressors are heavier, expensive and difficult in construction for the same pressure ratio as compared to centrifugal compressors. So, in rare cases only axial compressor is being employed.

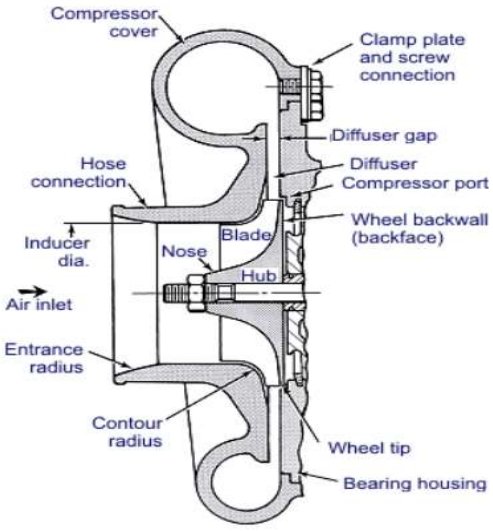

Fig. 6 Compressor stage operating components (Magdi K. Khair, 2017)

Compressor Performance

Compressor performance is ascertained using compressor map. Efficiency lines for operation are also visible in the map. The non-dimensional parameters mass flow parameter and speed parameter are used to make it independent of inlet temperature and pressure conditions and the map of a compressor remains the same at every location for analysis. The compressor map has three vital areas which are visible in figure 7. The leftmost part of the map indicates the Surge line while the rightmost part shows the choke region (Gcg.com.au, 2016). The central part where maximum efficiency is achieved is the heart region of the map. The engine operations are bound to happen in the efficient and stable heart region of the map while it's margined from unstable surge and choke regions. Surge is an unstable condition that occurs in operation when the compressor operates at reduced mass flow rates but with a constant pressure ratio. In the Surge phenomenon due to insufficient mass flow rate, the inlet velocity reduces which attacks the blades at inappropriate angles and thus resulting in inducer stall. As the flow does not have enough energy at the impeller outlet so it begins to re circulate

because of boundary layer separation. Thus, the surge condition results in highly inefficient operation and energy loss. It also results in instability because of vibrations. This condition can be avoided by diffuser recess optimisation and map width enhancement (Fisher, 1988).

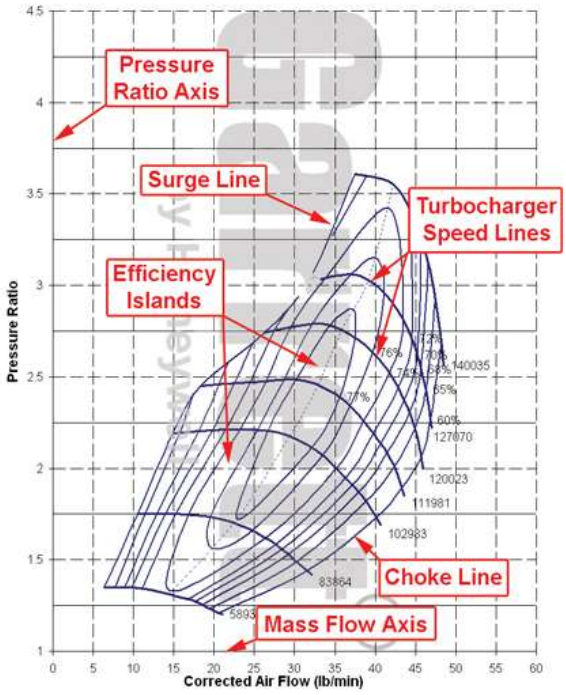

Fig. 7 Compressor map showing critical regions of operation (Gcg.com.au, 2016)

Fig. 8 Diffuser recess optimisation (Books, 2015)

Another unstable operating phenomenon is Choke which occurs when flow enters with higher velocity. The higher mass flow rate can be achieved at higher operating speeds. The flow rate is high enough that the impeller throat becomes blocked. In the case of choke Mach number at the impeller outlet goes beyond 1 resulting in shockwaves. An MWE slot at the compressor end is a way of reducing the possibility of choke (Fisher, 1988).

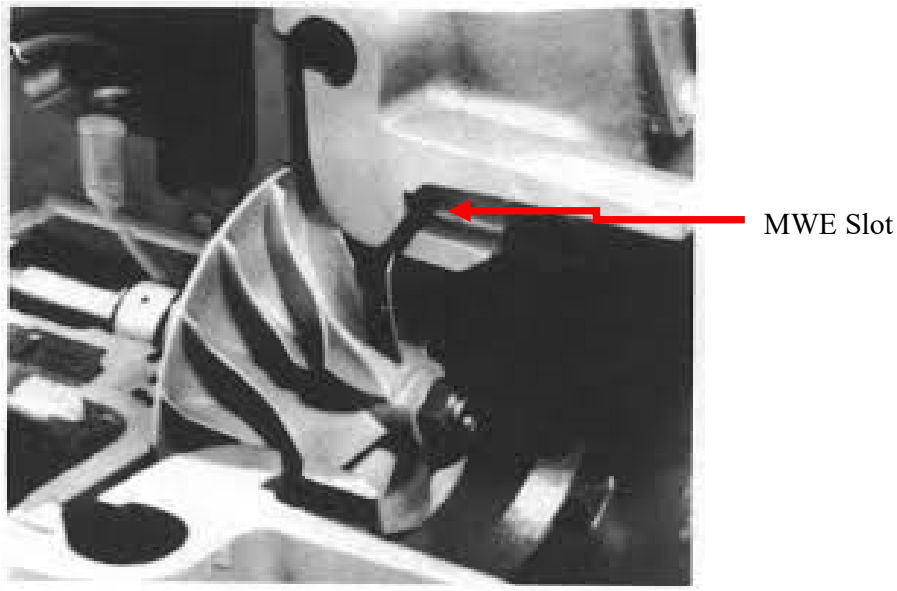

Fig. 9 MWE slot to resolve surge and choke (Fisher, 1988)

Compressor Wheel

Radial compressor sucks in the fresh air and then turning the flow at a right angle to supply the compressed and higher density air into the inlet manifold to achieve desired pressure ratio, which is not like axial compressors. Various compressor trims and geometries are available to support the desired mass flow rate and engine matching. The compressor wheel is affected by various design parameters which are given below and shown in figure 10 (Books, 2015):

1. Diameter of Inducer
2. Width of Impeller Tip
3. Trim
4. Splitter blade
5. Full blade
6. Compressor back face

7. Diameter of impeller tip
8. Tip of Impeller
9. Nose

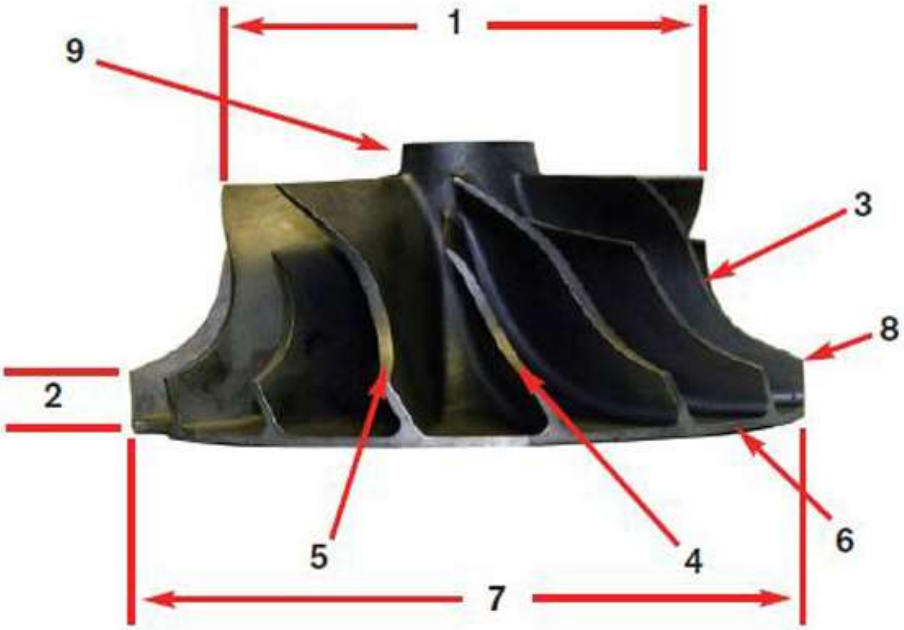

Fig. 10 Impeller geometric parameters (Books, 2015)

The two-plane balancing is used for compressor wheels. It is balanced on the nose and wheel back face (Books, 2015). As the turbocharger rotor rotates at very high speeds so balancing is crucial for the operation otherwise it could cause serious accidents. The balancing cuts are visible on the nose and back face of the wheel in figure 11.

Fig. 11 Two plane balancing of an impeller on nose and back-face (Books, 2015)

There are various types of compressor wheel blade designs available which are preferred according to their own application. Straight radial vanes were employed in an application where diesel engines operate on small RPM range. So, it's difficult to use the straight blade designs for automotive as the engine operates on a wide RPM range (Books, 2015). The full blade design is used for low turbocharger speed applications. It is unable to produce enough mass flow required for high-speed applications. The splitter blade design is a widely used form of impeller design as it maintains the required mass flow rate.

Fig. 12 Straight vanes of an impeller (Books, 2015)

Fig. 13 Full blades of an impeller (Books, 2015)

Fig. 14 Splitter blade design (Books, 2015)

The backward curved blade design wheels are of the most widely used type (Books, 2015). The design helps in the formation of enlarged compressor map which is suitable for modern day applications. It begins the fluid diffusion within the wheel and helps to increase compressor efficiency. The figure 15 below shows the velocity diagram of backward curved impeller:

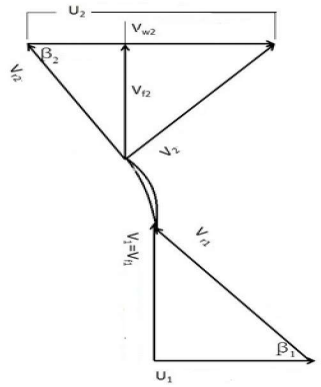

Fig. 15 Velocity triangle for backward curved vanes (Khin Nwe Zin Tun, 2014)

Compressor Housing

The housing plays a significant role in transporting the air flow into the inlet manifold at the designed pressures. The high velocity and highly compressed air gains its static pressure in the diffuser region, which is further supplemented by increasing the cross-section area of the volute. The figure 16 below shows the compressor housing exterior view and its components (Books, 2015):

1. Volute
2. Discharge
3. Eye
4. Inlet connection diameter

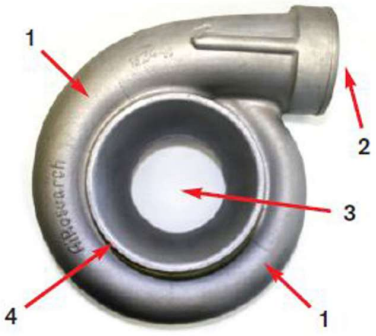

Fig. 16 Exterior outlook of Compressor volute (Books, 2015)

The inside view of the compressor housing along with its components is shown in the figure 17 below (Books, 2015) :

1. The contour of compressor cover
2. Inducer diameter of the cover
3. Connections of bearing housing
4. Diffuser face wall

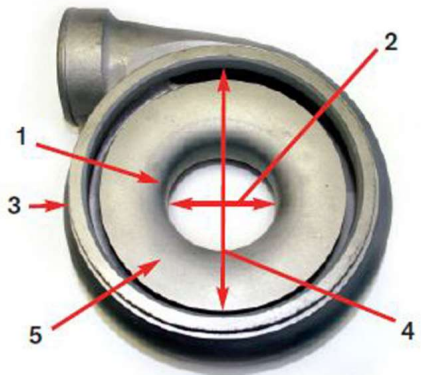

Fig. 17 Inner outlook of compressor volute (Books, 2015)

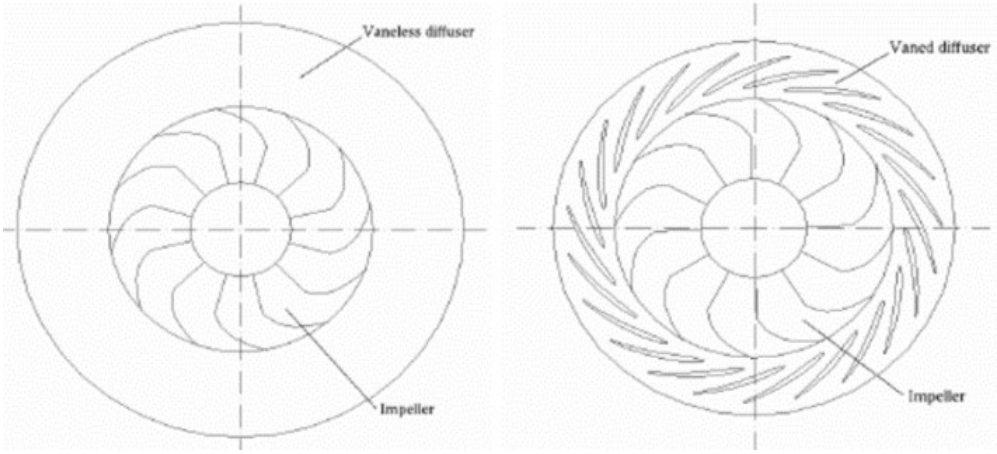

Fig. 18 Vaneless and vaned diffuser (Turunen-Saaresti, 2004)

Turbine Stage

Turbine Operation

The turbine is a vital part of the turbocharger. It is the driver which drives impeller pulling in fresh air (Books, 2015). It derives power from combustion gases which impinge on turbine blades. In the turbine, the exhaust gases enter radially inwards and exit axially outwards into the diffuser and then released to the atmosphere after passing it through after-treatment devices.

The components of the turbine stage are shown in the figure 19 below:

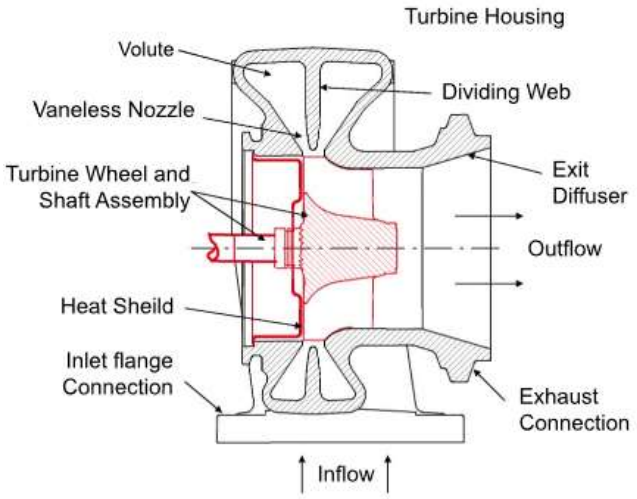

Fig. 19 Cut section view of turbine side of turbocharger © Cummins

Turbine Performance

Turbine stage performance is also indicated by the turbine map which gives the flow at a certain turbine speed and expansion ratio. The isentropic efficiency plots are superimposed to indicate the best matching area with the compressor for operation. The non-dimensional parameters are used for plotting the graph to make it universal for use in every region for a specific turbine stage.

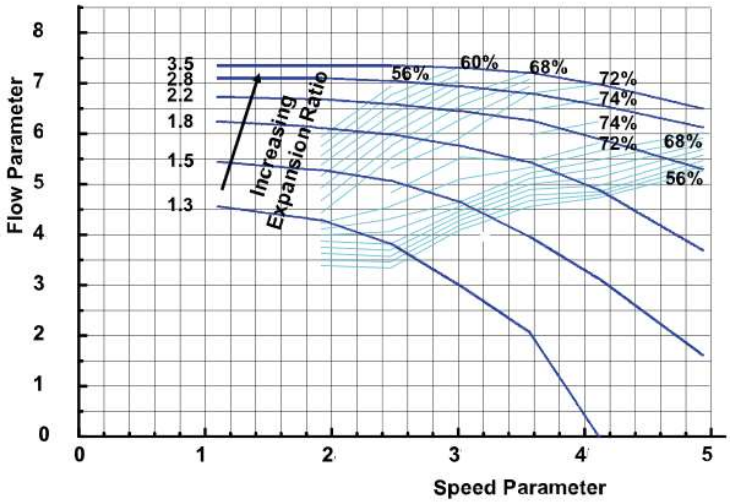

Fig. 20 Turbine map showing the performance with scaled values © Cummins

The turbine performance is also judged by the graph which is plotted generally between the speed parameter and the efficiency. Another way of plotting the map is given below:

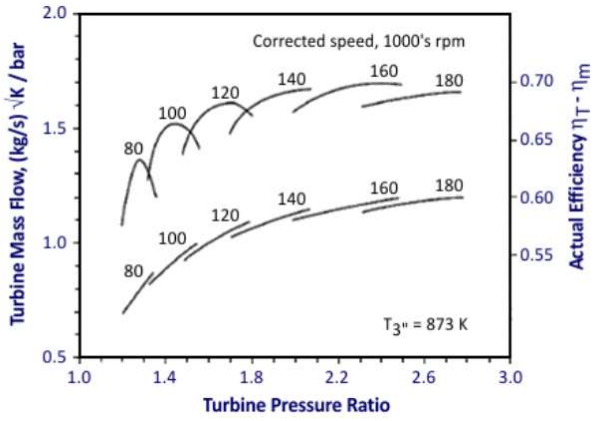

Fig. 21 Turbine efficiency plot (Hannu Jääskeläinen, 2017)

In the above map, a continuous line is drawn at each turbine speed at peak efficiency points which help to denote the best possible operating conditions for the turbine. The lower curve shown in figure 21 indicates air intake capability of turbine and upper curve indicates efficiency of turbine. A/R ratio is number indicating the air intake capability of the volute. Another important parameter to estimate the turbine efficiency is the blade speed ratio which has been discussed in detail in the chapter of Methodology with reference to radial and mixed flow turbine wheel. It indicates that for the radial inlet turbine wheel higher performance is visible at U/C of 0.7.

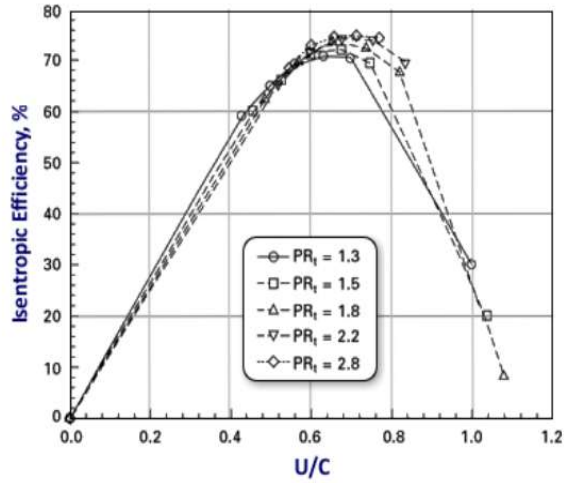

Fig. 22 Graph showing relationship between efficiency and U/C (Hannu Jääskeläinen, 2017)

Turbine Shaft and Wheel

Turbine wheel is friction welded to the shaft and it is always available as a single unit. The turbine shaft and wheel is the major part of the turbocharger unit and it is one of the costliest part. The wheel is made up of Inconel to bear higher operating temperatures and thermal stresses while the shaft is made up of stainless steel and is induction hardened to avoid wear and tear. The various components of the assembly are shown in figure 23 (Books, 2015):

1. Diameter of exducer
2. The contour of the turbine wheel
3. Turbine tip
4. Seal ring
5. Surface for Journal Bearings
6. Step shaft
7. Turbine wheel
8. Shaft
9. Shoulder
10. Rolled threads

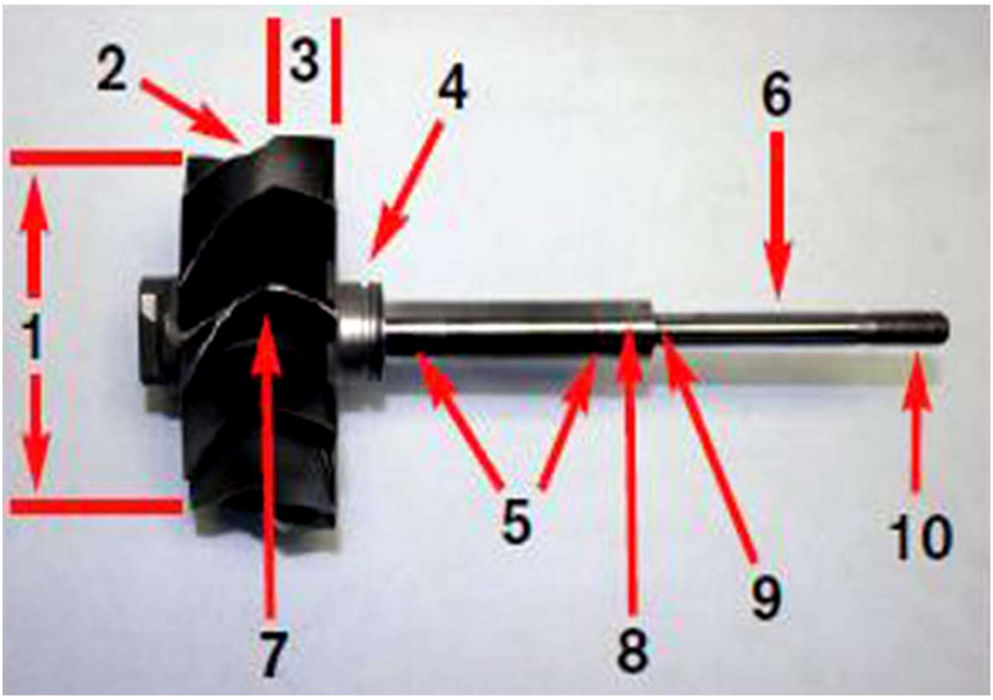

Fig. 23 Shaft and wheel parameters (Books, 2015)

The shaft has rolled threads for mounting the compressor wheel instead of cut threads (Books, 2015). The rolled threads have higher strength in comparison to cut threads as the grain boundaries remain intact but in compressed form. The figure 24 below elaborates it more.

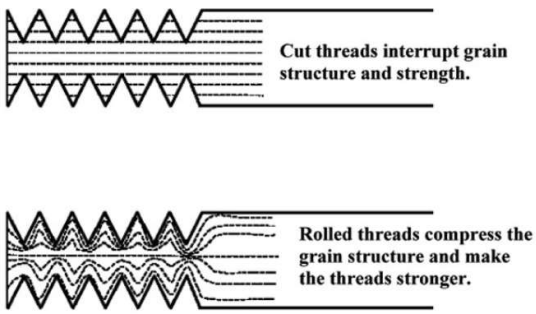

Fig. 24 Rolled threads on the shaft vs Thread cutting (Books, 2015)

Turbine Housing

Turbine volute is the most important part of turbine stage carrying exhaust gases from the exhaust manifold to the outlet. There are various types of turbine housing designs based on turbocharger application like waste-gate or VGT. The most common ones are the single entry and divided entry turbine housings. The divided entry is generally used for the pulsating flow to capture the entry of each pulse. This design is helpful in transporting maximum available energy to the turbine tip for expansion over the wheel in case of low-speed operations. Single entry is generally preferred in operations with high RPM and with a steady flow of exhaust gases (Books, 2015). In those applications, the twin entry results in loss of energy due to obstruction in the flow path. The volute goes on decreasing in cross-section as visible in figure 25 below to impart maximum velocity to exhaust gases.

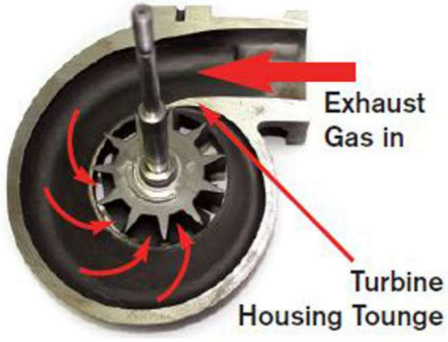

Fig. 25 Exhaust gas flow inside the turbine housing (Books, 2015)

Fig. 26 Tangential entry single and twin entry turbine housing (Books, 2015)

Another important design factor impacting the mass flow rate into the turbine stage is A/R ratio. A/R ratio also impacts the pressure and energy extraction from the exhaust gases so most of the turbine housings in the market are labelled with this number. The term A denotes the tongue area of the volute while R is the distance from the axis of rotation to the centroid of the volute tongue (Books, 2015). Figures 27 and 28 give a description of the parameter.

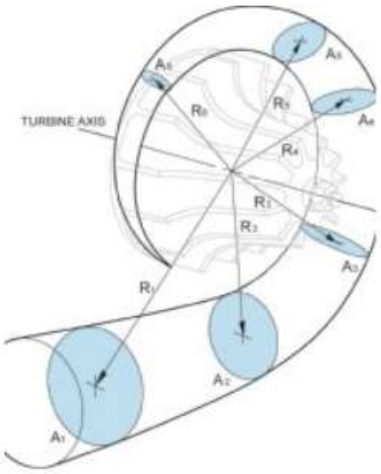

Fig. 27 A/R constant throughout the volute (Enginebasics.com, 2010)

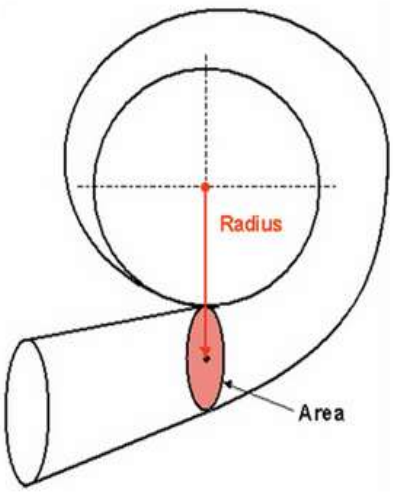

Fig. 28 A/R parameter (Enginebasics.com, 2010)

The turbine housings are manufactured of cast iron to sustain high temperature and pressure during the operation. They must have the ability to sustain the bust containment test to be customer and operation friendly. A/R ratio determines volume

of combustion gases that turbine can intake which affects the flow parameter and the pressure ratio. The effect is described in the figure 29 below:

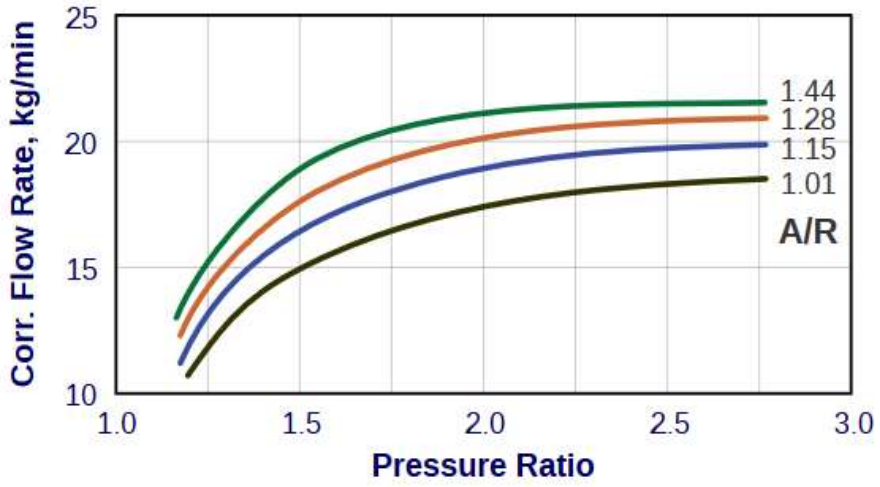

Fig. 29 A/R effect on the mass flow rates (Hannu Jääskeläinen, 2017)

A/R can improve the mass flow rates which help to improve the performance at low speeds of the engine resulting in higher torques. Lower A/R ratio also helps to diminish the smoke levels in the vehicle when operated at speeds less than peak torque. Lower A/R ratio chokes at smaller speeds with less flow rate so larger A/R is preferred to get high energy output.

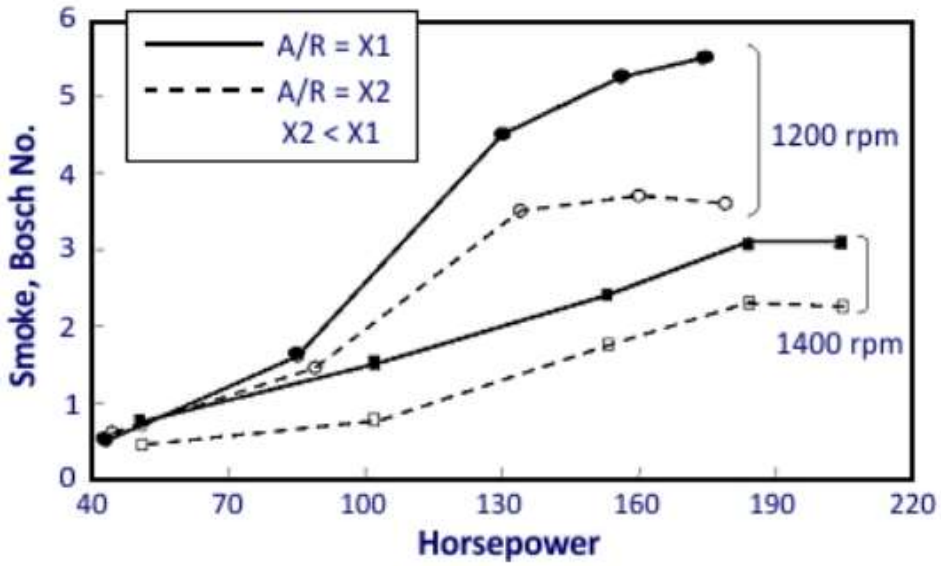

Fig. 30 Effect of low A/R on emissions (Hannu Jääskeläinen, 2017)

Exhaust Brake and After-treatment Devices:

An exhaust brake is a device which is used in vehicles as a supplementary braking system which helps to stop heavy and loaded vehicles down the hill. They are made of hard anodized aluminium and stainless steel. Exhaust brake operates in a manner that they obstruct the path of exhaust gases (En.wikipedia.org, 2016) and the gases are trapped inside the exhaust manifold and engine cylinder. This results in the generation of opposite torque on the engine and thus slows it down to stop the vehicle. The benefits of the exhaust brake are that it supports the normal braking system, causes the engine to decelerate and prevents vehicle accidents down the hill. On the other side, it affects turbocharger operation by reducing operating clearances, causing higher blow by and causing oil leakage. The operation describing the brake is shown in figure 31 below:

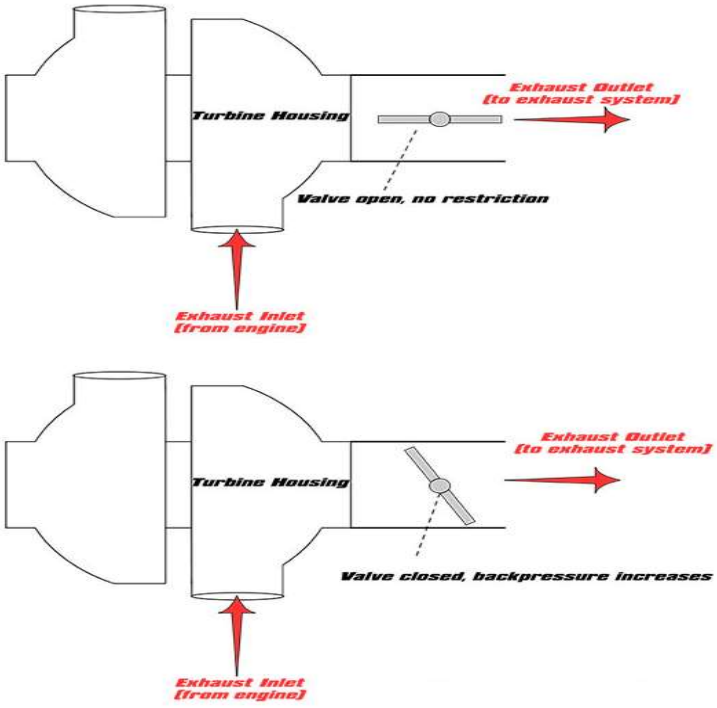

Fig. 31 Exhaust brake operation (Dieselhub.com, 2009)

The after-treatment devices ensure that the vehicular emissions are within the acceptable norms of the environmental regulations. So, the exhaust gases are treated before they are released into the atmosphere (Dieselhub.com, 2009). Exhaust brake has also been employed in vehicles to generate the optimum temperature required for the efficient working of after treatment device. The exhaust brake's effect on the thrust bearing and load evaluation is the main part of the current research work.

Bearing and seals

Seals

Seals are very important for the turbocharger functioning to prevent oil leakage and to reduce blow by. Seals are provided at rotor ends. During low turbocharger speeds and during exhaust braking the pressure behind the impeller wheel drops lower than the bearing housing pressure which results in oil leakage on the compressor side. Moreover, during the exhaust braking, the turbine side pressures may increase more than the bearing stage pressure which results in the transfer of exhaust gases to the bearing compartment resulting in higher blow-by. The oil leakage on the compressor end contaminates the charged flow which is transferred to the inlet manifold and affects compressor stage efficiency. While the blow-by from turbine end adds to blow-by from engine which increases pressure on the filtration unit for disposal of gases to the environment. Seals are of various types depending upon the applications (Worldturbocharger.com, 2018). There are single seals, twin seals with a single groove and two seals with two grooves.

Fig. 32 Twin seal grooves for two seals (Worldturbocharger.com, 2018)

Journal Bearings

To stabilise the turbocharger in the radial position, it's necessary for the turbocharger rotor to be supported by journal bearings. The journal bearing prevents rotor misalignment during operating conditions of the turbocharger and supports the rotor during critical shaft motions which are conical, bending and cylindrical. Journal bearings are of floating type which provides oil lubrication to rotating shaft and oil helps to create the required film for diminishing the power loss in a turbocharger

(Books, 2015). The bearing clearances between the shaft and the bearing housing, combined with oil film are significant to shaft critical motions during rotor operation. So, the balancing of all components is very significant. Both grooved and non-grooved journal bearing with oil holes is preferred in turbocharger operation.

Fig. 33 Journal bearings (Books, 2015)

Ball Bearings

It can also be used as it eliminates the need to oil the bearings and help in decreasing the turbo lag. Ball bearings are usually helpful in racing cars as it provides better transient response than the journal bearings but steady state response is nearly the same. It also tend to eliminate the need for separate thrust bearing which is responsible for maximum frictional loss in rotor operation and help to avoid the oil viscous drag (Books, 2015).

Fig. 34 Ball bearings (Books, 2015)

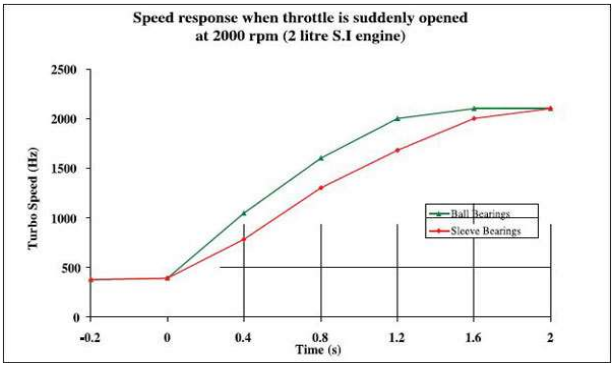

Fig. 35 Ball bearing vs Journal bearing response (Books, 2015)

Thrust Bearing

Thrust bearings are useful for counteracting the axial rotor motion. It contributes nearly 30% under no load condition while this effect goes to scale up as the thrust forces are encountered in turbocharger operation (Lüddecke *et al.*, 2015). The aerodynamic forces impinging on the rotor wheels and creating the difference of pressure at rotor ends creates axial loads which are counteracted by oil lubricated bearing. It is fixed in bearing housing and it is placed between oil slinger and thrust collar (Nguyen-Schäfer, 2012). Oil slinger and the thrust collar shows relative motion with shaft rotation. The micro clearances are present along with oil slinger and thrust collar. Reaction force is applied on either the thrust collar or the oil slinger to keep the rotor axially stable. The oil film squeezed with operating thrust bearing parts generates the reaction force. The force variation is in inverse to the oil film thickness (Nguyen-Schäfer, 2012).

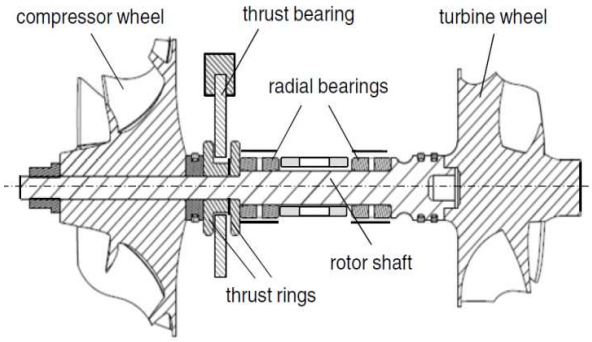

Fig. 36 Turbocharger rotor system (Nguyen-Schäfer, 2012)

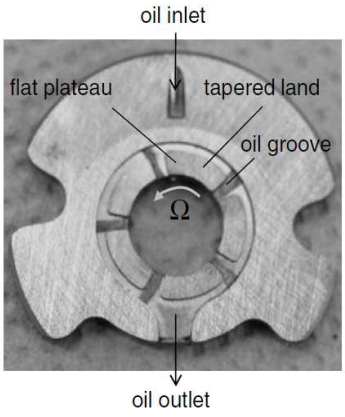

Fig. 37 Thrust Bearing (Nguyen-Schäfer, 2012)

Operating Principle

The thrust bearing is designed to bear the axial thrust loads on both sides. It consists of a tapered surface which merges with the flat surface. The thrust bearing consists of oil holes present on the surface to lubricate the bearing during operation and to generate the hydrodynamic film. The hydrodynamic film is responsible for squeeze film action and the wedging action which together contribute to the reacting thrust force (Nguyen-Schäfer, 2012). The thrust bearing is generally made up of brass or bronze. The hydrodynamic effect during the operation is result of the equation proposed by the Reynolds which is given below:

$$\frac{\partial}{\partial x}\left(h^3\,\frac{\partial p}{\partial x}\right)+\frac{\partial}{\partial z}\left(h^3\,\frac{\partial p}{\partial z}\right)=6\eta U\frac{\partial h}{\partial x}+12\eta\frac{\partial h}{\partial t} \qquad (1)$$

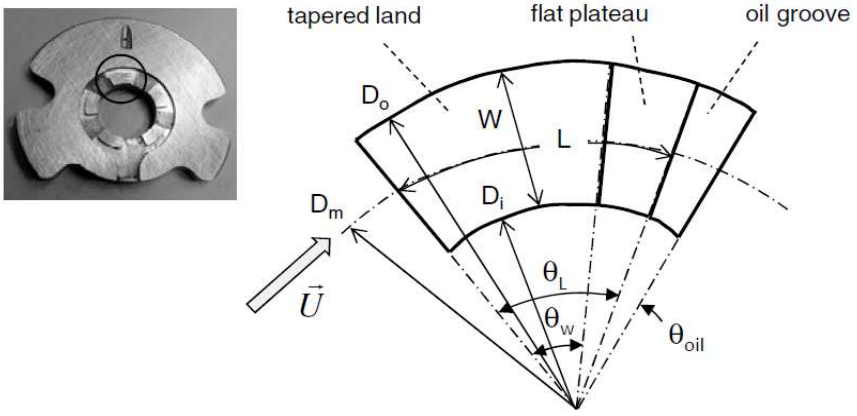

Fig. 38 Thrust bearing design (Nguyen-Schäfer, 2012)

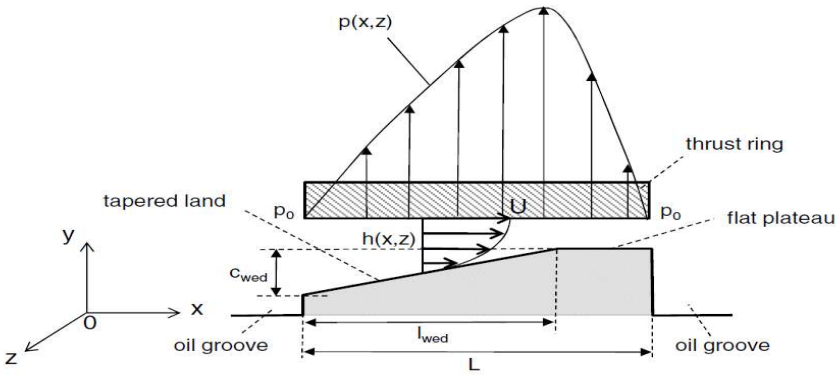

Fig. 39 Hydrodynamic effect on thrust bearing (Nguyen-Schäfer, 2012)

Types of Turbochargers

Fixed Geometry

The fixed geometry turbocharger is one with a fixed turbine and compressor geometries and that there are no means to control the boost pressure. It's generally preferred for specific speed range. Generally, it's preferred for the generators. The fixed geometry turbocharger is inefficient in the transient response and at low engine speeds (Hannu Jääskeläinen, 2014). For the passenger car applications, fixed geometry turbocharger is unsuitable.

Fig. 40 Fixed geometry turbocharger (Cummins Inc., 2019)

Waste-gated Turbocharger

The waste gated turbocharger is an improvement over the fixed geometry in which the wastegate valve is applied on the turbine end to bypass the exhaust gases which can over speed or result in over boosting (Hannu Jääskeläinen, 2014). The use of waste gated turbocharger has made the capability of using smaller A/R ratio turbine housing which can help to provide the optimum boost at low exhaust flows. Moreover, it has improved the boost at lower operating speeds.

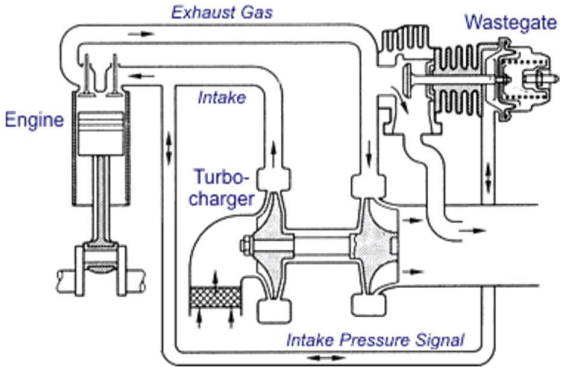

Fig. 41 Waste gated turbocharger (Hannu Jääskeläinen, 2014)

The figure 42 below shows that the waste gated turbocharger performs well when operated at low mass flow rates.

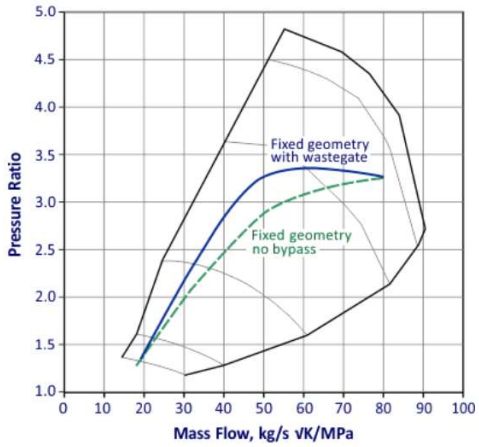

Fig. 42 Comparison between fixed geometry and waste gated turbochargers (Hannu Jääskeläinen, 2014)

The figure 43 below compares the waste-gated turbocharger with fixed geometry which causes over speeding and over boost. The waste gated valves are either pressure controller or electronically controlled.

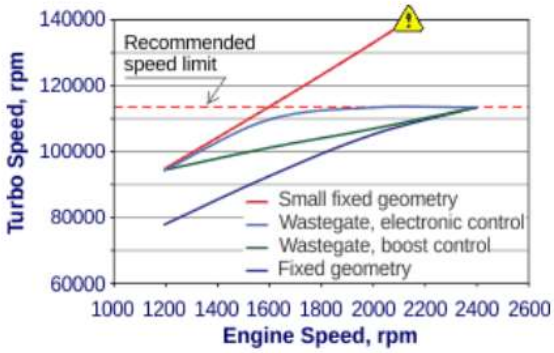

Fig. 43 Performance comparison of various turbochargers (Hannu Jääskeläinen, 2014)

Variable Geometry Turbine (VGT)

The variable geometry turbochargers eliminate most of the limitations of the fixed geometry turbochargers and waste gated turbochargers (Hannu Jääskeläinen, 2014). On the variable geometry turbocharger, the turbine side geometry is varied either by opening and closing of vanes mounted on the shroud plate or keeping the guide vanes fixed while moving the shroud plate. Figure 44 is the one showing the movable vanes

on fixed shroud plate while figure 45 shows the movable shroud plate VGT turbo with fixed vanes.

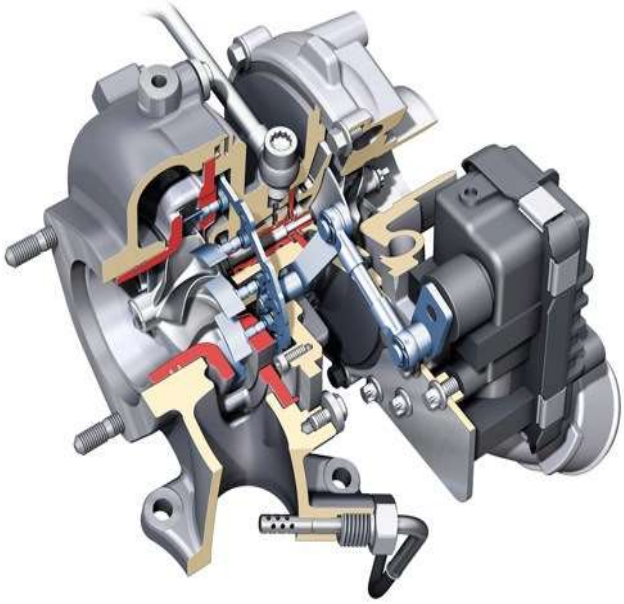

Fig. 44 Movable vane turbocharger (AUDI AG, 2019)

Fig. 45 Movable shroud plate VGT turbo (Cummins Inc., 2019)

The variable geometry turbochargers are extremely costly so they are rarely employed. The specialities of VGT turbocharger are (Hannu Jääskeläinen, 2014):

1. Higher torque at lower engine speeds
2. Allows flexibility over the pressure ratios and mass flow rates
3. Helpful in engine braking
4. Reduces the turbo-lag

5. Transient response in better
6. A wider range of speed availability to provide a boost

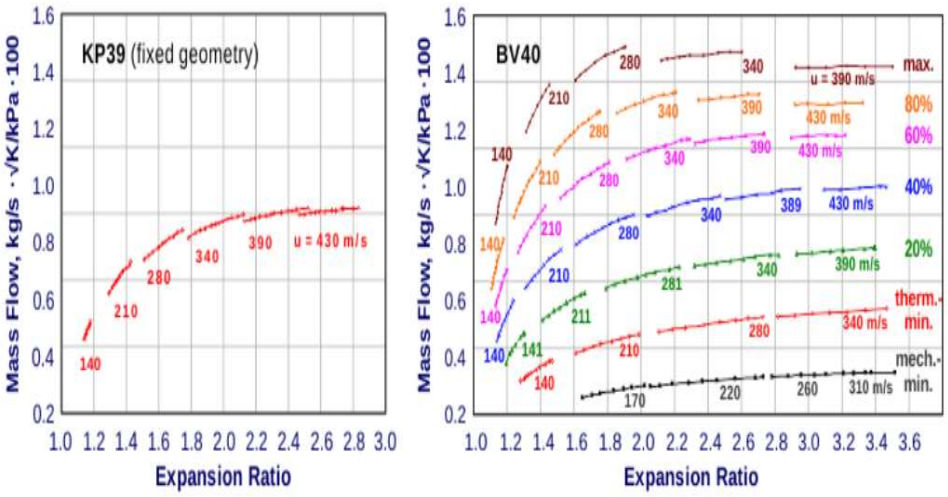

Fig. 46 Fixed and VGT comparison (Hannu Jääskeläinen, 2017)

Figure 46 shows that at one-speed multiple expansion ratios and flow rates can be achieved. So, it adds complexity in analysing the VGT as turbocharger due to higher degrees of freedom involved. The efficiency of the VGT's is depending upon the opening and closing of vanes. The efficiency is maximum at vane opening of 60% which tends to decrease when the opening gets to reduce.

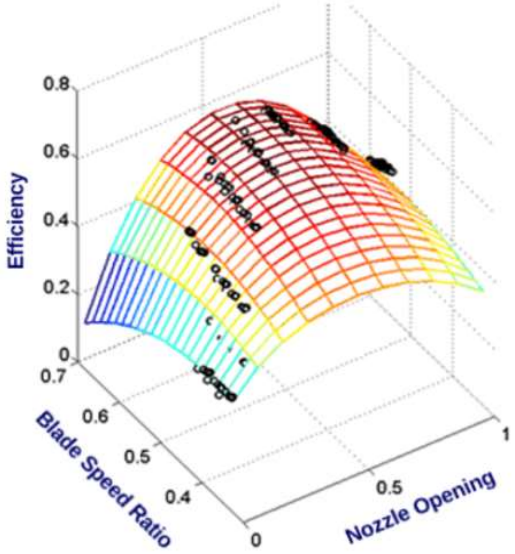

Fig. 47 VGT efficiency plot (Hannu Jääskeläinen, 2017)

Gaussian Process Regression (GPR)

Gaussian process regression (Ebden, 2015) is the machine learning approaches of performing regression and training the data and then predicting the results for any noisy data sets. The models are based on the Gaussian probability and it makes use of kernels to specify the covariance domain. Based on the kernels the Gaussian regression models are classified as (The MathWorks, 2019):

1. Squared Exponential Kernel
2. Exponential Kernel
3. Rational Quadratic
4. Matern 3/2
5. Matern 5/2

The advantages of the GPR are:

1. The interpolation of the observations is possible with this approach
2. Most realistic problems follow Gaussian distribution, so it can easily fit the random and noisy data set
3. As the approach depends on various kernels to vary co-variance domain so it is flexible to fit various types of data sets

The disadvantages are:

1. It loses importance when the dimensional space increases in high numbers
2. It overestimates when the data set is small

CHAPTER 4: METHODOLOGY

Chapter 4 is about the methodology undertaken to achieve the objectives of the project. It also talks about the specific reasons for undertaking a specific approach. The diagram below shows the steps taken to achieve project targets.

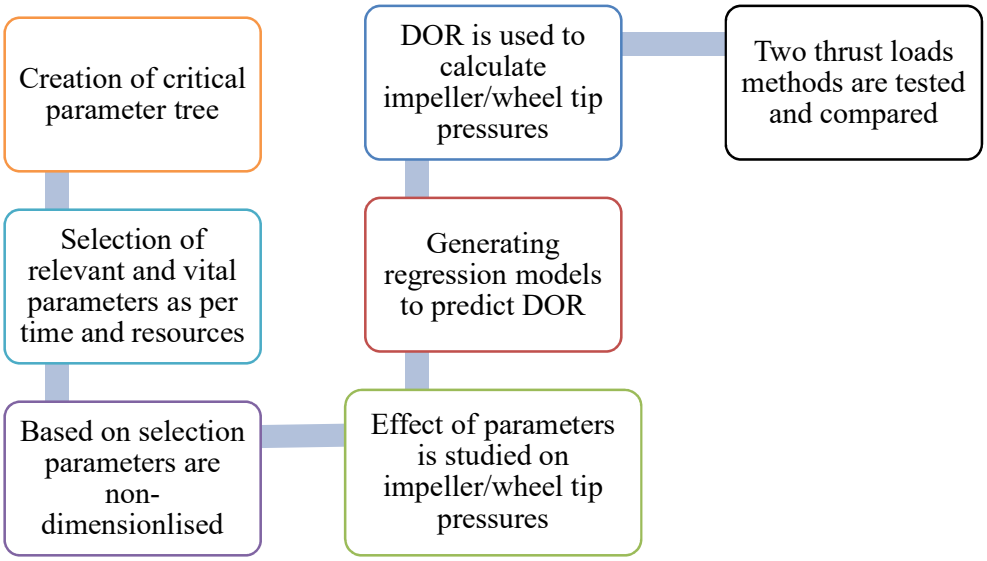

Critical Parameter Tree

The major aim of the building the new approach is to eliminate the hypothesis of a DOR which was taken 0.5 both on compressor and turbine stage. This assumption has been taken because the degree of reaction depends upon many factors. To make the prediction easier for thrust loads, DOR has been assumed the same both compressor and turbine stage. The research thesis aims to bridge this gap in the literature and has come up with a method to predict the degree of reaction considering relevant factors. Degree of reaction is given by the formula (Nguyen-Schäfer, 2012):

- For compressor side (Nguyen-Schäfer, 2012)

$$rc = \frac{\Delta hc}{\Delta hst} = \frac{1-(\frac{p2*}{p1})^{\frac{\gamma-1}{\gamma}}}{1-(\frac{p2.}{p1})^{\frac{\gamma-1}{\gamma}}} \quad (2)$$

- For turbine side (Nguyen-Schäfer, 2012)

$$\mathrm{rt} = \frac{\Delta ht}{\Delta hst} = \frac{1-(\frac{p4}{p3*})^{\frac{\gamma-1}{\gamma}}}{1-(\frac{p4}{p3})^{\frac{\gamma-1}{\gamma}}} \quad (3)$$

So, to get the correct value of the degree of reaction its necessary to know impeller tip pressure p2* and turbine tip pressure p3*. These values of pressures are not available in the pressure tapped experimental approach of determining thrust loads and it's very difficult to determine these pressures as the wheel is rotating are very high speeds and it's difficult to mount the pressure sensors. Moreover, on the turbine side, the temperatures are extremely critical for measurement and data collected may not be reliable. So there came a need to develop a critical parameter tree to determine the parameters affecting the degree of reaction.

Compressor Stage CP Tree and Parameter Analysis:

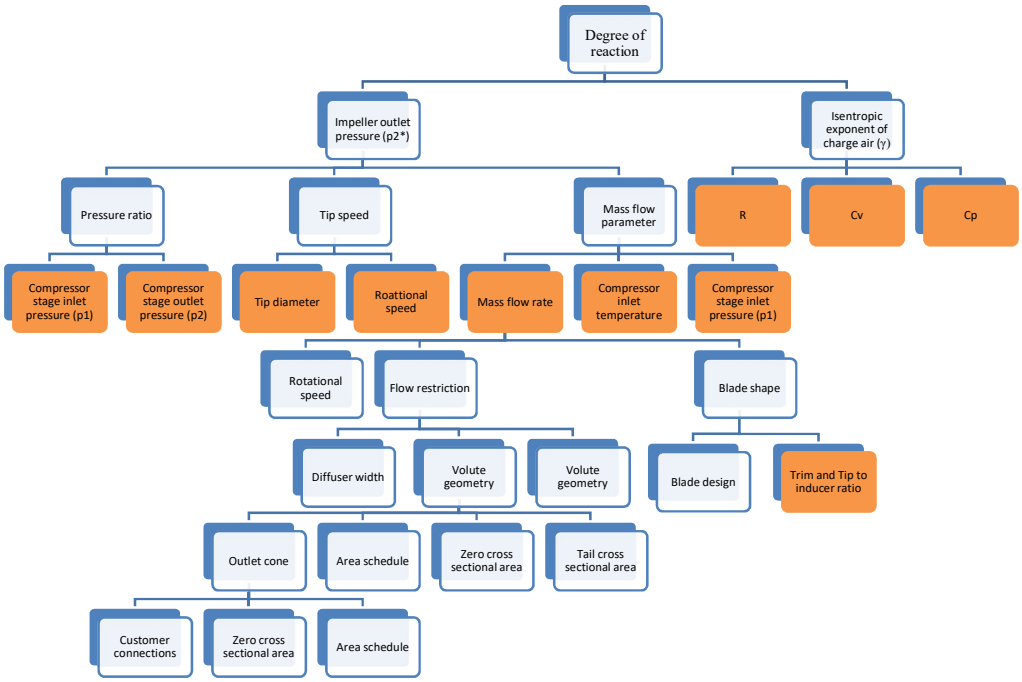

Figure 48 Compressor side parameters to predict the degree of reaction © Cummins

Using this critical parameter tree, the non-dimensional parameters (N.WATSON, 1982) suitable for the degree of reaction determination are obtained which are listed below:

1. True Mass Flow Parameter (TMFP)

   Compressor map uses mass flow parameter which is given below but it is not dimensionless (Hannu Jääskeläinen, 2017):

$$\text{Mass flow parameter} = \frac{\dot{m}}{P} \times \sqrt{T} \tag{4}$$

   So, to make it dimensionless it is divided by the area of inducer and multiplied by the square root of gas constant (www.grc.nasa, 2018)

$$\text{TMFP} = \left(\frac{\dot{m} \times \sqrt{R} \times \sqrt{T}}{P \times A}\right) \tag{5}$$

   The true mass flow parameter takes care of compressor inlet temperature, mass flow rate, compressor stage inlet pressure, area of the inducer and gas constant.

$$A = \text{Area of inducer} = \frac{\pi}{4} \times (\text{Inducer Diameter})^2 \tag{6}$$

2. Non-Dimensional Speed Parameter (NDSP)

   The speed parameter (Hannu Jääskeläinen, 2017) used for the compressor map is also not dimensionless which also complicates the process to generalise over complete turbocharger frames. It is given by:

$$\text{Speed parameter} = \frac{N}{\sqrt{T}} \tag{7}$$

   So, to make it non-dimensionless it has been divided by the speed of sound entering turbocharger. So, it takes care of parameters like a gas constant, isentropic exponent of charged air which takes care of gas properties, impeller tip diameter and rotational speed. The new non-dimensional speed parameter is given below (Dinescu and Tazerout, 2010):

$$\text{NDSP} = \frac{\pi \times D \times N}{60 \times \sqrt{\gamma \times R \times T}} \tag{8}$$

3. Pressure Ratio (PR)

   The pressure ratio (Hannu Jääskeläinen, 2017) is crucial in terms of determining the impeller outlet pressure so it is taken as an important parameter. It is the ratio of compressor stage outlet pressure and compressor stage inlet pressure. The volute

geometry of compressor significantly affects the compressor outlet pressure (Abdelmadjid, Mohamed and Boussad, 2013).

$$PR = \frac{P2}{P1} \tag{9}$$

To study the effects of the above three non-dimensionless parameters on the impeller outlet pressure (p2*) the CFD compressor stage data was obtained and the trends were plotted which are visible in figures 49 and 50 below:

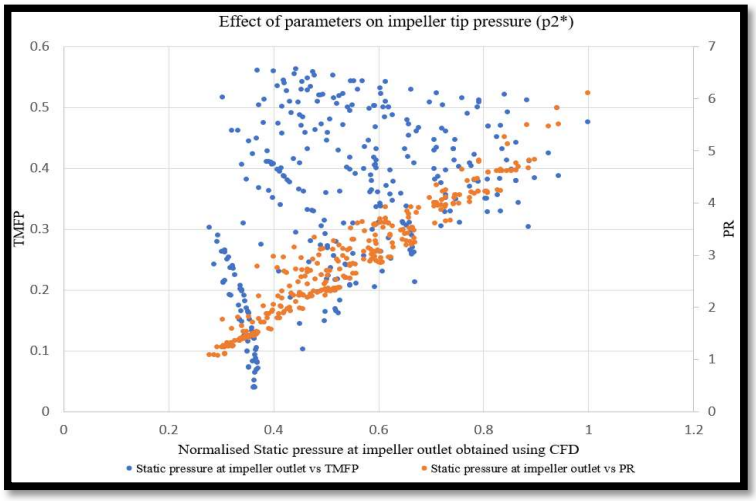

Fig. 49 Effect of parameter TMFP and PR on impeller outlet pressure © Cummins

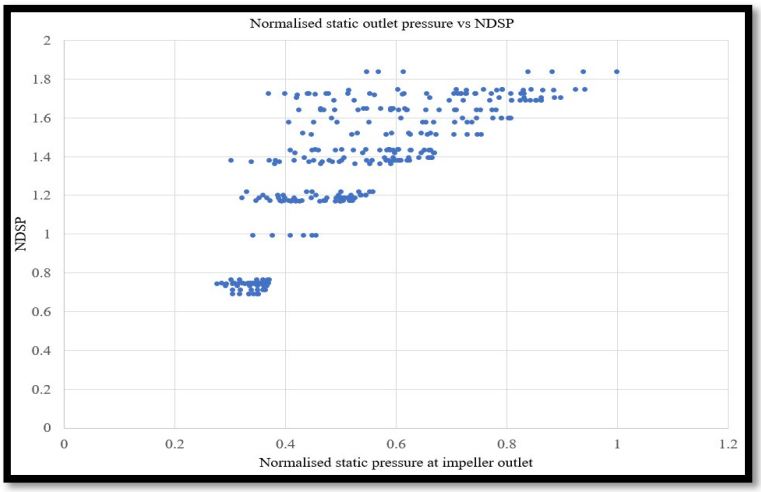

Fig. 50 Variation of impeller outlet pressure with NDSP © Cummins

If the impeller outlet pressure changes then there is a change in the value of the degree of reaction. The CFD data collected from Cummins turbo technologies for compressor stage has compressor stage data from lowest to higher mass flow range. The flow restriction parameters have been left out of the study as it requires extensive data, time

and resources. Also, most of the volute selections are customer dependent and on the mass flow rate required by the customer. It has been found that trim does impact the pressures. So, both the factors trim and tip/inducer ratio has been put to study their combined effect based on the research (Miltykh and Sotnyk, 2016). The trim is given by the equation below:

$$\text{Trim} = \frac{\text{Inducer diameter}}{\text{Exducer diameter}} \tag{10}$$

Using Minitab, the pressure contours were plotted when the tip to inducer ratio is same but trim is different which are shown below:

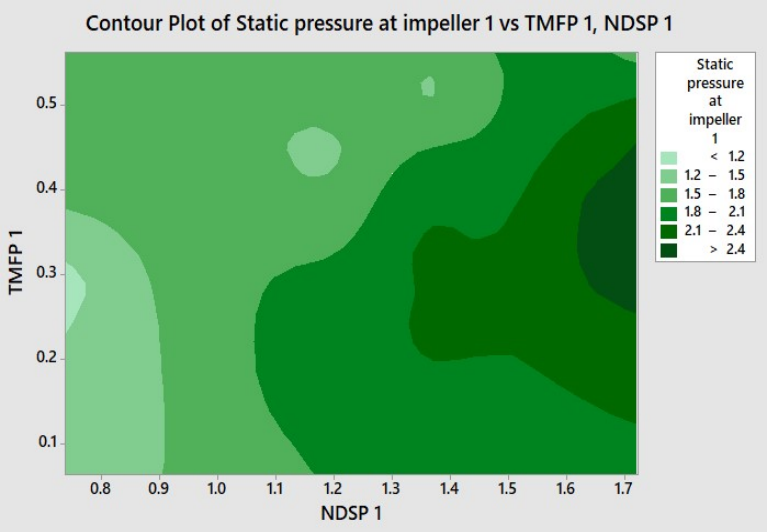

Fig. 51 Pressure contour plot with higher trim © Cummins

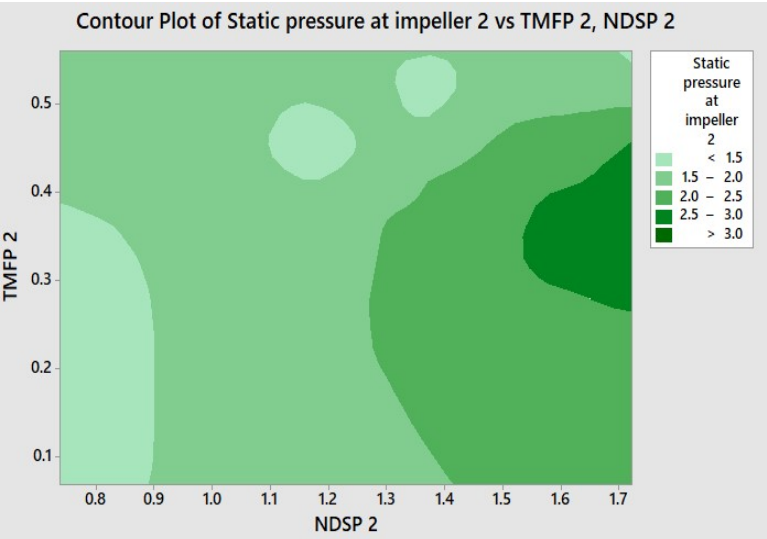

Fig. 52 Pressure plot with lower trim © Cummins

To visualise the combined effect of trim and tip width, another parameter tip/ inducer ratio has been taken into consideration which poses a considerable impact on pressure of impeller outlet. The parameter is given by the formula:

$$\frac{\text{Tip}}{\text{Inducer area}} = \frac{\text{Exducer area}}{\text{Inducer area}} \tag{11}$$

The effect of the above parameter is shown in figures 53 and 54 below:

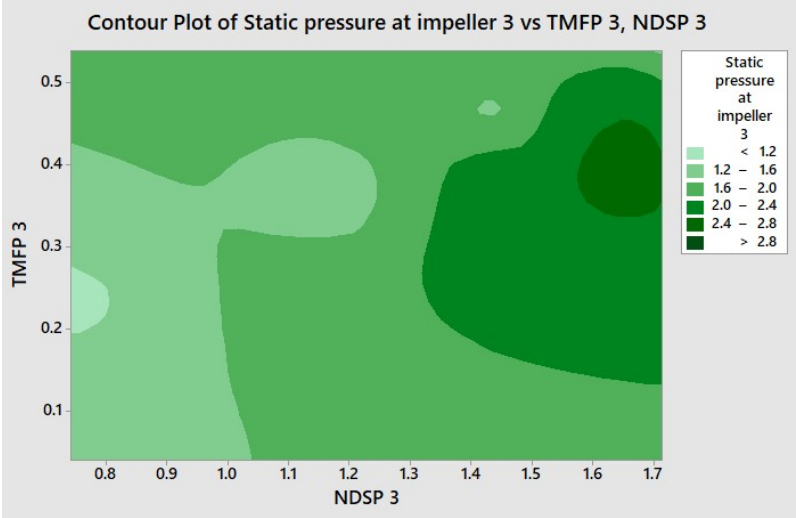

Fig. 53 Impeller outlet pressure variation with lower trim and tip/inducer ratio © Cummins

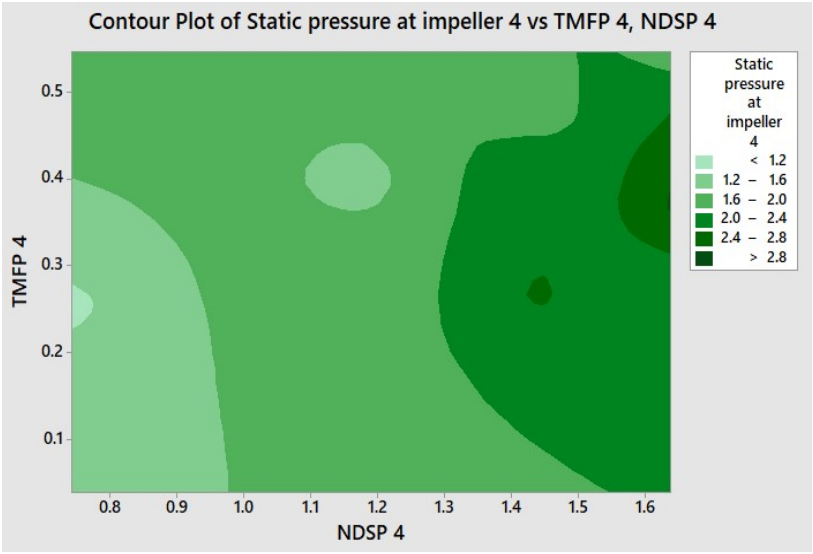

Fig. 54 Impeller outlet pressure variation based on higher trim and higher tip/inducer ratio © Cummins

The five parameters have been finalised for predicting the value of the degree of reaction on the compressor end which are TMFP, NDSP, PR, Trim and Tip to inducer ratio.

Turbine Stage CP Tree and Parameter Analysis:

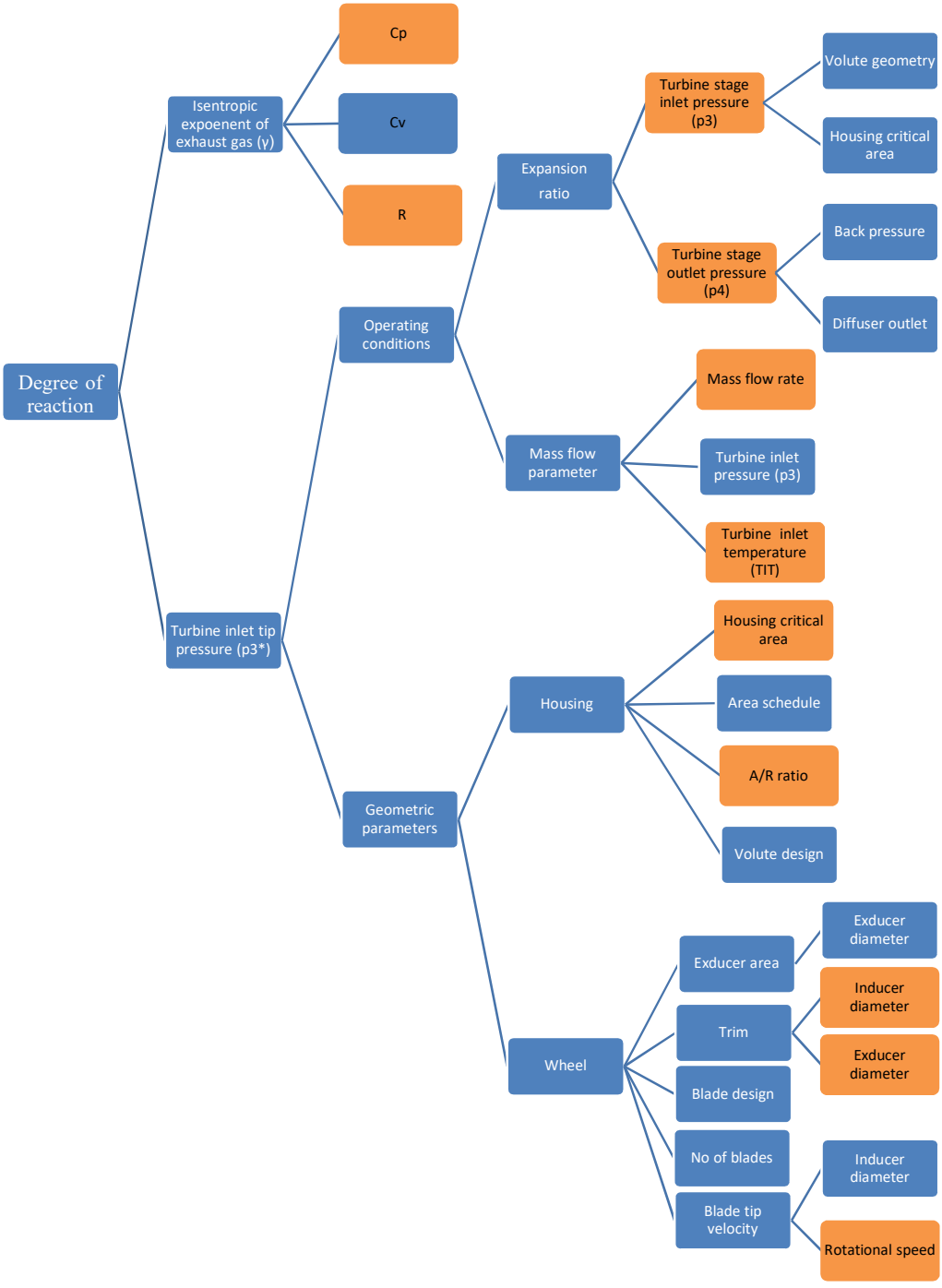

Fig. 55 Turbine side parameters to predict DOR © Cummins

On turbine wheel side, critical parameter tree is highly complicated and involves a good number of parameters affecting the DOR. Moreover, the turbine geometry is highly variable having radial and mixed flow turbine wheels. Besides different flows, the wheels are scalloped and un-scalloped. The scalloped wheels are generally preferred over un-scalloped wheels. The differences don't just stop at the turbine geometry but it further goes down the way the turbine is operated, which is whether it is fixed, waste-gated or variable geometry turbine. Considering all these complexities it was not possible to come up with non-dimensional numbers based on turbine map. So, going into the basics of fluid machinery, Buckingham Pi theorem has been adopted (A., ÇENGEL and CIMBALA, 2001). Using the theorem, the non-dimensional parameters has been formulated which can predict the DOR. The procedure is given below in steps:

- Initially, the parameters are selected based on the turbine map analysis and CFD studies which are highlighted in green in figure 55
- Combining with a degree of reaction on turbine total number of parameters amount to 12, but the degree of reaction is a ratio so the number of critical parameters remains 11
- The next step is to choose the number of repeating variables which depend upon the fundamental variables which are M, L, T and θ. Generally, the numbers of repeating variables are 3 which are usually M, L, T but they can be 4 if there are temperature terms in the parameters. In this case, the number of repeating variables is 4 in number. The reason for choosing four repeating variables is listed below:
  1. Turbine stage inlet pressure = p3 = $[ML^{-1}T^{-2}]$
  2. Turbine stage outlet pressure = p4 = $[ML^{-1}T^{-2}]$
  3. Specific heat capacity at constant pressure = C_p = $[L^2T^{-2}\theta^{-1}]$
  4. Gas constant = R = $[L^2T^{-2}\theta^{-1}]$
  5. Mass flow rate = $\dot{m} = [MT^{-1}]$
  6. Rotational speed = N = $[T^{-1}]$
  7. Turbine inlet temperature = TIT = $[\theta]$
  8. Inducer diameter = [L]
  9. Exducer diameter = [L]
  10. Housing critical area = A_{cr} = $[L^2]$
  11. A/R ratio = [L]

The parameters when written in fundamental variables contain M, L, T and θ so the repeating variables are four in number.

- The repeating variables chosen for predicting the seven dimensionless parameters are also given below that have been chosen as per fluid machinery principles:
    1. Rotational velocity = $[T^{-1}]$
    2. Inducer diameter = [L]
    3. Turbine inlet temperature = [θ]
    4. Mass flow rate = $[MT^{-1}]$
- Therefore, the number of π terms is the total number of variable parameters minus the number of repeating variables. So, the π terms are seven in number which are listed below (A., ÇENGEL and CIMBALA, 2001).

$$\pi_1 = \frac{\text{p3}\times\text{Inducer diameter}}{\text{N}\times\dot{m}} \tag{12}$$

$$\pi_2 = \frac{\text{p4}\times\text{Inducer diameter}}{\text{N}\times\dot{m}} \tag{13}$$

$$\text{Trim of the turbine wheel} = \pi_3 = \frac{\text{Exducer diameter}}{\text{Inducer diameter}} \tag{14}$$

$$\pi_4 = \frac{\text{Critical area of housing}}{(\text{Inducer area})^2} \tag{15}$$

$$\pi_5 = \frac{\left(\frac{\text{A}}{\text{R}}\right)\text{ratio}}{\text{Inducer diameter}} \tag{16}$$

$$\pi_6 = \frac{\text{TIT}\times\text{Cp}}{\text{N}^2\times\text{Inducer diameter}^2} \tag{17}$$

$$\pi_7 = \frac{\text{TIT}\times\text{R}}{\text{N}^2\times\text{Inducer diameter}^2} \tag{18}$$

- Combining π terms π_1 and π_2

$$\text{Expansion ratio} = \pi_{12} = \frac{\text{p3}}{\text{p4}} \tag{19}$$

- Combining π terms π_6 and π_7

$$\pi_{67} = \frac{\pi_6}{\pi_7} = \frac{\text{C}_\text{p}}{\text{R}} \tag{20}$$

The term π_{67} has been neglected as it is a constant term while π_5 has been left out of consideration as a turbine housing critical area is already there in π_4. The other parameters that can be taken for determining the degree of reaction on the turbine side are blade speed ratio $\frac{\text{U}}{\text{C}}$ and true mass slow parameter (TMFP). The effect of various parameters on turbine inlet tip pressure has been put to study. To study the parameters the CFD analysis data for the turbine side has been collected for the range of

turbocharger frames. It consists of frames from low, medium to heavy duty. This covered the large operating range in which the turbochargers operate in the industry. But the data availability for the turbine stage was lesser than the compressor stage due to some limitations within the company. The graphs below show the effect of parameters on the wheel inlet pressure.

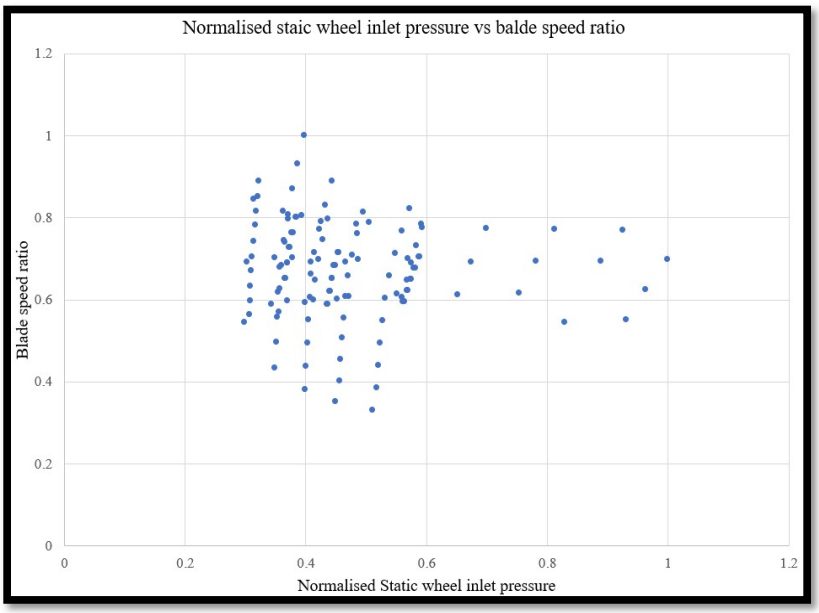

Fig. 56 Effect of blade speed ratio on turbine wheel inlet pressure © Cummins

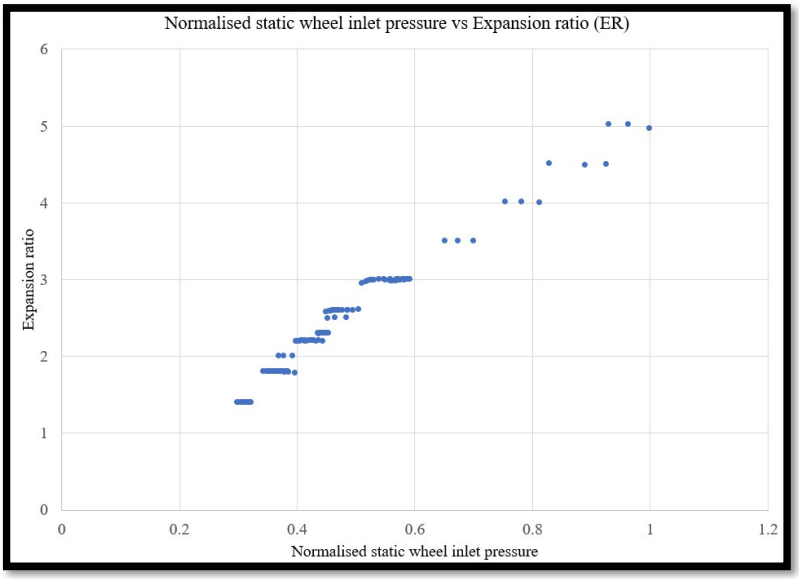

Fig. 57 Effect of expansion ratio on static wheel inlet pressure © Cummins

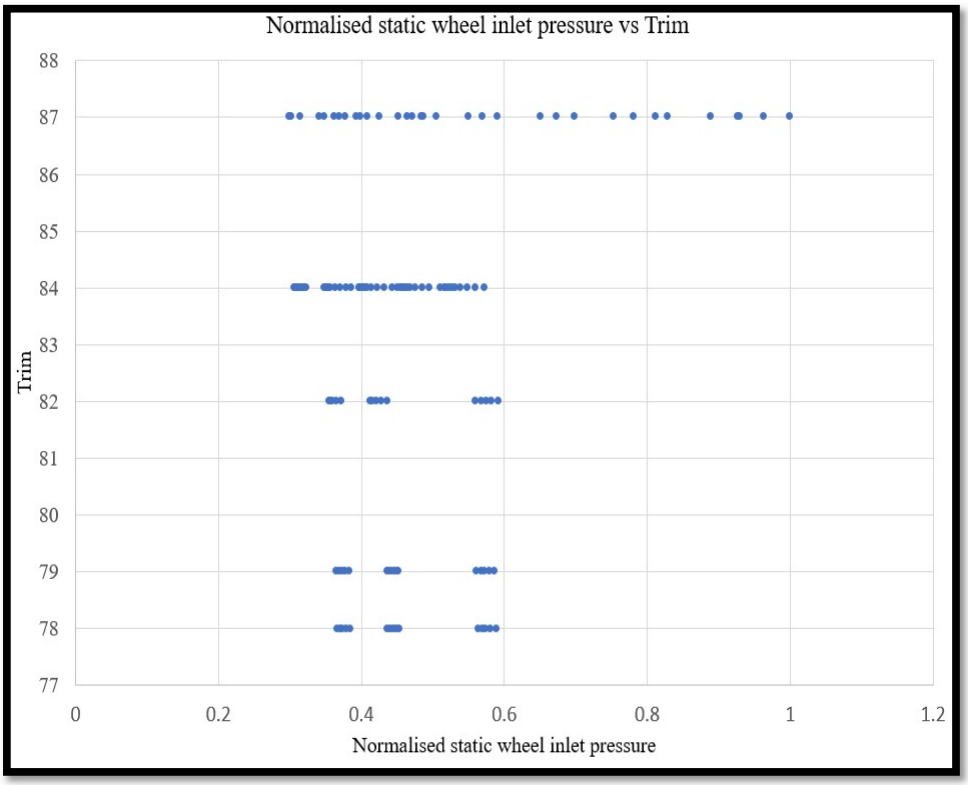

Fig. 58 Effect of trim on static wheel inlet pressure © Cummins

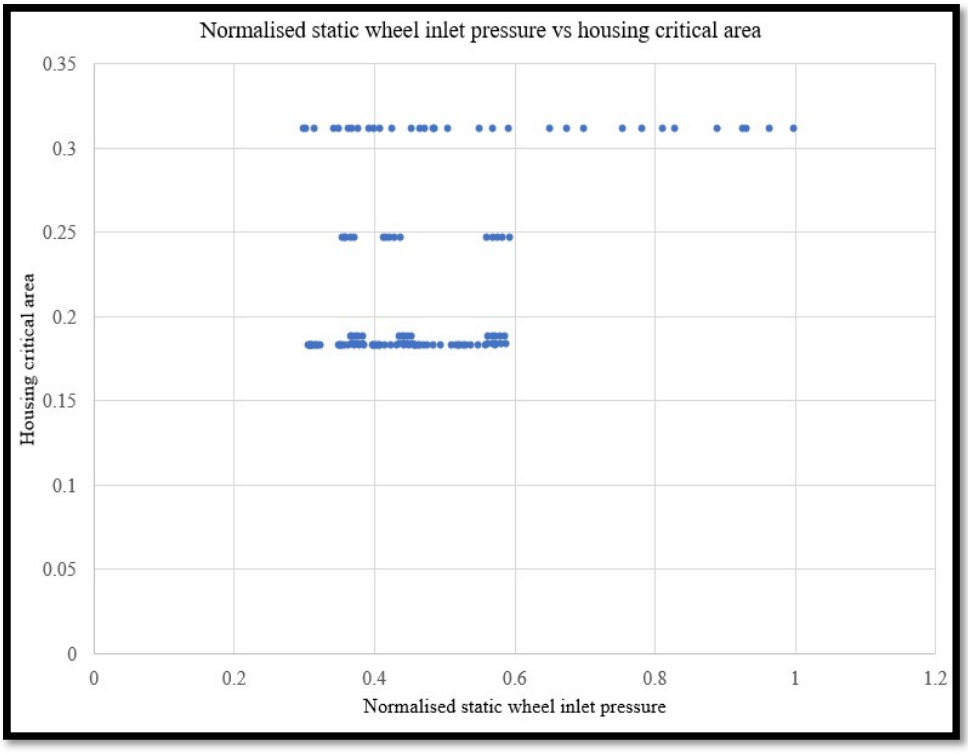

Fig. 59 Effect of housing critical area on static wheel inlet pressure © Cummins

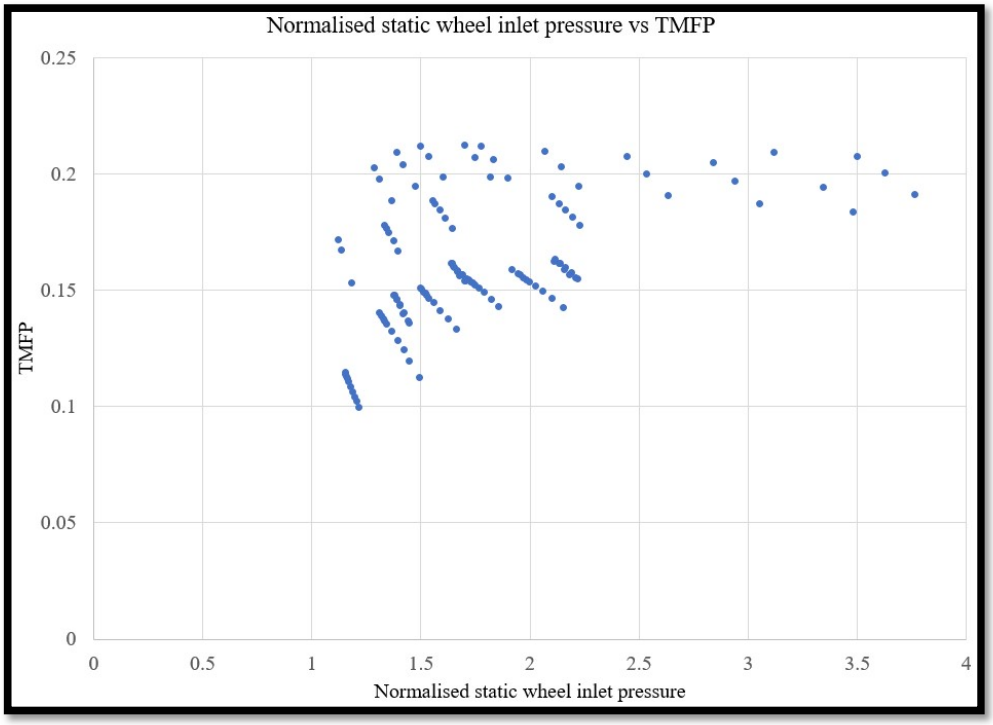

Fig. 60 Effect of TMFP on static wheel inlet pressure © Cummins

Importance of Blade Speed Ratio as a Parameter

The blade speed ratio is the ratio of velocity imparted to blade resulting in rotor rotation with the spouting velocity in the turbine stage. The spouting velocity is the velocity attained by the gas because of isentropic expansion from the inlet conditions to the turbine exit. It is a method of comparing the various turbocharger turbine stages as it is a non-dimensional parameter. The formula is given below (Lüddecke, Filsinger and Ehrhard, 2012):

$$\frac{\text{Blade Tip velocity}}{\text{Isentropic nozzle velocity}} = \frac{U}{C} = \frac{\pi \times D \times N}{60 \times \sqrt{2 \times C_P \times T \times \left(1 - \left(\frac{1}{ER}\right)^{\frac{\gamma-1}{\gamma}}\right)}} \qquad (21)$$

The radial inflow turbines have U/C ratio as 0.7 for maximum efficiency but when it is compared with mixed flow turbines it's lower to 0.59. This implies that the mixed flow turbines can perform better even at decreased engine speeds. It improves transient response of turbocharger. Under mixed flow conditions, the combined effect of mass flow and efficiency generates higher power (Lüddecke, Filsinger and Ehrhard, 2012). So, when U/C is maximum then the brake specific fuel consumption would be lower.

The figures 61, 62 and 63 show the MFT wheel geometry and their effect on the non-dimensional parameter.

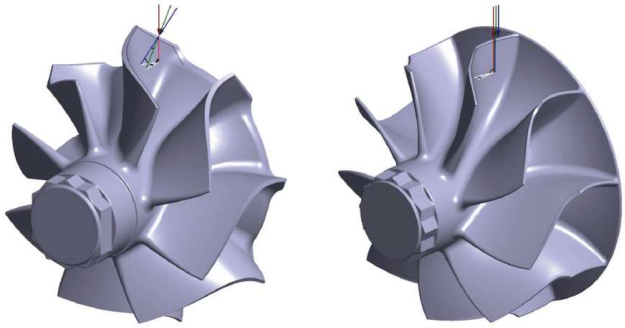

Fig. 61 MFT (Left) and RFT (Right) (Lüddecke, Filsinger and Ehrhard, 2012)

In a MFTwheel, the combustion gases incident on turbine blade tip has both axial and radial components while this effect is missing in the radial wheel.

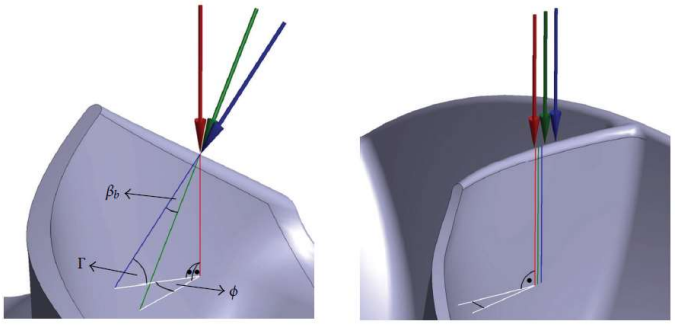

Fig. 62 The velocity triangles on the incident flow (Lüddecke, Filsinger and Ehrhard, 2012)

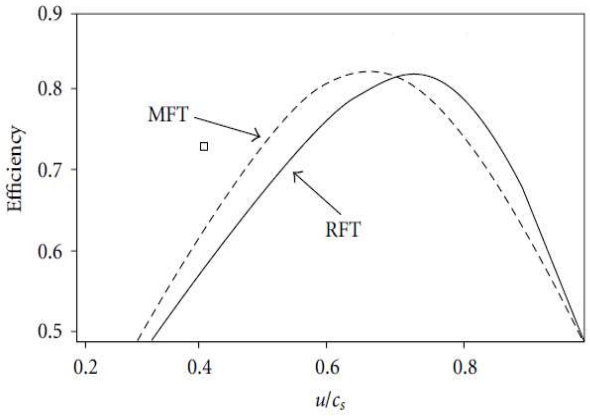

Fig. 63 The effect of mixed (MFT) and radial flow turbine wheels (RFT) on U/C when the pressure ratio is 1.5 to 3 (Lüddecke, Filsinger and Ehrhard, 2012)

Regression Analysis

The CFD data collected for studying the parameters would be put to regression study in which the aim is to get a trained equation or model that can predict the degree of reaction values closely. First, the correlation was established with CFD data and then it was put to test with test cell data. The process followed to achieve the target is detailed below.

Minitab

Initially, the idea was to generate the regression equation to predict the degree of reaction for both compressor and turbine end. So first the compressor end data was taken for taken and put to test. The results for the higher order regression analysis were better than the lower order regression fit curve. Generalised linear regression models have been used to do regression.

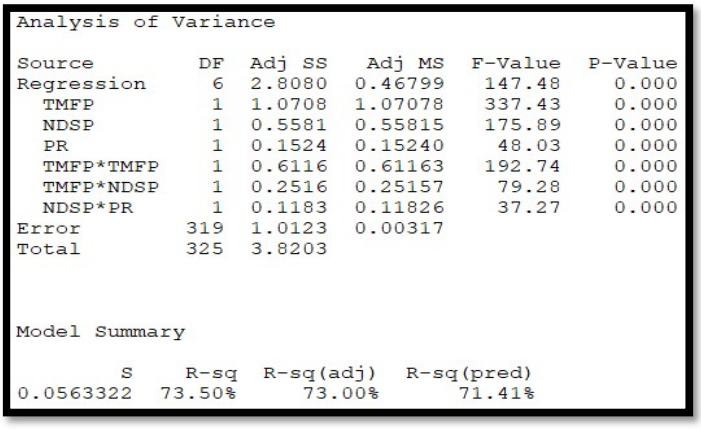

Analysis of Variance

Source	DF	Adj SS	Adj MS	F-Value	P-Value
Regression	6	2.8080	0.46799	147.48	0.000
TMFP	1	1.0708	1.07078	337.43	0.000
NDSP	1	0.5581	0.55815	175.89	0.000
PR	1	0.1524	0.15240	48.03	0.000
TMFP*TMFP	1	0.6116	0.61163	192.74	0.000
TMFP*NDSP	1	0.2516	0.25157	79.28	0.000
NDSP*PR	1	0.1183	0.11826	37.27	0.000
Error	319	1.0123	0.00317		
Total	325	3.8203			

Model Summary

S	R-sq	R-sq(adj)	R-sq(pred)
0.0563322	73.50%	73.00%	71.41%

Fig. 64 Second order regression analysis © Cummins

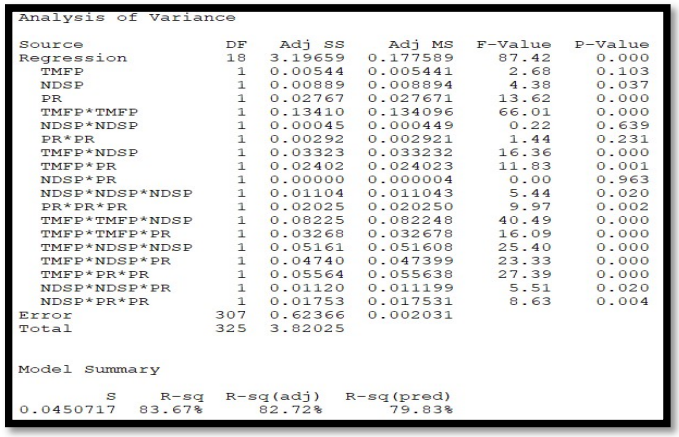

Analysis of Variance

Source	DF	Adj SS	Adj MS	F-Value	P-Value
Regression	18	3.19659	0.177589	87.42	0.000
TMFP	1	0.00544	0.005441	2.68	0.103
NDSP	1	0.00889	0.008894	4.38	0.037
PR	1	0.02767	0.027671	13.62	0.000
TMFP*TMFP	1	0.13410	0.134096	66.01	0.000
NDSP*NDSP	1	0.00045	0.000449	0.22	0.639
PR*PR	1	0.00292	0.002921	1.44	0.231
TMFP*NDSP	1	0.03323	0.033232	16.36	0.000
TMFP*PR	1	0.02402	0.024023	11.83	0.001
NDSP*PR	1	0.00000	0.000004	0.00	0.963
NDSP*NDSP*NDSP	1	0.01104	0.011043	5.44	0.020
PR*PR*PR	1	0.02025	0.020250	9.97	0.002
TMFP*TMFP*NDSP	1	0.08225	0.082248	40.49	0.000
TMFP*TMFP*PR	1	0.03268	0.032678	16.09	0.000
TMFP*NDSP*NDSP	1	0.05161	0.051608	25.40	0.000
TMFP*NDSP*PR	1	0.04740	0.047399	23.33	0.000
TMFP*PR*PR	1	0.05564	0.055638	27.39	0.000
NDSP*NDSP*PR	1	0.01120	0.011199	5.51	0.020
NDSP*PR*PR	1	0.01753	0.017531	8.63	0.004
Error	307	0.62366	0.002031		
Total	325	3.82025			

Model Summary

S	R-sq	R-sq(adj)	R-sq(pred)
0.0450717	83.67%	82.72%	79.83%

Fig. 65 Third order regression analysis © Cummins

So, the R-square for the third order generalised linear regression model is 82.72% while for second order it's 73%. So as per the R-square value, the linear equation with third order must fit better. Then it was tested with the test data for a turbocharger and the results are given in figure 66.

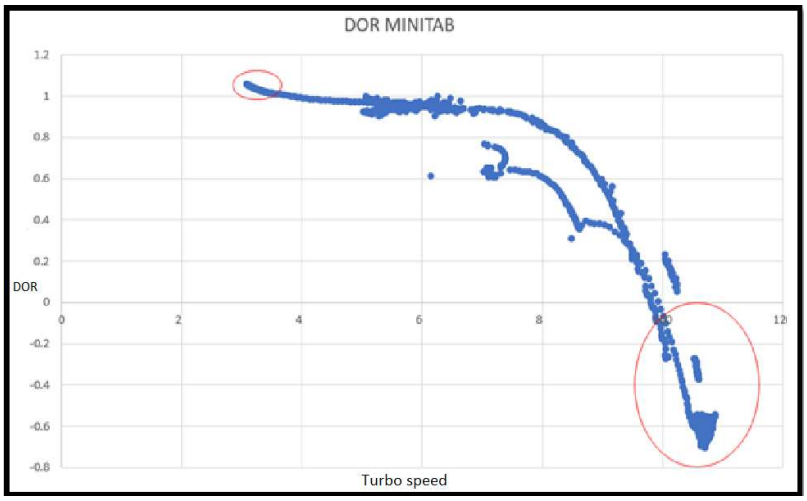

Fig. 66 Value of DOR predicted by linear regression models © Cummins

The degree of reaction (DOR) values obtained using Minitab are reported to be under predicted and over predicted in the data which is the major reason for rejecting the general linear regression models. The DOR value cannot go beyond 1 and below 0, it must be within 0 and 1. So MATLAB machine learning regression tool called Regression learner app has been applied to train the data and predict the degree of reaction. Initially, it has been tested for the compressor end. The results are summarised in figure 67.

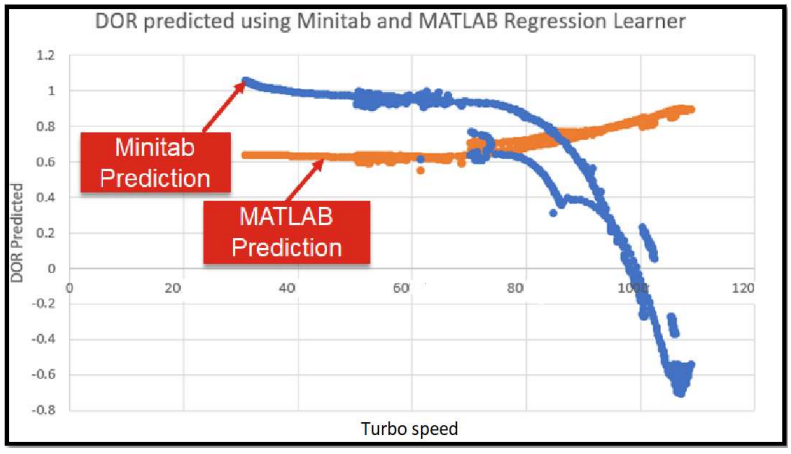

Fig. 67 Comparison of Minitab method and machine learning approach © Cummins

The results in the figure 67 show that the degree of reaction predicted by the machine learning tool is better than the general linear regression model. The value which is obtained is within 0 and 1.

MATLAB Regression Models and CFD Trained Data

- Compressor Stage

Initially, the parameters chosen for regression analysis for predicting the degree of reaction of compressor stage are taken TMFP, PR and NDSP which are explained under Compressor stage CP tree and parameter analysis. Taking the variables, the CFD data taken as the base was trained. The automated process of training the model has been followed in which the data has been run on all the 19 available regression models. The results for the lowest root mean square model (RMSE) have been summarised below:

Fig. 68 RMSE values for all regression models © Cummins

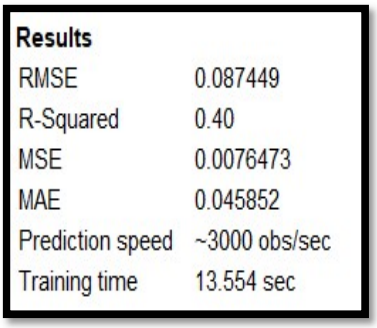

Fig. 69 R-square value of highlighted model © Cummins

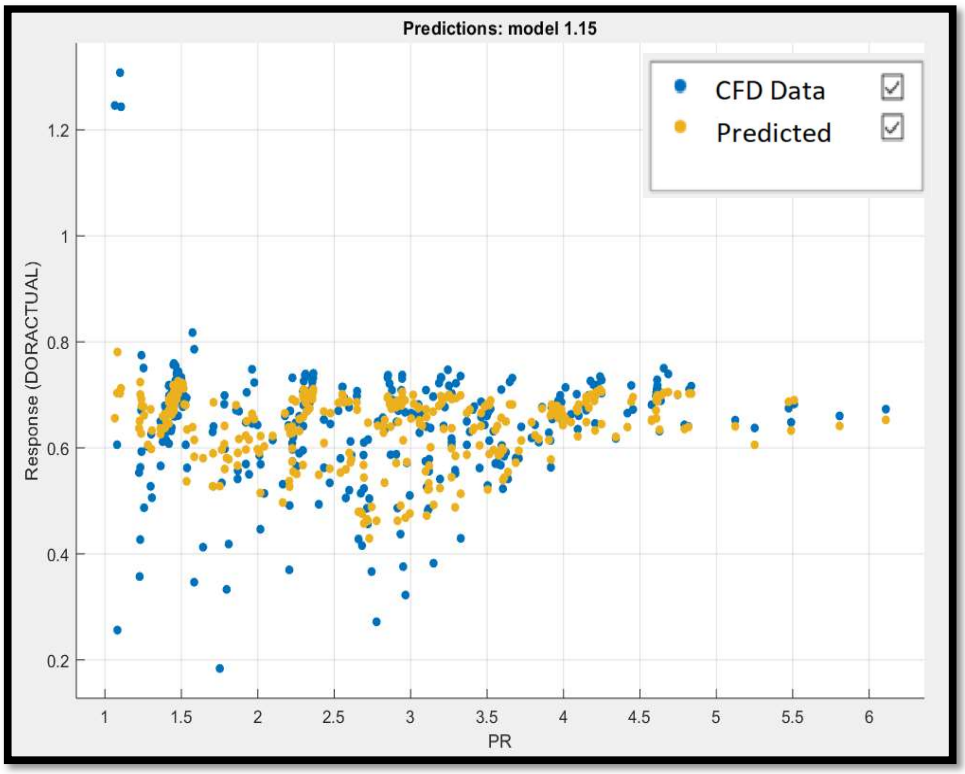

Fig. 70 Plot of data fit with respect to PR © Cummins

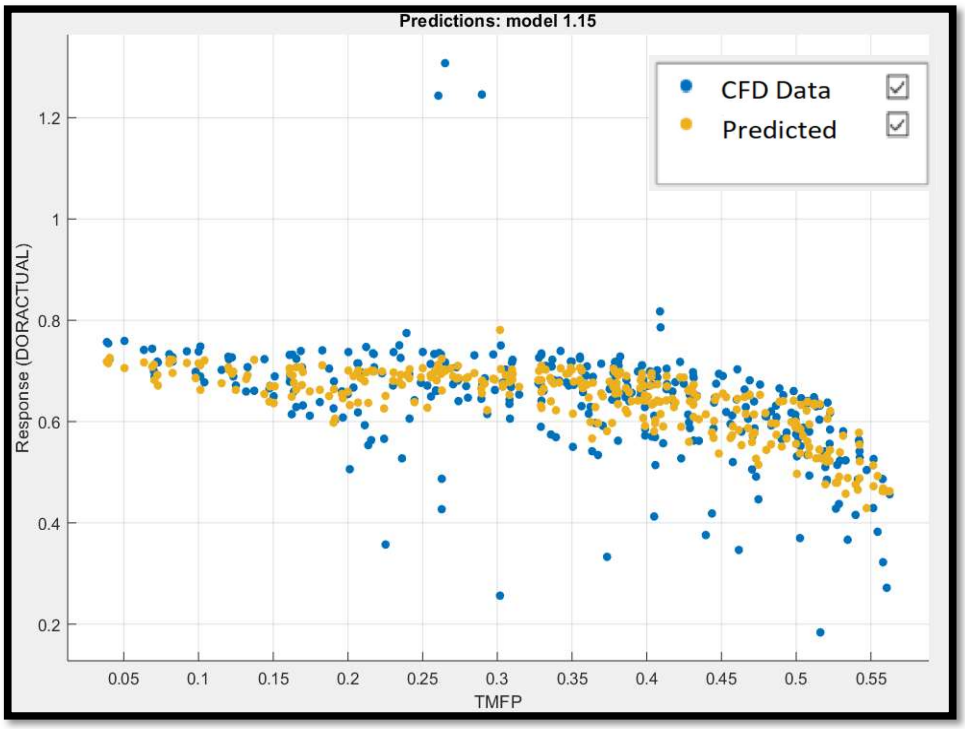

Fig. 71 Plot of data fit with respect to NDSP © Cummins

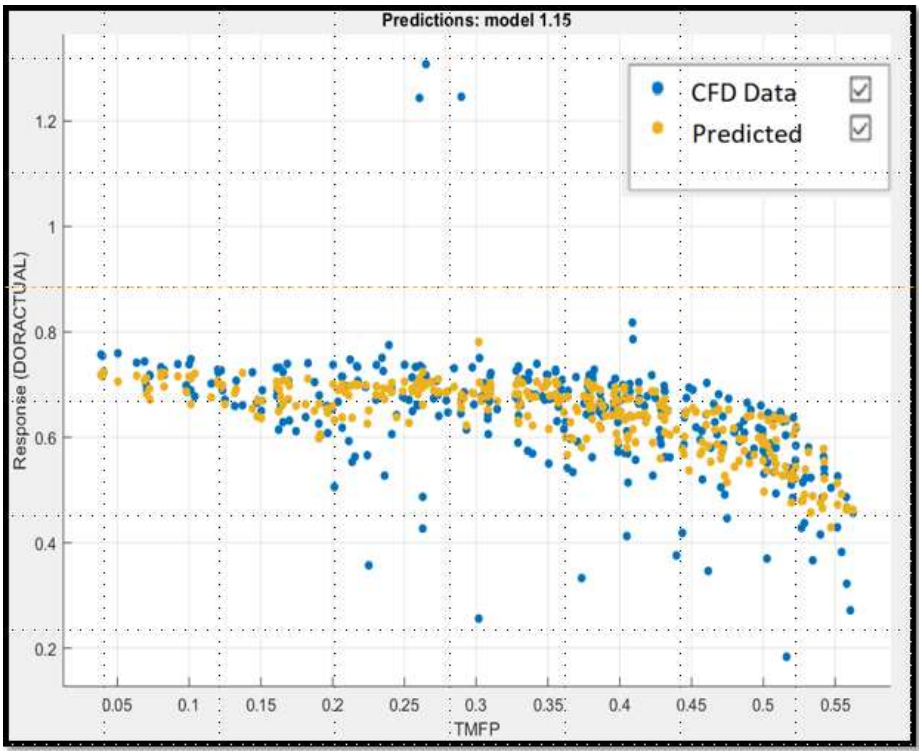

Fig. 72 Data plot showing curve fit with TMFP © Cummins

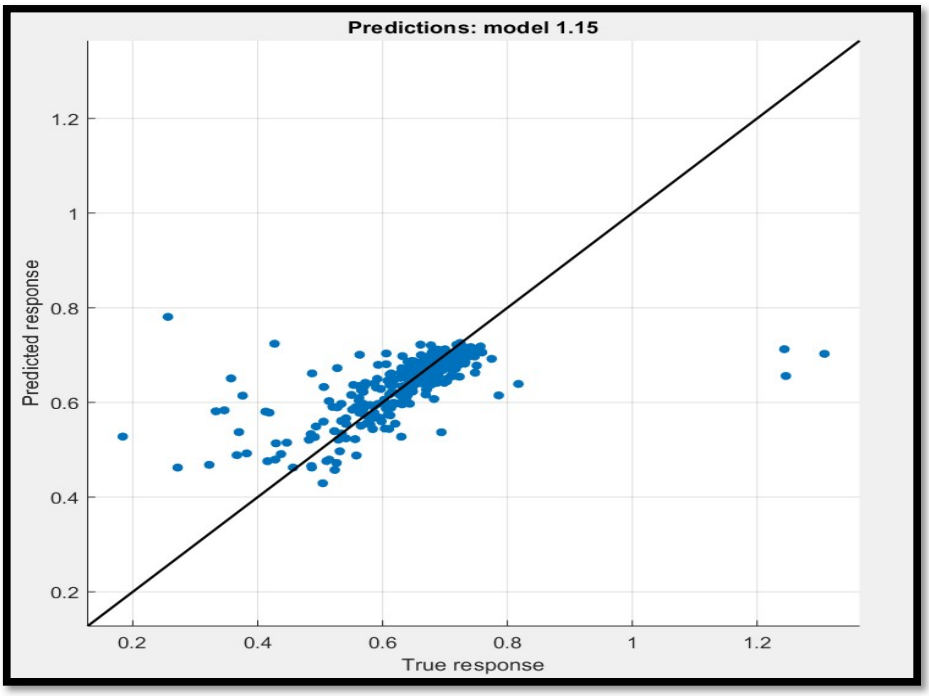

Fig. 73 Curve fit plot with the data © Cummins

The R-square value is 0.4 which indicates that there is lack of predictors and the data does not well fit with a regression curve. So geometric parameters have been added

stepwise. Initially, the predictor Trim has been added which makes the predictor to four. The models have been put to training and results are listed in figures below:

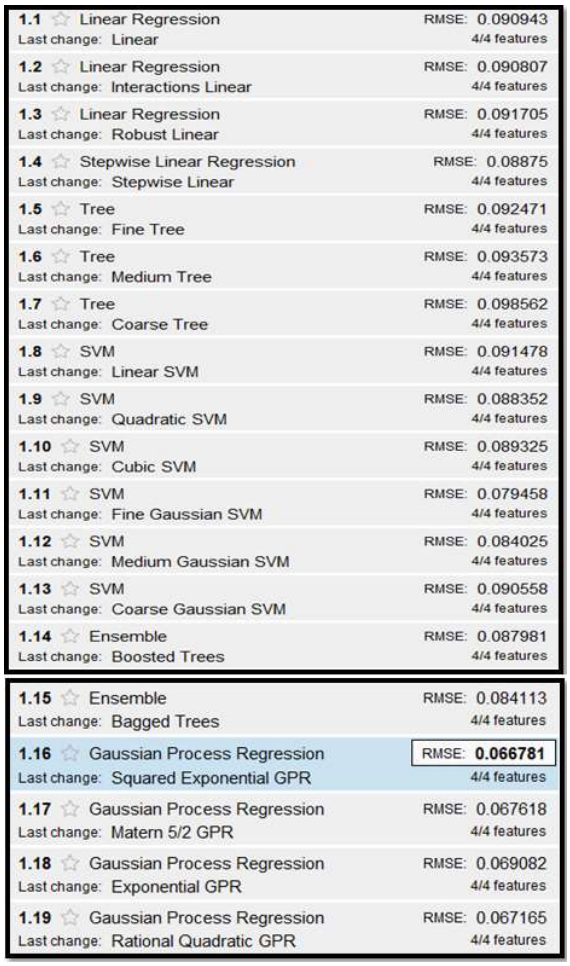

Fig. 74 Regression models run on CFD data © Cummins

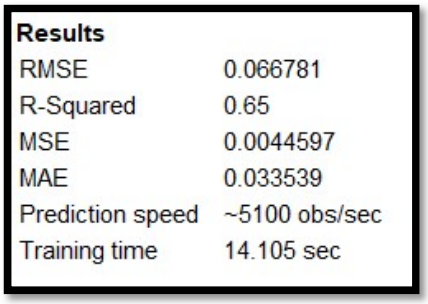

Fig. 75 The R-square value improvement © Cummins

The regression model has changed from Bagged tress to Squared exponential GPR with improved R-square from 0.4 to 0.65.

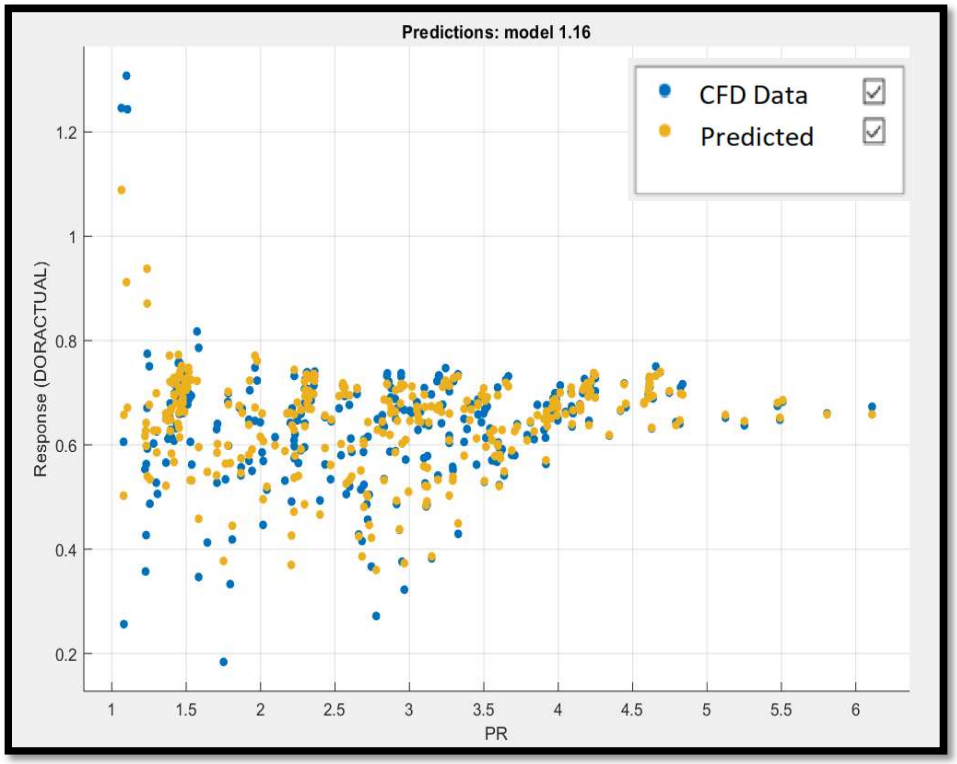

Fig. 76 Variation of predicted values with PR © Cummins

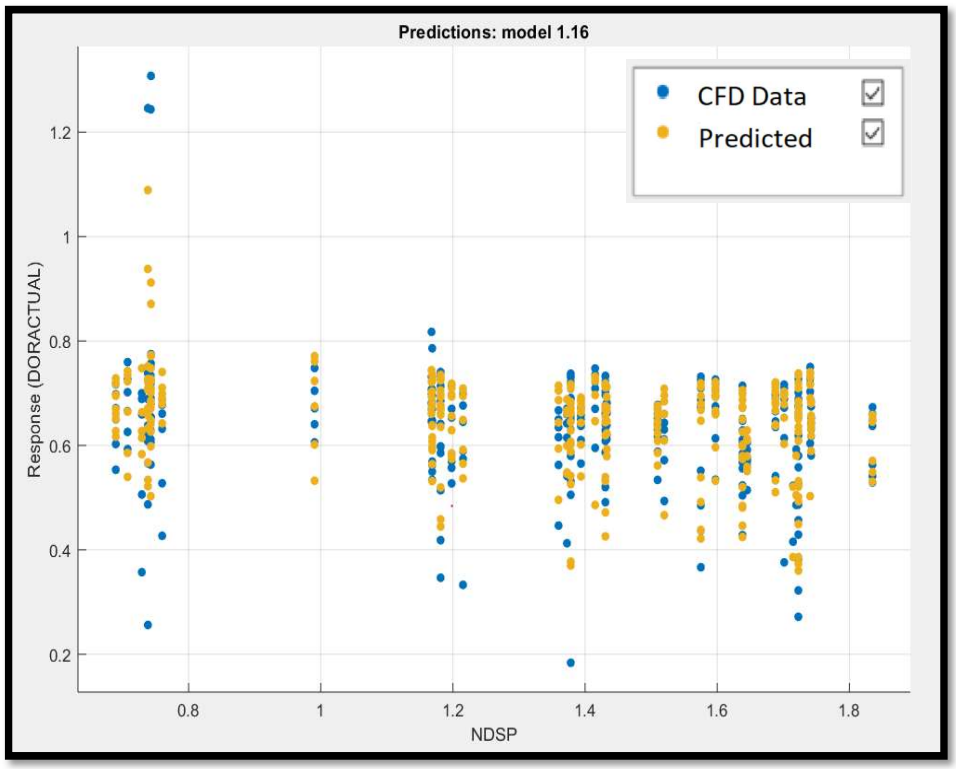

Fig. 77 Variation of predicted values with NDSP © Cummins

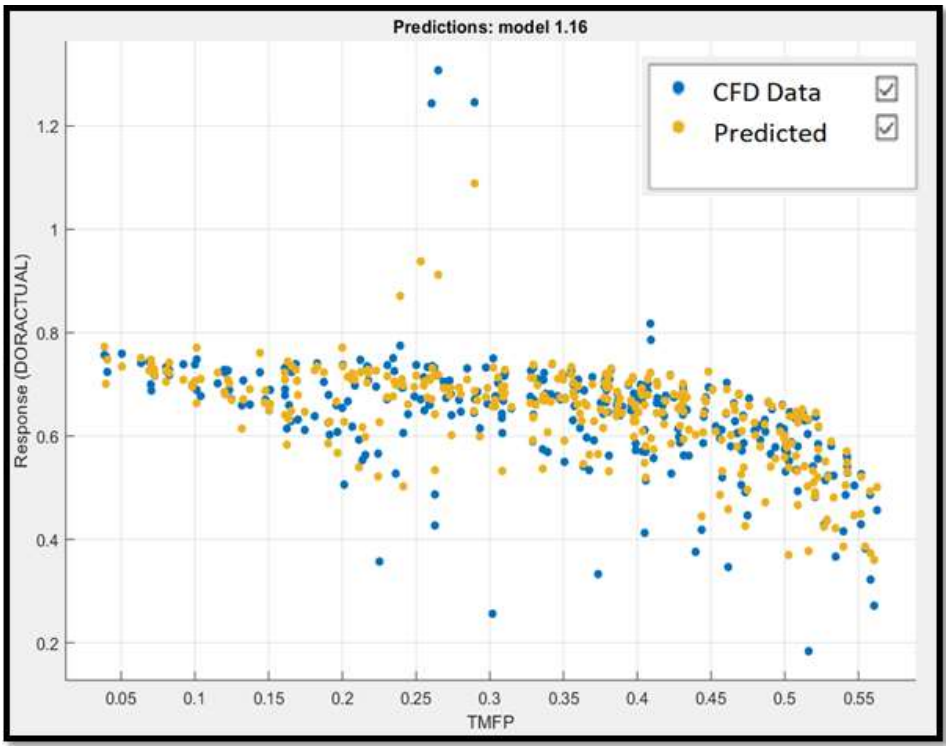

Fig. 78 Variation of TMFP with CFD data © Cummins

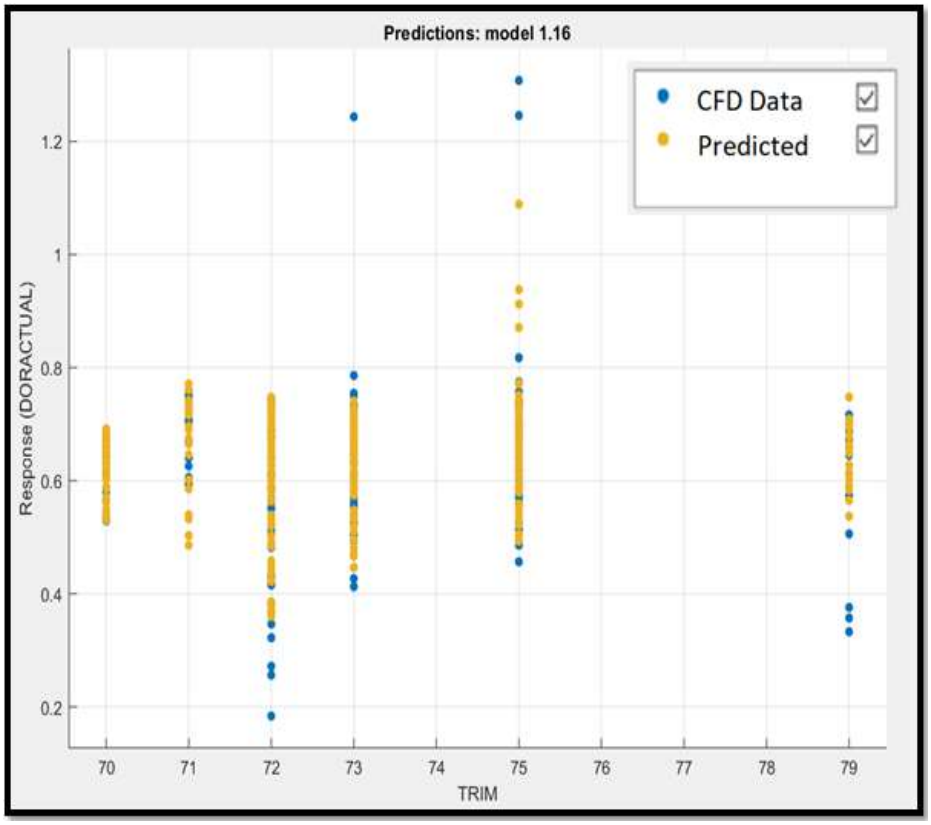

Fig. 79 Variation of Trim with CFD data © Cummins

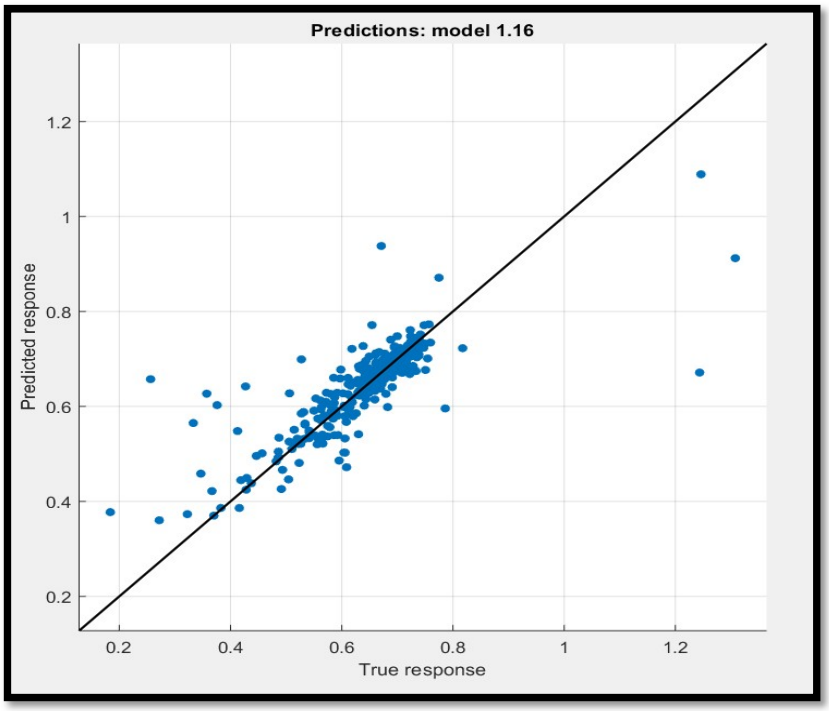

Fig. 80 Curve fit plot of CFD data © Cummins

The regression fit is better than the previous model and it is made better by adding additional geometric parameter mean value of Tip to inducer ratio. The data has been again trained to make prediction better using MATLAB. The regression analysis has been run all 19 models, the results of which are given below:

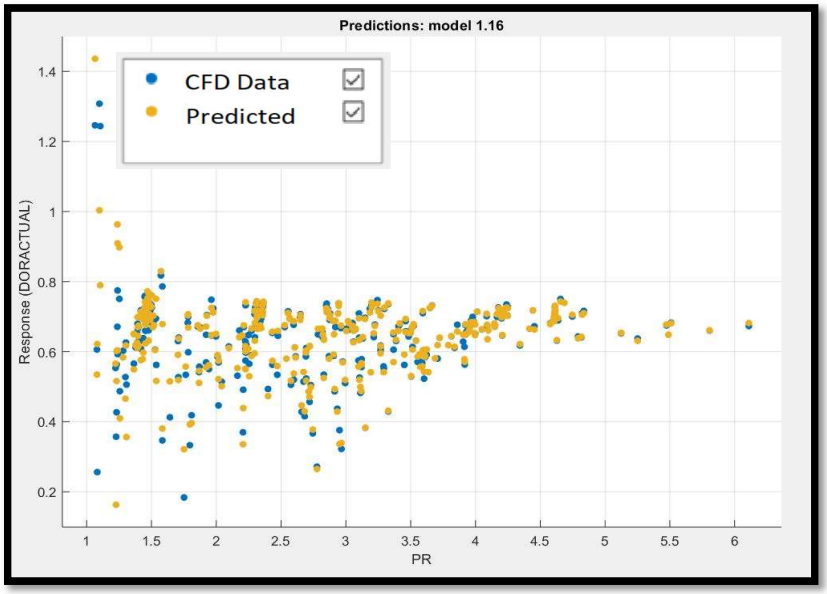

Fig. 81 Model fitting better with PR © Cummins

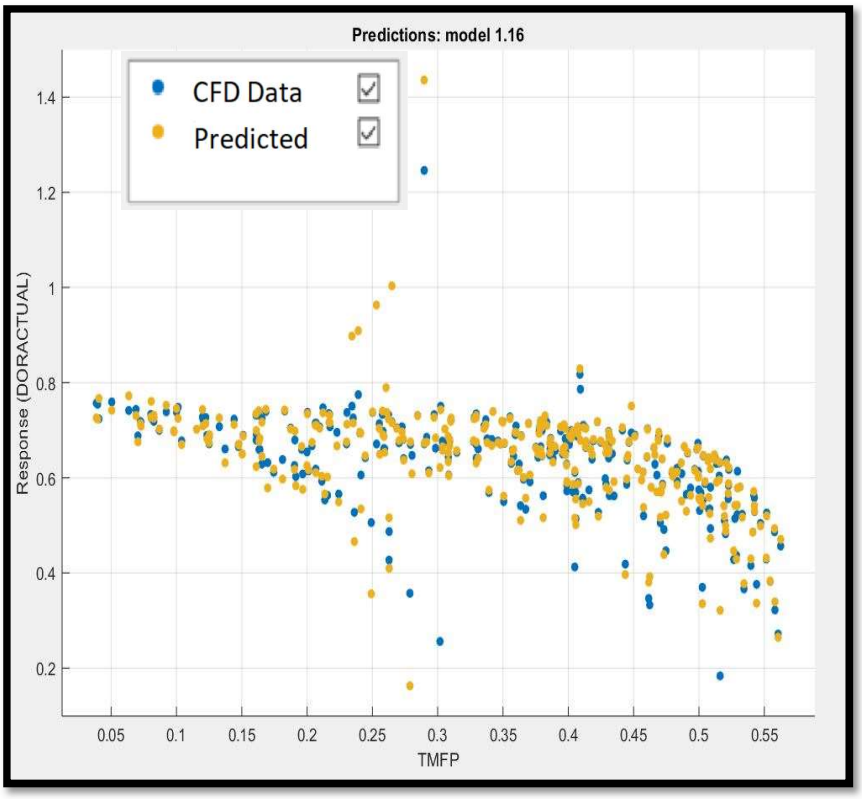

Fig 82 Perfect fit with TMFP © Cummins

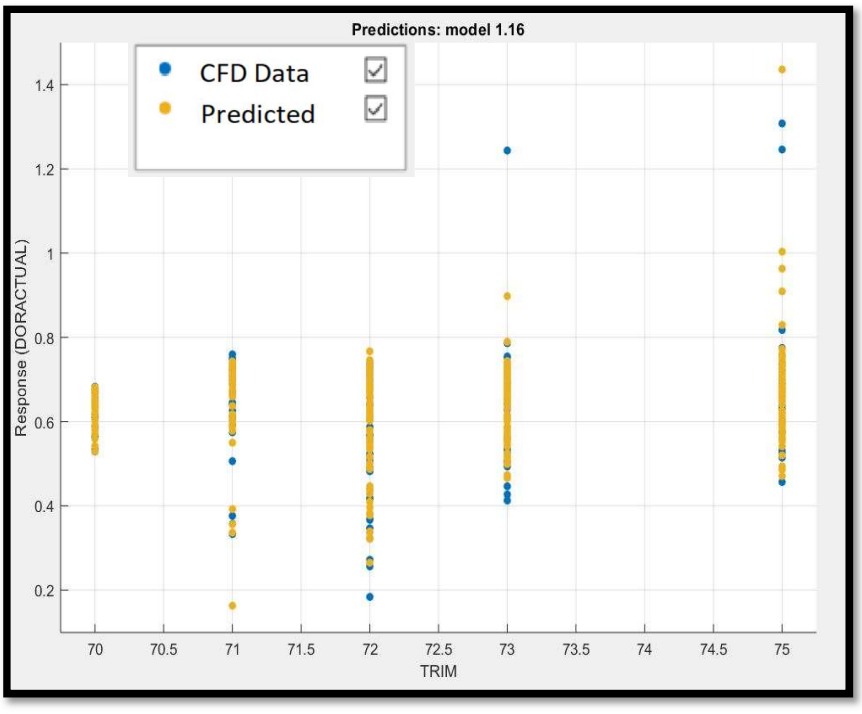

Fig. 83 Perfect fit with Trim © Cummins

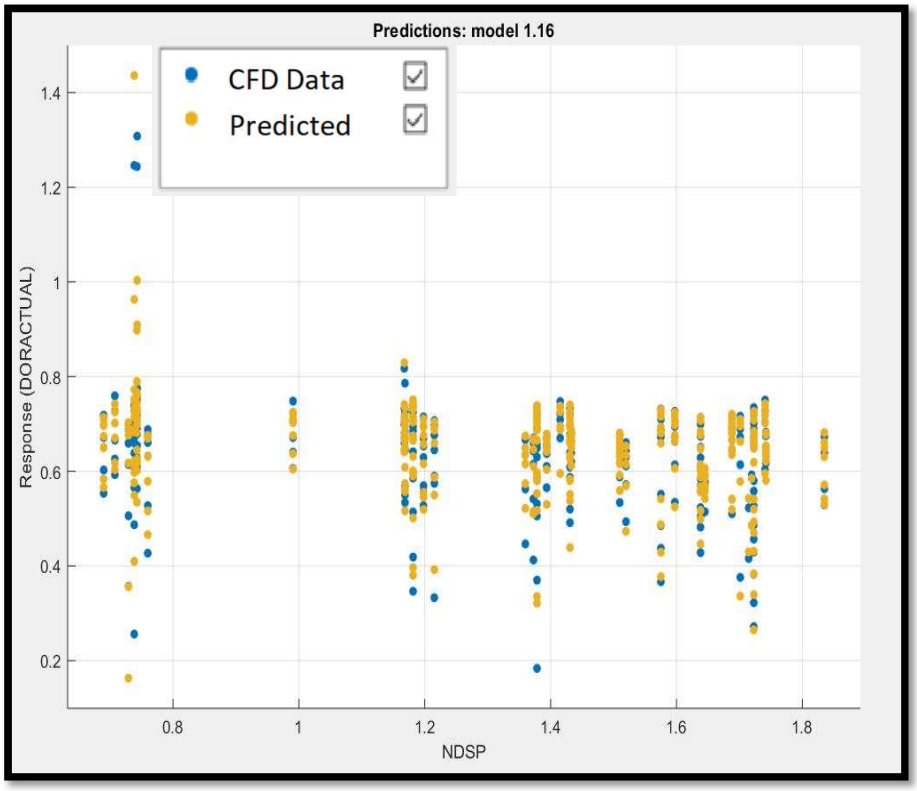

Fig. 84 Perfect fit with NDSP © Cummins

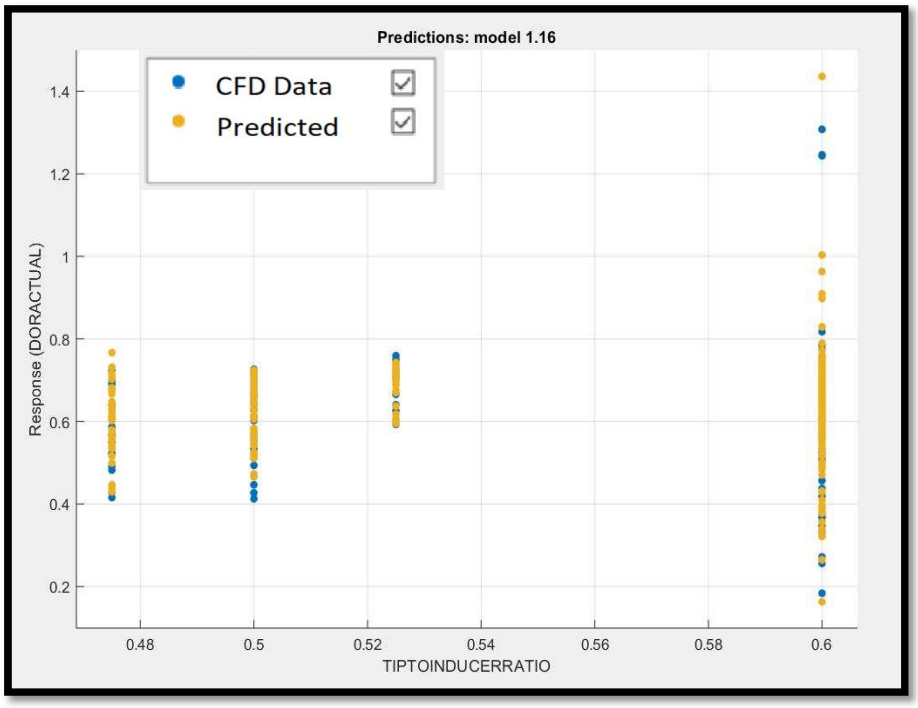

Fig. 85 Perfect fit with Tip to inducer ratio © Cummins

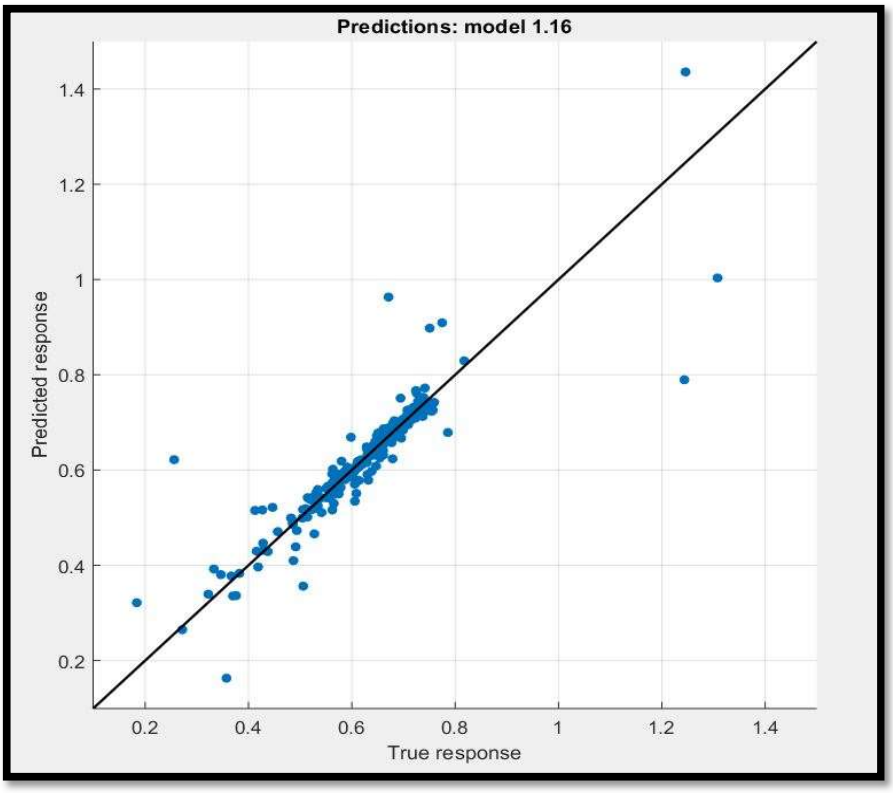

Fig. 86 Curve fit © Cummins

The best of the curve fit was obtained using all the five parameters in steps. The R-square has improved from 0.4 to 0.81 which is quite a drastic change. The prediction of DOR is improved as the root mean square error with this approach is quite less as compared to the previous. The value of R-square is shown in figure 87.

Results	
RMSE	0.049597
R-Squared	0.81
MSE	0.0024598
MAE	0.018898
Prediction speed	~4400 obs/sec
Training time	18.799 sec

Fig. 87 The best model R square © Cummins

The best of all the 19 models tested for the CFD data for the analysis of the compressor side to predict the degree of reaction. So, the best of the model came out under Gaussian Progress Regression which is squared exponential in nature. The model has improved from three degrees of reaction predictors to five. The model is chosen based on the least value of root mean square value

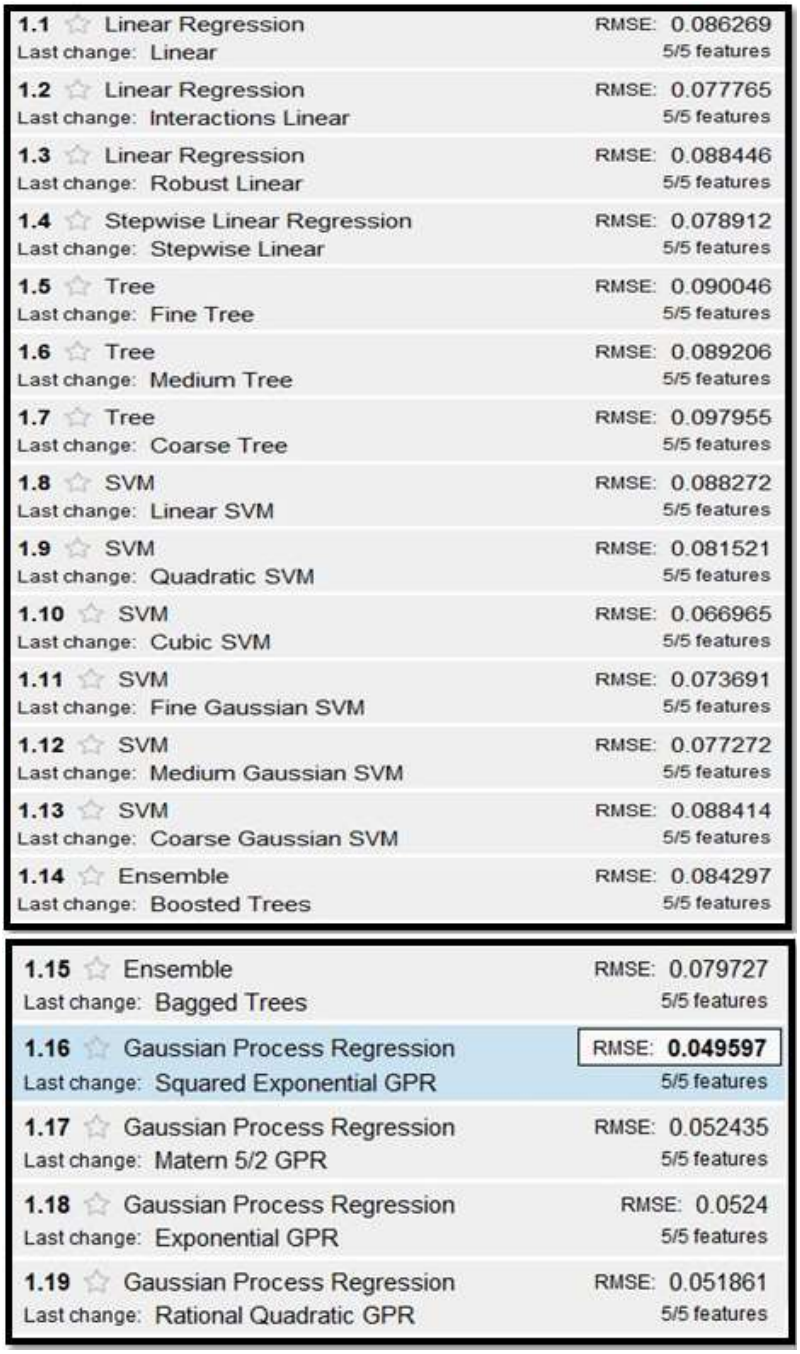

Fig. 88 Best model to predict the degree of reaction for compressor © Cummins

- Turbine Stage

Initially, for the turbine stage the parameters three parameters have been chosen which were obtained using Buckingham Pi theorem. These are trim, arc parameter which considers the critical area of housing and expansion ratio (ER). The MATLAB regression learner app was used to predict the best model. The results of which are detailed below:

1.1 ☆ Linear Regression Last change: Linear	RMSE: 0.045197 3/3 features
1.2 ☆ Linear Regression Last change: Interactions Linear	RMSE: 0.045063 3/3 features
1.3 ☆ Linear Regression Last change: Robust Linear	RMSE: 0.045207 3/3 features
1.4 ☆ Stepwise Linear Regression Last change: Stepwise Linear	RMSE: 0.045758 3/3 features
1.5 ☆ Tree Last change: Fine Tree	RMSE: 0.041972 3/3 features
1.6 ☆ Tree Last change: Medium Tree	RMSE: 0.050105 3/3 features
1.7 ☆ Tree Last change: Coarse Tree	RMSE: 0.067503 3/3 features
1.8 ☆ SVM Last change: Linear SVM	RMSE: 0.045279 3/3 features
1.9 ☆ SVM Last change: Quadratic SVM	RMSE: 4.5752 3/3 features
1.10 ☆ SVM Last change: Cubic SVM	RMSE: 229.32 3/3 features
1.11 ☆ SVM Last change: Fine Gaussian SVM	RMSE: 0.048725 3/3 features
1.12 ☆ SVM Last change: Medium Gaussian SVM	RMSE: 0.042726 3/3 features
1.13 ☆ SVM Last change: Coarse Gaussian SVM	RMSE: 0.044255 3/3 features
1.14 ☆ Ensemble Last change: Boosted Trees	RMSE: 0.047407 3/3 features
1.16 ☆ Gaussian Process Regression Last change: Squared Exponential GPR	RMSE: 0.040182 3/3 features
1.17 ☆ Gaussian Process Regression Last change: Matern 5/2 GPR	RMSE: **0.040104** 3/3 features
1.18 ☆ Gaussian Process Regression Last change: Exponential GPR	RMSE: 0.042066 3/3 features
1.19 ☆ Gaussian Process Regression Last change: Rational Quadratic GPR	RMSE: 0.040182 3/3 features

Fig. 89 List of regression models run for analysis © Cummins

The R-square for the best-predicted model which is highlighted in blue is given below:

Results	
RMSE	0.040104
R-Squared	0.84
MSE	0.0016083
MAE	0.031098
Prediction speed	~7900 obs/sec
Training time	15.981 sec

Fig. 90 Low value of R square © Cummins

The prediction by the tool for the three parameters which were taken for analysis has not been better so far. The prediction varied largely and the predicted values were not able to fit well with data. The results are shown below with each parameter taken. So, it also helped to realise that the new parameter is needed to accurately determine the results.

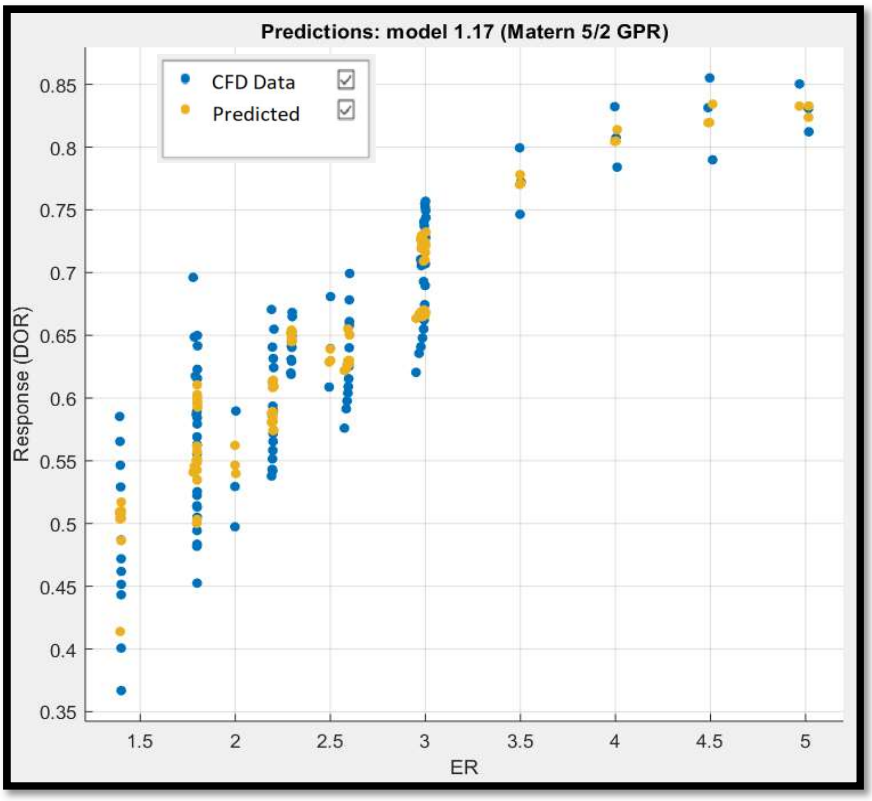

Fig. 91 Variation of prediction with ER © Cummins

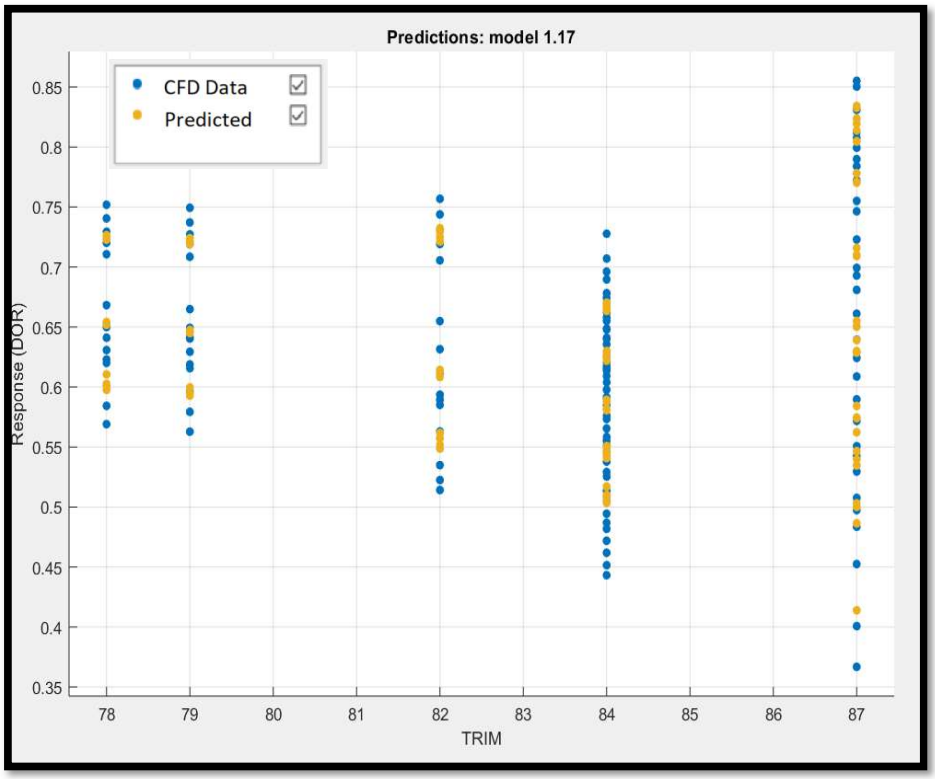

Fig. 92 Variation of trim with respect to CFD data © Cummins

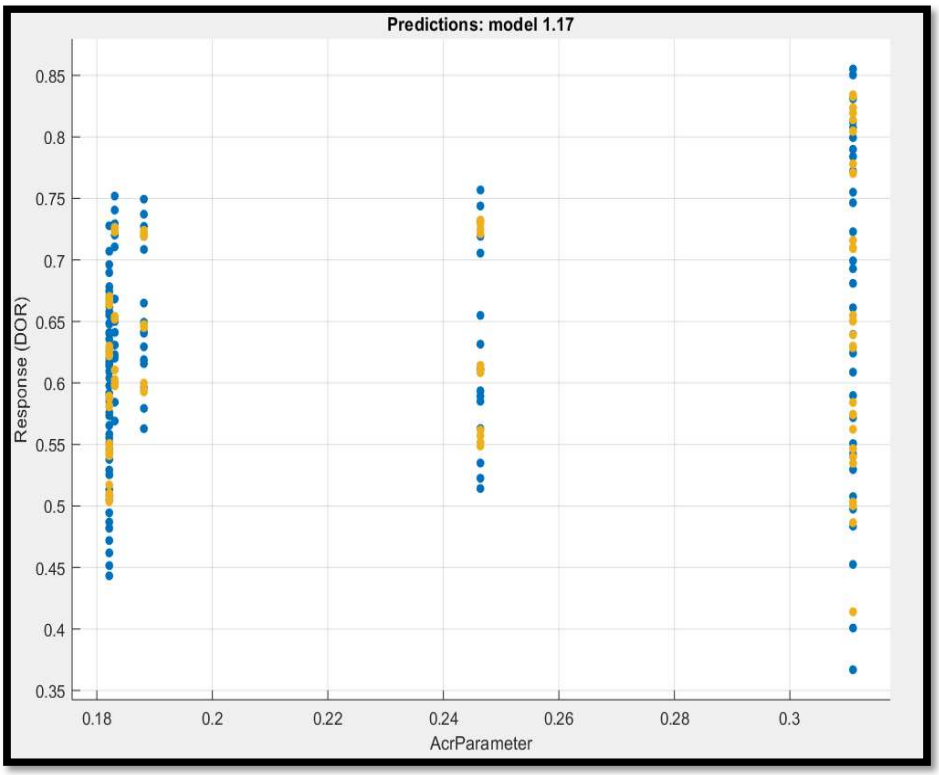

Fig. 93 Variation of housing critical parameter with CFD data © Cummins

So, another parameter which is the fourth one in the list is U/C that has been added to the predictors. The R-square value related to the analysis has seen a large improvement. This reason led to dropping off an extra parameter true mass flow parameter (TMFP) for the turbine side. The model and the R-square valued with four predictors are listed below along with the curve fit plot showing the improvement in the results of predicting the degree of reaction on the turbine side. The R-square value is 1 because the data set for the turbine was small.

Fig. 94 Trained turbine data models with four parameters © Cummins

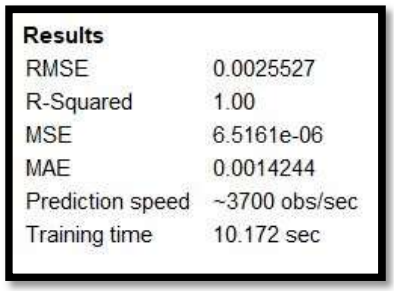

Fig. 95 The table shows the R-square value © Cummins

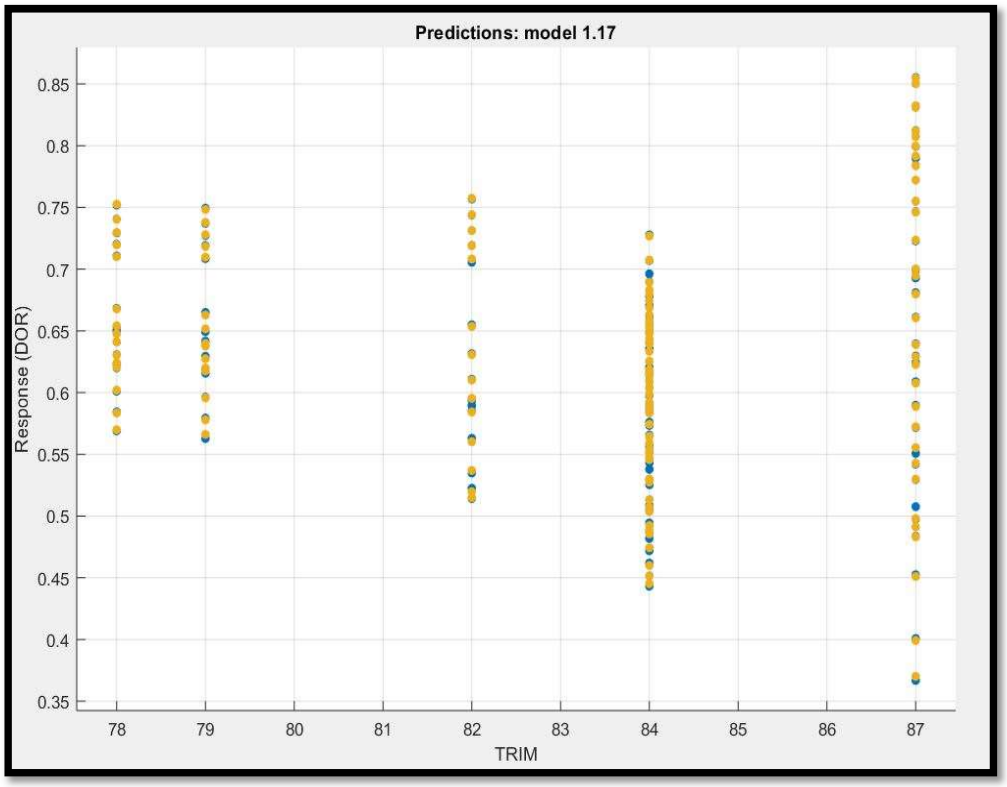

Fig. 96 Variation of selected model with Trim © Cummins

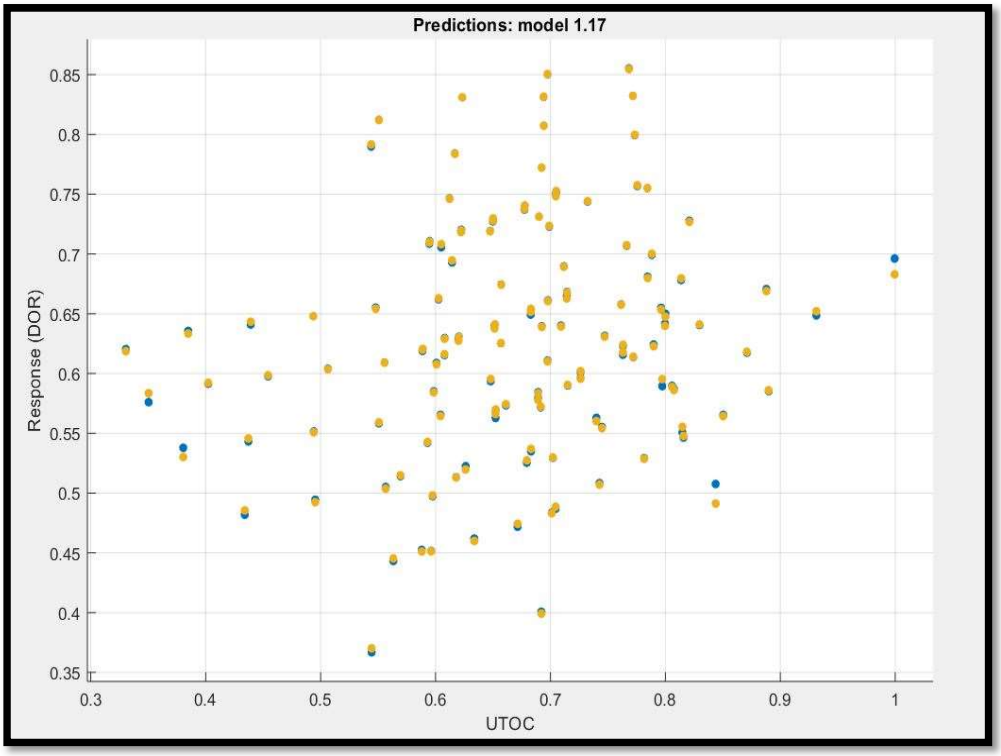

Fig. 97 Variation of selected model with blade speed ratio (U/C) © Cummins

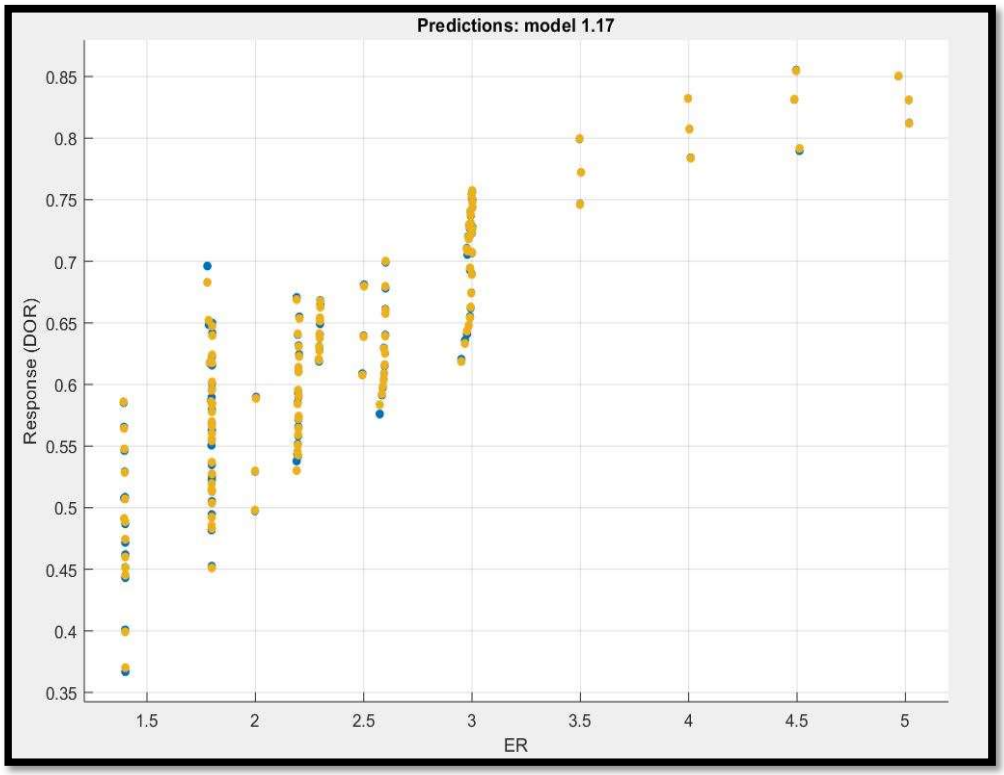

Fig. 98 Variation of selected model with expansion ratio © Cummins

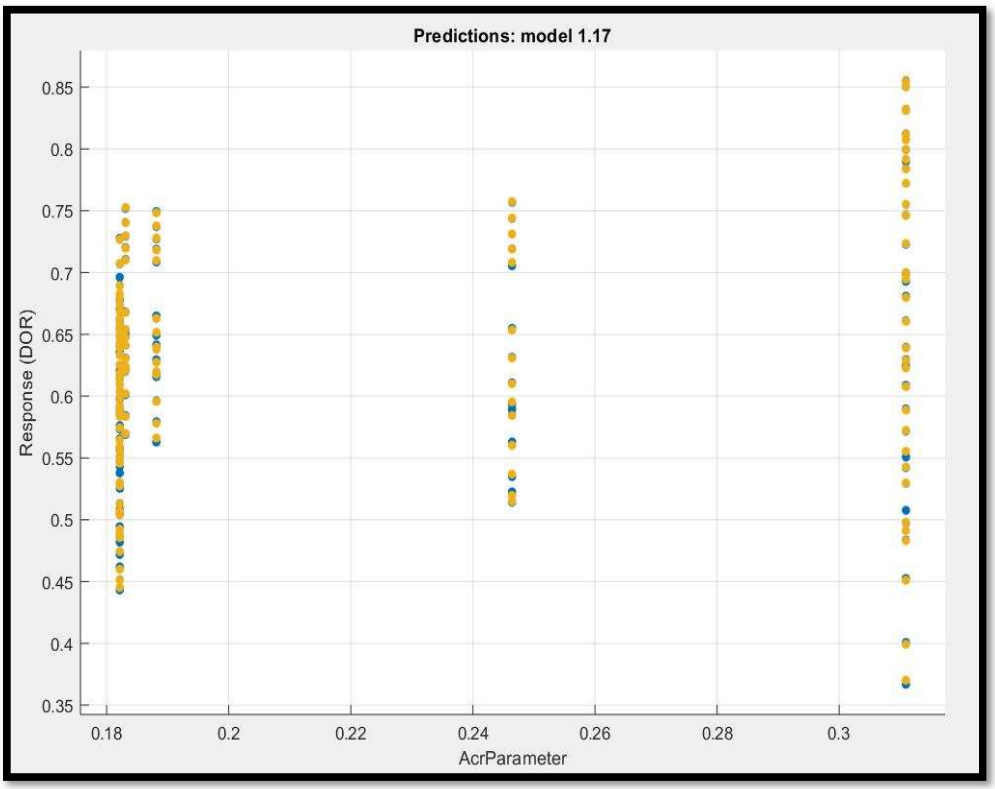

Fig. 99 Variation of selected model with housing critical area © Cummins

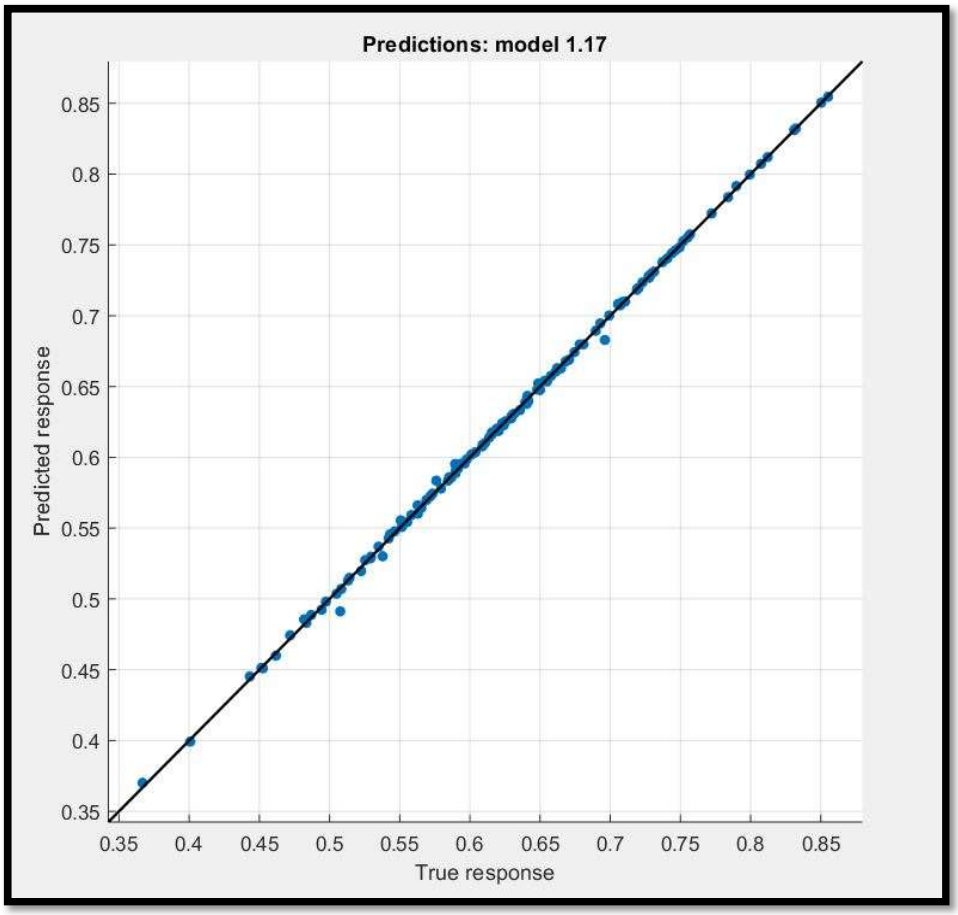

Fig. 100 The curve fit with selected model © Cummins

The best possible prediction of the degree of reaction is given by the model by Gaussian process regression under category 5/2 Matern with both three and four predictors. The highest R-square have been observed with this model and the least root mean square error but R-square close to 1 leads to over fitting so the model with three parameters has been chosen for prediction with R-square 0.84.

The regression analysis tool helped to eliminate the biggest assumption of constant and equal degree of reaction on both sides which have been followed in various literature studies so far. It can help to predict the changes in the degree of reaction values when the geometric and operating parameters tend to change with the change in turbocharger frames and applications. Now that the models can be used to predict the degree of reaction values then the values of impeller outlet tip (p2*) and wheel inlet tip (p3*) can be predicted.

Techniques Used for Predicting Thrust Loads

- Analytical Method

The procedure applied is based on previous research studies with improvements. As the aim is to develop a model which is less complicated and can give results with adequate accuracy so the momentum forces have been neglected considering the steady state operation of the turbocharger (Lüddecke *et al.*, 2015). Moreover, the regression models that have been utilised to predict the values of degree of reaction for compressor and turbine stage using steady-state CFD data for training in regression learner app. Another reason is that the flow physics at the impeller/wheel blade is complicated (Lüddecke *et al.*, 2015) and it's not well defined so their contribution to the net thrust loads is not very significant. Instead of determining the pressure points for complete geometry of the impeller and turbine wheel, certain pressure locations (impeller/wheel tip and seal pressures) have been used to predict the net thrust loads which are different from the experimental pressure tapping approach (Lüddecke *et al.*, 2015). The figure 101 below shows the forces that have been utilised to predict net thrust loads.

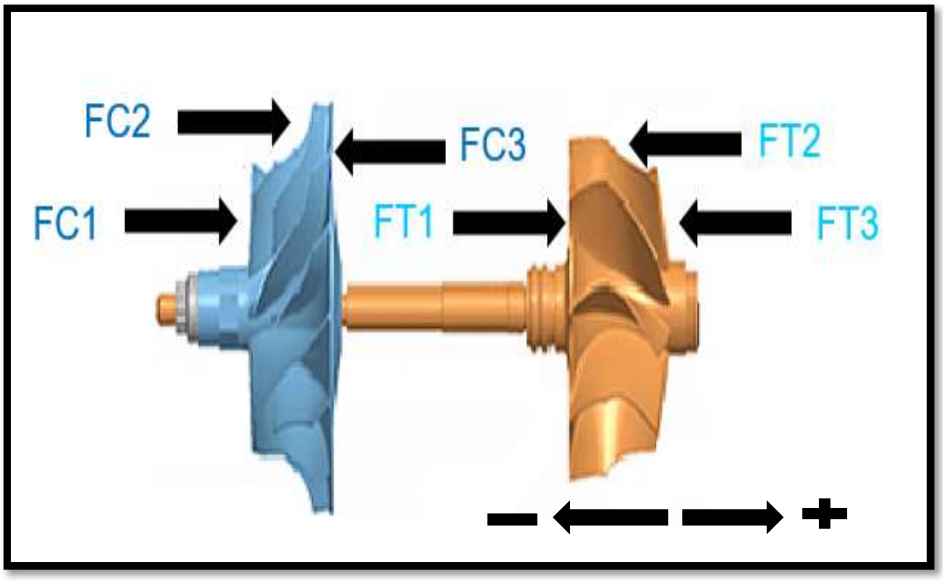

Fig. 101 Forces acting on the turbocharger (Elnemr, 2011)

FC1 is the force acting on the impeller inducer section while FC2 is the load affecting blade curvature known as shroud. FC3 is the load impacting backward face of wheel. FC3 is a dominating force while turbocharger is in operation (Lüddecke *et al.*, 2015). FT1 load affects back face of wheel and FT2 affects turbine wheel shroud. FT3 is the load exerted at exducer portion (Lüddecke *et al.*, 2015). The net force is the resultant

of all the forces. The sign convention for the axial load direction is negative towards compressor end and positive for the turbine end.

The projected areas have been taken for analysis on the compressor side which are detailed below:

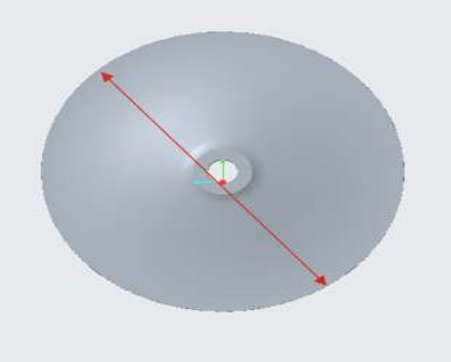

Fig. 102 Area at back face © Cummins

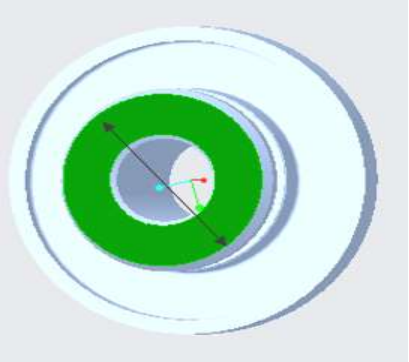

Fig. 103 Slinger diameter in contact with back face © Cummins

Fig. 104 Inducer area © Cummins

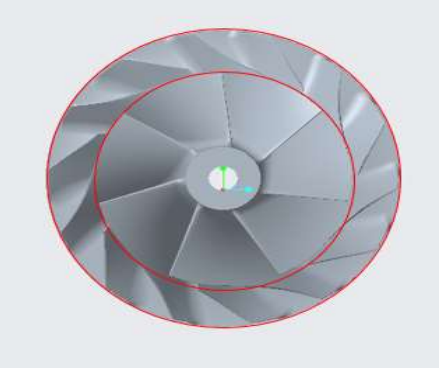

Fig. 105 Shroud projected area © Cummins

The projected areas have been taken for analysis on the turbine side which are detailed below (Lüddecke *et al.*, 2015) :

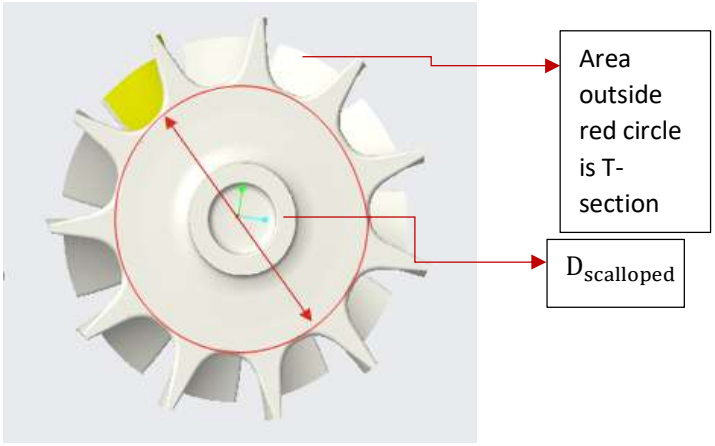

Fig. 106 Back face wheel area © Cummins

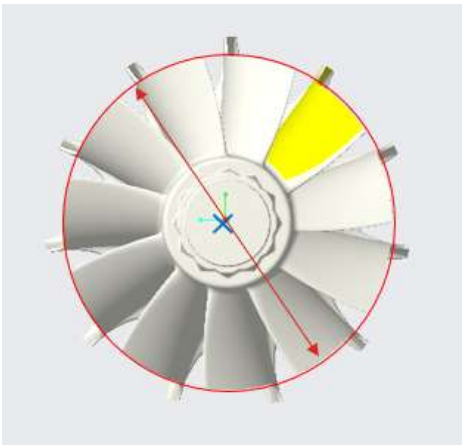

Fig. 107 Exducer area © Cummins

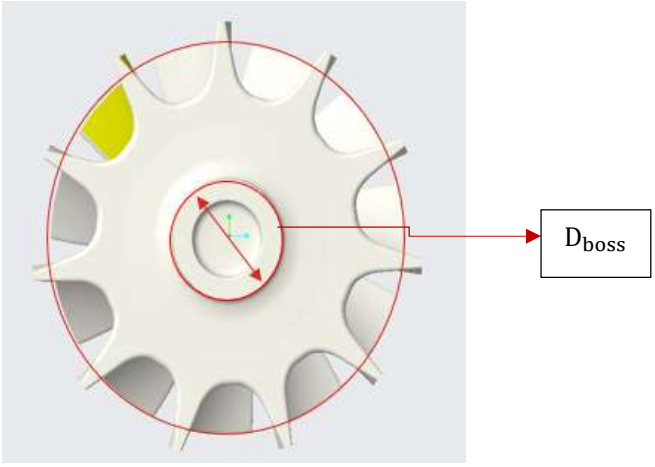

Fig. 108 Shroud area © Cummins

Making use of projected area and pressures the forces are estimated which are detailed. As the impeller outlet pressure (p2*) and turbine inlet pressure (p3*) are unknown in the analysis because of which the regression models have been developed for prediction of the degree of reaction.

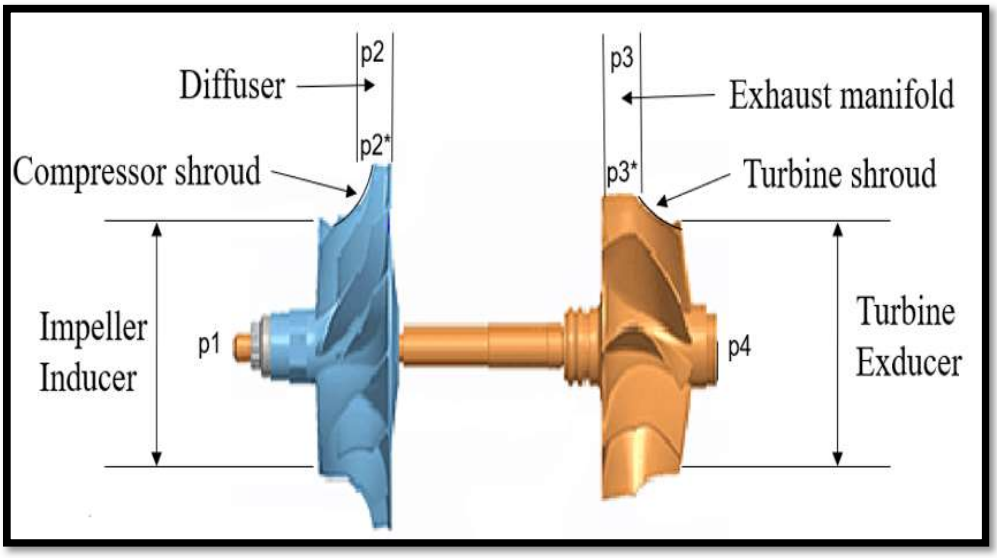

Fig. 109 Pressure and geometric parameters (Elnemr, 2011)

- Compressor stage forces (Nguyen-Schäfer, 2012)
  1. Inducer force

$$FC1 = \left(\frac{\pi}{4} \times D^2_{inducer}\right) \times (p1) \quad (22)$$

  2. Shroud force

$$FC2 = \left(\frac{\pi}{4} \times \left(D^2_{impeller\ tip} - D^2_{inducer}\right)\right) \times \left(\frac{p1+p2^*}{2}\right) \quad (23)$$

  3. Back-face force

$$FC3 = \left(\frac{\pi}{4} \times D^2_{impeller\ tip} - D^2_{slinger}\right) \times (p2^*) \quad (24)$$

The formula for back face is taken with the assumption that distance between wheel back face and bearing housing is greater than 1mm. Moreover, in the shroud portion of the impeller, the pressure variation definitions are complex so the mean of the compressor stage inlet pressure (p1) and impeller tip pressure (p2*) has been taken. The exact areas of contact of forces are very complicated to estimate as the blade geometry is changing so the projected areas have been taken for the analysis of the thrust loads. To determine the impeller tip pressure the value of the degree of reaction from trained regression models is utilised and used in formula which is given in equation- and derived taking isentropic process assumptions.

$$p2* = \ p1 \times (1 + rc \times \left((\frac{p2}{p1})^{\frac{\gamma-1}{\gamma}} - 1 \right)^{\frac{\gamma}{\gamma-1}} \quad (25)$$

- Turbine stage forces (Nguyen-Schäfer, 2012)

4. Turbine back-face force (Sun *et al.*, 2010)

$$FT1 = (\frac{\pi}{4} \times (D^2_{scalloped} - D^2_{boss})) \times (p\text{-back}) + (\frac{p3* + pback}{2}) \times (\text{T-section projected area}) \quad (26)$$

$$p\text{-back} = p3* - \rho \times \frac{\omega^2}{8} \times (\frac{\pi}{4} \times D^2_{scalloped} - \frac{\pi}{4} \times D^2_{boss}) \quad (27)$$

The turbine back force is a combination of the force acting on the scalloped wheel and T-section of the wheel. T-section region remains after the subtraction of the scalloped diameter region (Lüddecke *et al.*, 2015). The pressure at the turbine back which is assumed to be the pressure near the turbine seal is used to get the force in the scalloped part of the wheel. The wheel inlet pressure (p3*) is obtained using the models trained using CFD data to predict the degree of reaction for the turbine wheel which is given by equation (28) below (Nguyen-Schäfer, 2012) :

$$p3* = p4 \times [1 + rt \times ((\frac{p3}{p4})^{-(\frac{\gamma-1}{\gamma})} - 1)]^{\frac{-\gamma}{\gamma-1}} \quad (28)$$

5. Shroud force

$$FT2 = ((\frac{\pi}{4} \times D^2_{scalloped} + T - \text{section area}) - (\frac{\pi}{4} \times D^2_{exducer})) \times (\frac{p4 + p3*}{2}) \quad (29)$$

As the pressures in the shroud region are very complicated to accurately estimate so the mean of the turbine outside pressure (pout) and wheel inlet tip pressure (p3*) have been taken.

6. Exducer force

$$FT3 = (\frac{\pi}{4} \times D^2_{exducer}) \times (p4) \quad (30)$$

The exducer force is the load exerted on the exducer projected area when acted upon by the turbine outlet pressure. This force is critically important at times when there is an obstruction in the flow path of exhaust gases which results in increasing the back pressure and thus affecting the axial load direction. The net axial thrust loads (Lüddecke *et al.*, 2015) is a summation of all the forces as per their sign convention.

$$F_{net} = (FC1 + FC2 - FC3) + (FT1 - FT2 - FT3) \quad (31)$$

The summation of FC1, FC2 and FC3 is net load acting on the compressor wheel and summation of FT1, FT2 and FT3 is the net load acting on the turbine wheel (Nguyen-Schäfer, 2012).

- Experimental Method

In the experimental technique, the test data is obtained using the pressure sensors which tap the pressures at impeller back face and turbine. The pressures are tapped as shown in the figure 110 below:

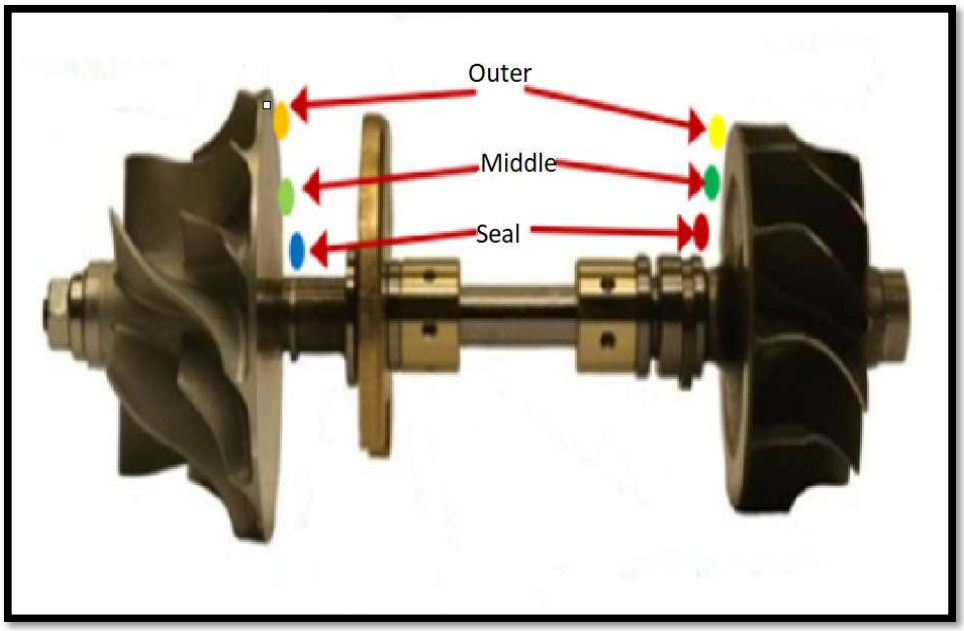

Fig. 110 Pressures tapped to estimate thrust loads (Charitopoulos et al., 2018), (Sun et al., 2010)

The pressure tapped at the top of the impeller/wheel is labelled as outer while the pressure tapped near the shaft and close to seals are seal pressures. The pressures tapped in between them are called middle pressures. Making use of the pressures at specific pressure points the forces are calculated. In this approach, the pressures at the impeller outlet tip and wheel inlet tip are not estimated due to the complexity involved in the pressure tapped approach. So, from this, it can be inferred that the two approaches which are analytical and experimental make use of different pressures to estimate the thrust loads. Moreover, the equations in the analytical approach are based on theoretical assumptions which cannot represent the practical situation of the critical operating conditions of the turbocharger. Taking the pressure tapped approach as the base and

taking it as the correct prediction of thrust loads, the analytically calculated forces have been compared with experimentally derived forces. The calculation of the inducer force for the compressor side and the exducer force for the turbine side remain the same for the experimental approach. The changes are made in a shroud and back face forces of impeller and turbine wheel. There is a difference in the way the forces are calculated in the turbine back face and shroud face because mostly turbine wheels are scalloped and do not contain complete back-face. So, the tip pressure is not estimated. On the other hand, the compressor shroud force formula remains unchanged.

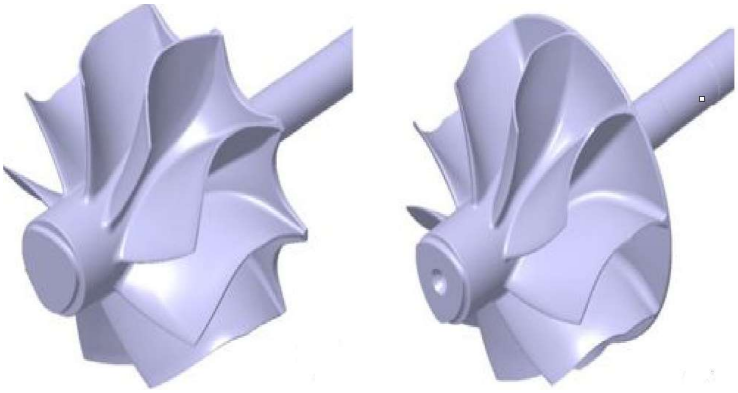

Fig. 111 Scalloped wheel (L) and Un scalloped wheel (R) (Hannu Jääskeläinen, 2017)

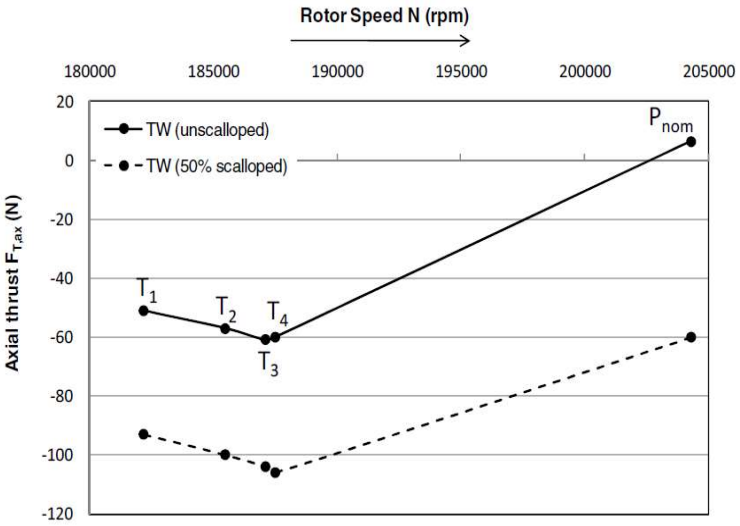

Fig. 112 Effect of scalloping on the net axial load of the turbocharger (Nguyen-Schäfer, 2012)

The turbine wheels are scalloped so that the thrust loads remain towards the compressor side. It also improves the working of the turbocharger by decreasing the turbine wheel inertia. It largely affects the net axial loads on the turbine wheel and lowers it down in

comparison to the net axial loads on the compressor side (Nguyen-Schäfer, 2012). Even at higher turbocharger speeds if the scalloped wheels are used then net axial loads remain towards the compressor side as seen in figure 112. It is mostly desired as towards the compressor end the load-bearing capacity is higher than the load-bearing capacity towards the turbine. Under higher axial thrust loads it leads to the rubbing of the thrust bearing on either side which also leads to the loss of power. So, it is important to control the net axial loads for the efficient operation of the turbocharger in all operating conditions.

While selecting data for analysis data is sorted by under principle of pressure difference that pressures at wheel/impeller back outer are greater than middle and seal and middle pressure is greater than the seal pressure then only the backflow behind the wheels would occur.

CHAPTER 5: RESULTS AND DISCUSSIONS

After rigorous research study and studying all the parameters affecting the net thrust loads in a turbocharger, it has been established that the geometric and operating parameters have a significant effect. Due to some extent, this study has tried to fill in the gaps left by previous work but a lot more can be done to improvise the current model. The detailed steps followed to predict the thrust loads by experimental and analytical methods are given in chapter 4. The results of both the approaches and comparison with similar value of DOR approach are listed (Sun *et al.*, 2010). The variable degree of reaction has shown an improvement over the constant value of the degree of reaction approach available in the literature. The gap has been narrowed between the actual test results and predicted thrust loads. The new tool takes inputs which are listed below:

1. Ambient Pressure (Pa)
2. Turbine Outlet Pressure (Pa)
3. Turbine Inlet Temperature (K)
4. Expansion Ratio
5. Compression Ratio
6. Compressor Inlet Temperature (K)
7. DOR of Compressor (rc) dependent on critical parameters
8. DOR of Turbine (rt) dependent on critical parameters
9. Rotor Speed (Krpm)

The back-pressure force which is given in equation (26) has been added which requires turbine inlet temperature as new input. The engine has been run on the points shown in figure 113.

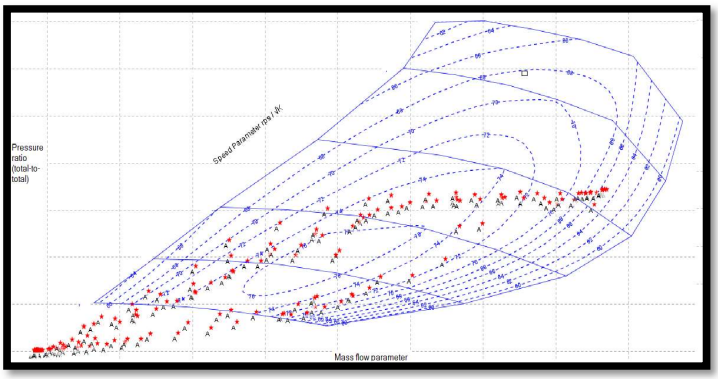

Fig. 113 Engine running points on compressor map © Cummins

Figure 113 shows that the engine has been run in the heart region of the compressor map. The thrust load results with comparison are detailed below:

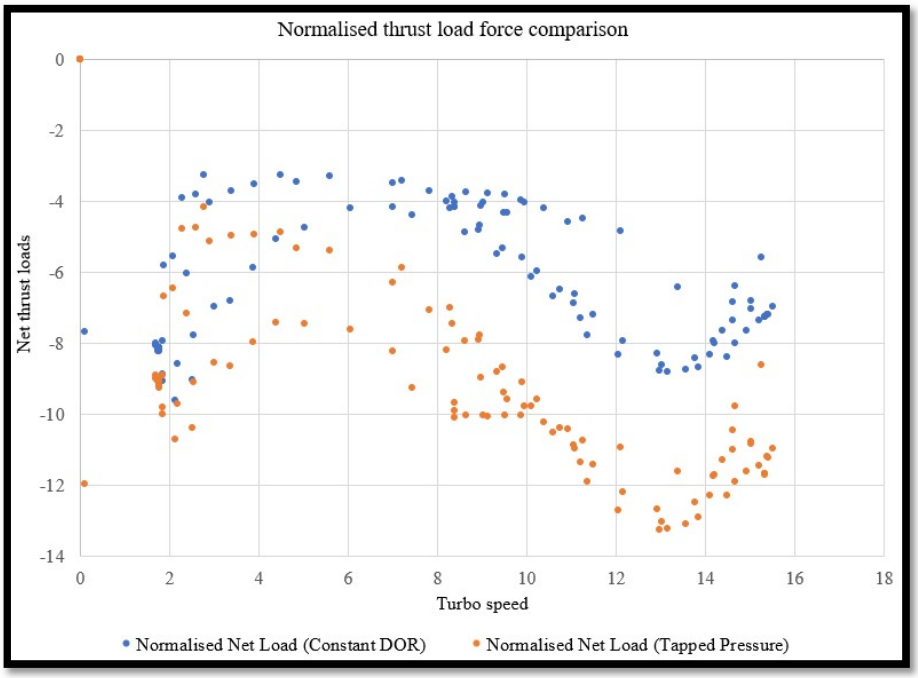

Fig. 114 Comparison of constant DOR method and pressure tapped thrust loads © Cummins

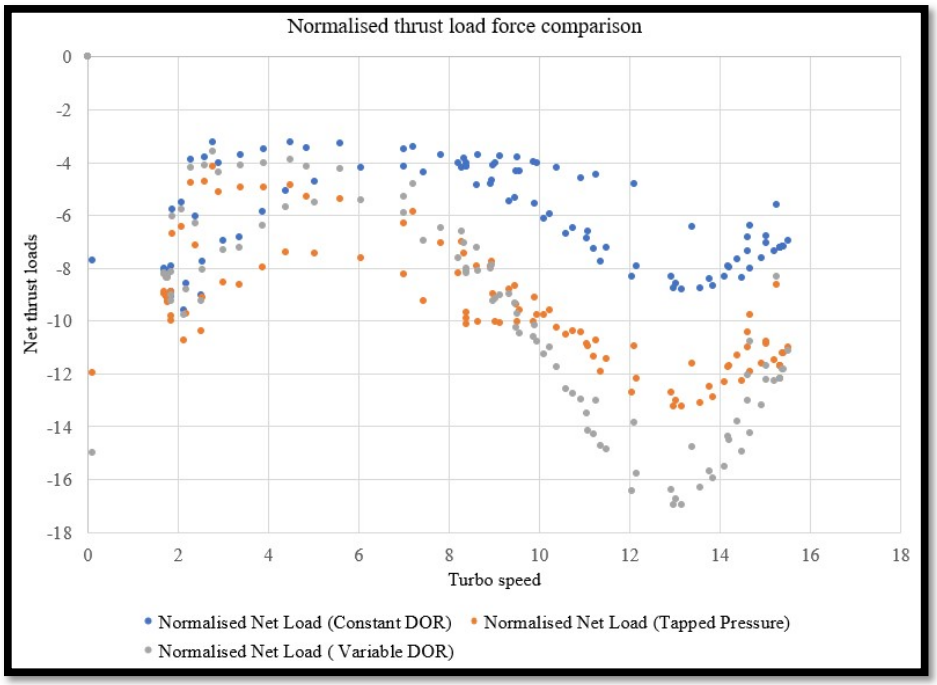

Fig. 115 Comparison of new variable DOR model with actual and previous constant DOR approach © Cummins

The figure 115 shows that the models have shown improvement over the previous constant DOR approach but there is still variation in the prediction. At lower turbocharger speeds, it under predicts the force while at higher turbocharger speeds it has over-predicted the force. In a medium range of speed, the model completely matches with test cell data results. But the variation with the actual loads is lower at low speeds while the gap is more at higher speeds. This data of the engine also has secondary brake valve operated so the comparison with the operation of additional brake valve is shown in figure 116 below:

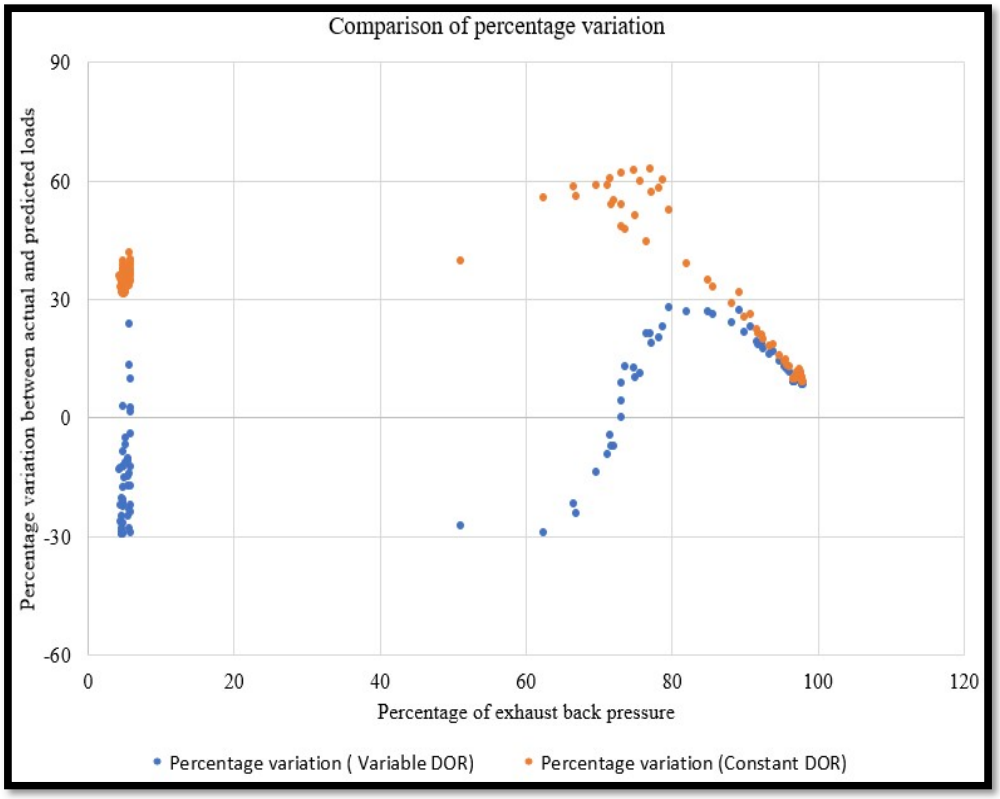

Fig. 116 Percentage change with previous constant DOR and variable DOR approach © Cummins

As per figure 116, it shows that the new method predicts much better than the previous approach as it considers many parameters which affect enthalpy change on the compressor and turbine stages. At lower exhaust back pressures variation is lesser than constant DOR approach. Even when the back pressures are moderately high the variation is lower than the previous method. At high back pressures both the approaches are nearly same but prediction by the new variable DOR approach is even better. So, it performs well better than the approach which takes the assumption of a degree of reaction as equal and constant for all operating conditions.

The reason for variation is that the pressure at the tip does not vary constantly at all operating conditions. The variation is lower in lower turbocharger speeds but higher at high speeds, because of which the model shows the under and overprediction in the results.

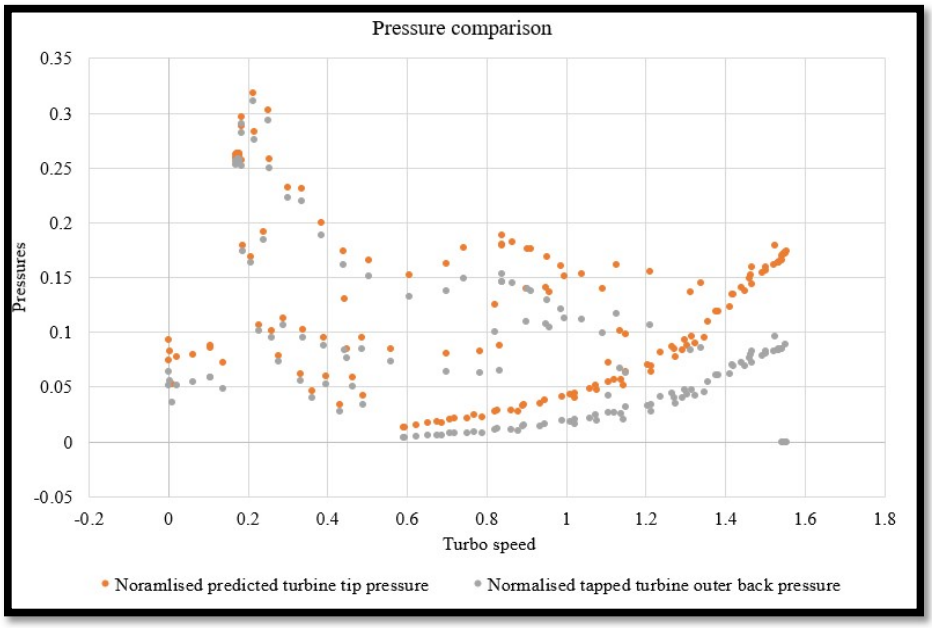

Fig. 117 Pressure variation between the predicted tip and tapped outer back pressure for turbine © Cummins

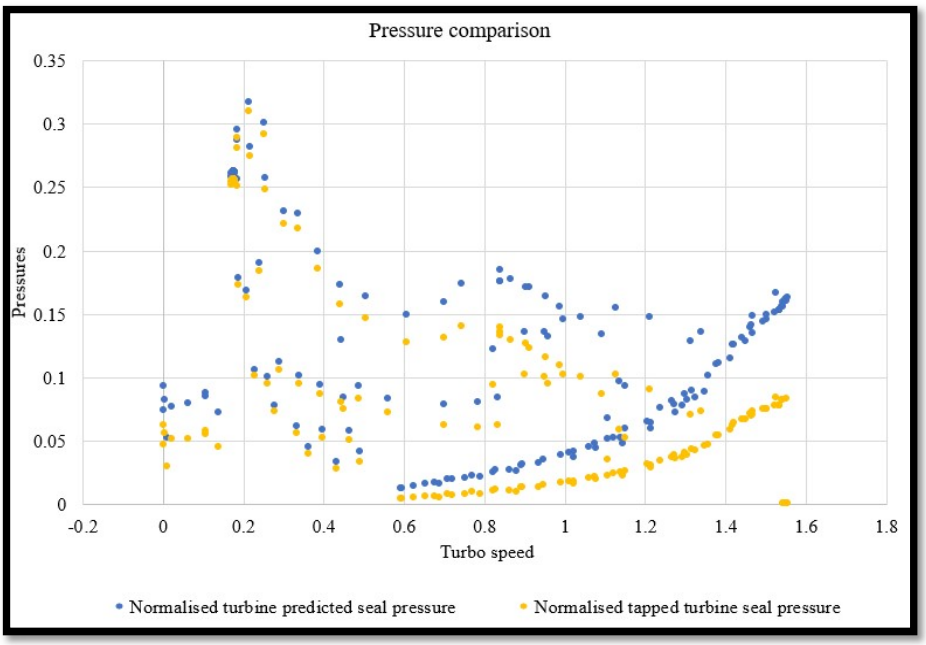

Fig. 118 Pressure variation between predicted seal and tapped seal pressure for turbine © Cummins

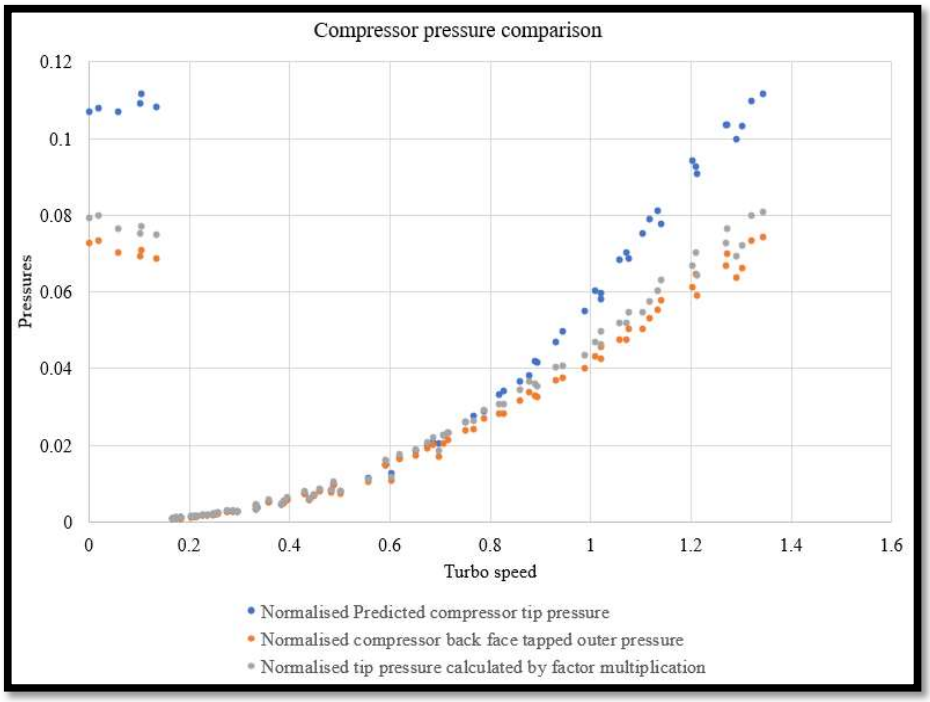

Fig. 119 Tip Pressure variation on compressor end © Cummins

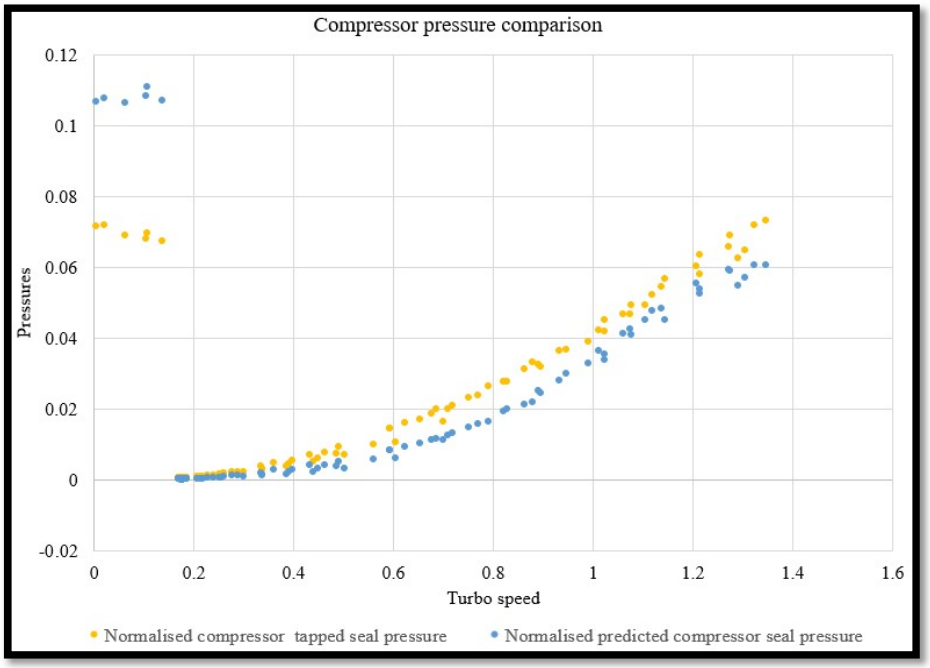

Fig. 120 Seal pressure variation on compressor end © Cummins

The pressures predicted for compressor tip are higher for higher turbocharger speeds due to which the loads shift towards negative side more resulting in overprediction at high speeds. On the other hand, for lower turbocharger speeds there is not a significant

variation. On the turbine side, the predicted pressures are higher for complete operating range and trend varies by predicting higher pressures at lower turbocharger speeds than at higher speeds. The new model has also been tested in under worst case operations of choke and surge. The results show the variation which is lesser than the previous approach even when the turbocharger is operated near choke points.

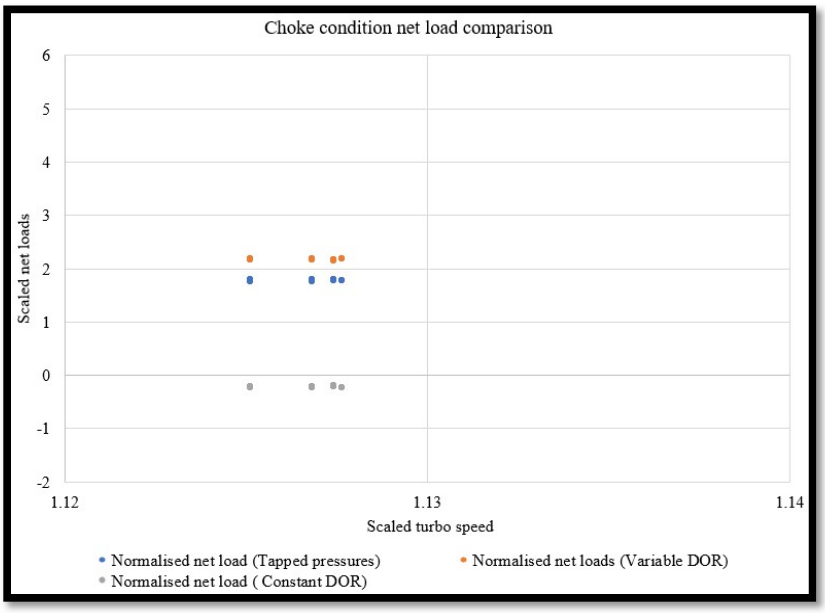

Fig. 121 Force comparison under choke test © Cummins

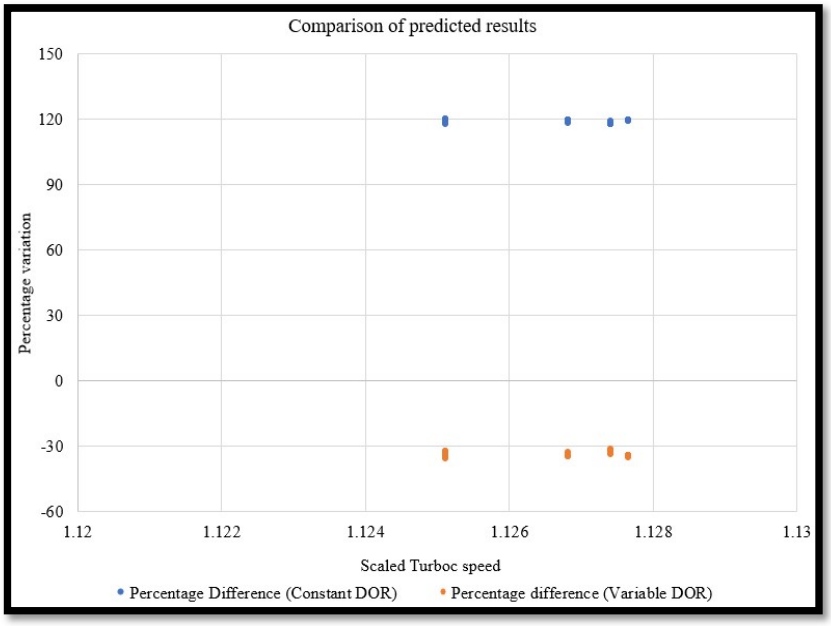

Fig. 122 Percentage variation is within lower than previous approach © Cummins

CHAPTER 6: CONCLUSIONS AND FUTURE SCOPE OF WORK

Chapter 6 gives insight into the developments made in the research work and the improvements that can be made in making the approach more robust and accurate. The findings of the research work are:

- CFD trained models can predict DOR and tip pressures with good relation which can reduce CFD computational efforts.
- Pressure tapping approach uses tapped pressures behind the wheel and impeller for thrust load prediction but the new approach uses tip and seal pressures based on theoretical assumptions.
- The CFD is not performed at compressor and turbine stage cavities so pressure behind wheels is difficult to be incorporated into the analytical model resulting in variation.
- The CFD trained approach shows good results with pressure tapped method under high exhaust back pressures and when the turbo operates in medium speed range. It under predicts at lower speeds but overpredicts at very high speeds.
- The CFD trained model is better than using the constant value of DOR as it considers various parameters affecting enthalpy changes and resulting a change in DOR.

With improved CFD and test analysis co-relation, accuracy can be increased further, which requires a lot of time and resources. More data needs to be collected to enlarge the data set so as the capture the variability of parameters and to predict better models by adding the new parameters, that can narrow down the variation. The steps that can be taken to improve the project in future are listed below:

- As the new model are trained to take CFD as the base so the gap between the CFD and actual test results must be reduced.
- Areas taken in new model is based on the control volume approach and as taken in previous research works so areas must be verified using CFD analysis.
- As an analytical method takes mean value of pressures in the shroud region so pressure variation in the blade region and the back face must be established.

- More data set for both the turbine side and compressor side is needed to come up with better regression models. Due to small data set on the turbine side, the parameter U/C has been dropped to avoid overprediction. The parameter U/C must be included to avoid making the fit better.

REFERENCES

A., Y., ÇENGEL, J. M. and CIMBALA (2001) FLUID MECHANICS: FUNDAMENTALS AND APPLICATIONS. 1st edn, McGraw-Hill. 1st edn. New York.

Abdelmadjid, C., Mohamed, S. A. and Boussad, B. (2013) 'CFD analysis of the volute geometry effect on the turbulent air flow through the turbocharger compressor', Energy Procedia. Elsevier B.V., 36, pp. 746–755. doi: 10.1016/j.egypro.2013.07.087.

AUDI AG (2019) EuroCarNews.com, Online. Available at: http://www.eurocarnews.com/29/0/1314/0/video-audi-turbochargers-with-variable-turbine-geometry.html (Accessed: 12 June 2019).

Books, C. (2015) Anatomy of a Turbocharger- CarTech Books, Online. Available at: https://www.cartechbooks.com/techtips/anatomy-of-a-turbocharger-whats-inside-and-how-it-works/ (Accessed: 8 June 2019).

Charitopoulos, A. et al. (2018) 'Design Optimization of an Automotive Turbocharger Thrust Bearing Using a CFD-Based THD Computational Approach', Lubricants, 6(1), p. 21. doi: 10.3390/lubricants6010021.

Chiatti, G., Chiavola, O. and Recco, E. (2017) 'Turbocharging a small displacement diesel engine for urban vehicles', International Journal of Mechanical Engineering and Technology, 8(7), pp. 1916–1928.

Cummins Inc. (2019) Holset Turbochargers, online. Available at: https://www.cummins.com/components/holset-turbo-technologies/holset-turbochargers (Accessed: 12 June 2019).

Deligant, M., Podevin, P. and Descombes, G. (2012) 'Experimental identification of turbocharger mechanical friction losses', Energy. Elsevier Ltd, 39(1), pp. 388–394. doi: 10.1016/j.energy.2011.12.049.

Dieselhub.com (2009) Exhaust-brake, Online. Available at: http://www.dieselhub.com/performance/exhaust-brake.html (Accessed: 8 June 2019).

Dinescu, D. C. and Tazerout, M. (2010) 'Mean value modelling of a Variable Nozzle Turbocharger (VNT)', UPB Scientific Bulletin, Series D: Mechanical Engineering, 72(1), pp. 109–116.

Ebden, M. (2015) 'Gaussian Processes: A Quick Introduction', (August). Available at: http://arxiv.org/abs/1505.02965.

Elnemr, Y. (2011) Acoustic Modeling and Testing of Exhaust and Intake System Components Licentiate Thesis in Technical Acoustics Stockholm, Sweden, 2011. KTH Royal Institute of Technology.

En.wikipedia.org (2016) Exhaust_brake. Available at: https://en.wikipedia.org/wiki/Exhaust_brake (Accessed: 8 June 2019).

Enginebasics.com (2010) AR turbo ratio, online. Available at: http://www.enginebasics.com/Advanced Engine Tuning/AR turbo ratio explained.html (Accessed: 8 June 2019).

Fisher, F. B. (1988) ‘Application of Map Width Enhancement Devices to Turbocharger Compressor Stages’, SAE Technical Paper Series.

Frene, J. (1978) ‘Tapered land thrust bearing operating in both laminar and turbulent regimes’, ASLE Transactions, 21(3), pp. 243–249. doi: 10.1080/05698197808982881.

Gcg.com.au (2016) MAPS-Compressor Maps, Online. Available at: https://gcg.com.au/component/rsticketspro/view-article/29-maps-compressor-maps (Accessed: 8 June 2019).

Gjika, K. and LaRue, G. D. (2008) ‘Axial Load Control on High-Speed Turbochargers: Test and Prediction’, ASME Turbo Expo 2008: Power for Land, Sea and Air, pp. 705–712. doi: 10.1115/GT2008-50756.

Hannu Jääskeläinen (2014) Fixed Geometry Turbochargers, DieselNet.com. Available at: https://www.dieselnet.com/tech/air_turbo_fixed.php (Accessed: 12 June 2019).

Hannu Jääskeläinen, M. K. K. (2017) Turbocharger Fundamentals, DieselNet.com. Available at: https://www.dieselnet.com/tech/air_turbocharger.php (Accessed: 30 August 2018).

Henry, Y., Bouyer, J. and Fillon, M. (2014) ‘An Experimental Hydrodynamic Thrust Bearing Device and Its Application to the Study of a Tapered-Land Thrust Bearing’, Journal of Tribology, 136(2), p. 021703. doi: 10.1115/1.4026080.

Hoepke, B. et al. (2015) ‘Analysis of Thrust Bearing Impact on Friction Losses in Automotive Turbochargers’, Journal of Engineering for Gas Turbines and Power, 137(8), p. 082507. doi: 10.1115/1.4029481.

Huebner, K. H. (1974) ‘A three-dimensional thermohydrodynamic analysis of sector thrust bearings’, ASLE Transactions, 17(1), pp. 62–73. doi: 10.1080/05698197408981439.

Jääskeläinen, H. (2017) Turbocharger Bearings, DieselNet.com. Available at: https://dieselnet.com/tech/air_turbo_bearings.php (Accessed: 9 August 2018).

Khan, P. M. et al. (2005) ‘Development and Evaluation of Exhaust Brake Systems for Light Commercial Vehicle’, SAE Technical Paper. doi: 10.4271/2005-26-063.

Khin Nwe Zin Tun, C. Z. (2014) ‘Design of Centrifugal Compressor for gas turbine’, IJSETR.

Lamquin, T. (2009) ‘Power Losses Identification on Turbocharger Hydrodynamic Bearing: Test and Prediction’, Proceedings of ASME Turbo Expo 2009: Power for Land, Sea and Air, pp. 1–10.

Lee, I. B., Hong, S. K. and Choi, B. L. (2018) ‘Investigation of the axial thrust load using numerical and experimental techniques during turbocharger operation’, Proceedings of the Institution of Mechanical Engineers, Part D: Journal of Automobile Engineering, 232(6), pp. 755–765. doi: 10.1177/0954407017706859.

Lüddecke, B. et al. (2015) ‘Unsteady Thrust Force Loading of a Turbocharger Rotor During Engine Operation’, Journal of Engineering for Gas Turbines and Power, 138(1), p. 012301. doi: 10.1115/1.4031142.

Lüddecke, B., Filsinger, D. and Ehrhard, J. (2012) 'On Mixed Flow Turbines for Automotive Turbocharger Applications', International Journal of Rotating Machinery, 2012, pp. 1–14. doi: 10.1155/2012/589720.

Magdi K. Khair, H. J. (2017) Superchargers -DieselNet, Online. Available at: https://www.dieselnet.com/tech/air_supercharger.php (Accessed: 8 June 2019).

Miltykh, V. and Sotnyk, M. (2016) 'Analysis of the impact of impeller outlet width on the steepness of pressure characteristic', Eastern-European Journal of Enterprise Technologies, 3(7(81)), p. 15. doi: 10.15587/1729-4061.2016.72122.

Muqeem, M., Ahmad, M. and Sherwani, A. F. (2015) 'Turbocharging of Diesel Engine for Improving Performance and Exhaust Emissions: A Review', IOSR Journal of Mechanical and Civil Engineering Ver. III, 12(4), pp. 2278–1684. doi: 10.9790/1684-12432229.

N.WATSON, M. S. J. (1982) 135336919-Watson-Janota-Turbocharging-the-Internal-Combustion-Engine.pdf. London: Macmillan Publishers Ltd.

Nguyen-Schäfer, H. (2012) Rotordynamics of Automotive Turbocharger. 2012th edn. Stuttgart, Germany: Springer. doi: 10.1007/978-3-642-27518-0.

Palanisamy, R. et al. (2018) 'Exhaust Braking System-Review Paper', IJIRT, 4(10), pp. 261–264.

Raetz, H. et al. (2017) 'Numerical Investigation of Aerodynamic Radial and Axial Impeller Forces in a Turbocharger', Proceedings of ASME Turbo Expo 2011, pp. 1–10. doi: 10.1115/GT2011-46360.

Rais, S. (2016) Turbocharger working gif-Speed Hounds, Online. Available at: http://www.speedhounds.com/2016/12/automobile-engine-types-automobilegyaan/turbocharger-working-gif/ (Accessed: 8 June 2019).

Sun, H. et al. (2010) 'Fault Diagnosis and Failure Prediction by Thrust Load Analysis for a Turbocharger Thrust Bearing', Proceedings of ASME Turbo Expo 2010: Power for Land, Sea and Air, (February), p. 8. doi: 10.1115/GT2010-22320.

The MathWorks, I. (2019) Gaussian-process-regression-models, Online. Available at: https://in.mathworks.com/help/stats/gaussian-process-regression-models.html (Accessed: 24 June 2019).

Tieu, A. K. (1991) 'Hydrodynamic Thrust Bearings: Theory and Experiment', J. Tribol., 113(3), pp. 633–638. doi: doi:10.1115/1.2920671.

Turunen-Saaresti, T. (2004) Vaneless and vaned diffusers-Researchgate, Computational and experimental analysis of flow field in the diffusers of centrifugal compressors. The Lappeenranta University of Technology, Lappeenranta, Finland. Available at: https://www.researchgate.net/figure/Vaneless-and-vaned-diffusers_fig1_34199536.

Watanabe, T. and Koike, T. (1996) 'Development of Turbocharger for Improving Passenger Car Acceleration', SAE Technical Papers, (41 2), p. 960018. doi: 10.4271/960018.

Worldturbocharger.com (2018) Technical-info, E&E TURBO. Available at: http://www.worldturbocharger.com/othercate/othername/Technical-info.html

(Accessed: 8 June 2019).

www.grc.nasa (2018) Mass flow choking, Online. Available at: https://www.grc.nasa.gov/www/k-12/airplane/mflchk.html (Accessed: 13 June 2019).